

UC Berkeley

UC Berkeley Previously Published Works

Title

Advances in the growth and characterization of magnetic, ferroelectric, and multiferroic oxide thin films

Permalink

<https://escholarship.org/uc/item/1gm2n89d>

Journal

Materials Science and Engineering R: Reports, 68(4-6)

ISSN

0927-796X

Authors

Martin, LW
Chu, YH
Ramesh, R

Publication Date

2010-05-20

DOI

10.1016/j.mser.2010.03.001

Peer reviewed



Advances in the growth and characterization of magnetic, ferroelectric, and multiferroic oxide thin films

L.W. Martin^{a,b,*}, Y.-H. Chu^c, R. Ramesh^{d,e,f}

^a Department of Materials Science and Engineering, University of Illinois, Urbana-Champaign, Urbana, IL 61801, USA

^b Frederick Seitz Materials Research Laboratory, University of Illinois, Urbana-Champaign, Urbana, IL 61801, USA

^c Department of Materials Science and Engineering, National Chiao Tung University, HsinChu 30100, Taiwan

^d Department of Materials Science and Engineering University of California, Berkeley, Berkeley, CA 94720, USA

^e Department of Physics, University of California, Berkeley, Berkeley, CA 94720, USA

^f Materials Science Division, Lawrence Berkeley National Laboratory, Berkeley, CA 94720, USA

ARTICLE INFO

Article history:

Received 22 March 2010

Accepted 24 March 2010

Available online 21 April 2010

Keywords:

Thin films

Multiferroic

Magnetic

ferroelectric

Complex oxides

ABSTRACT

The growth and characterization of functional oxide thin films that are ferroelectric, magnetic, or both at the same time are reviewed. The evolution of synthesis techniques and how advances in *in situ* characterization have enabled significant acceleration in improvements to these materials are described. Methods for enhancing the properties of functional materials or creating entirely new functionality at interfaces are covered, including strain engineering and layering control at the atomic-layer level. Emerging applications of these functional oxides such as achieving electrical control of ferromagnetism and the future of these complex functional oxides is discussed.

© 2010 Elsevier B.V. All rights reserved.

Contents

1. Introduction	90
2. The wide-world of complex oxides: structures and chemistry	90
3. Advances in the growth of oxide thin films	92
3.1. Thin film growth modes and epitaxy	92
3.2. Pulsed-laser ablation-based techniques	94
3.2.1. Laser-material interactions	95
3.2.2. Recent advances in pulsed laser deposition	96
3.3. Molecular beam epitaxy	97
3.4. Sputtering	97
3.5. Metal-organic chemical vapor deposition	97
3.6. Solution-based thin film deposition techniques	97
3.7. Low-temperature aqueous solution depositions	98

Abbreviations: AAO, anodized aluminum oxide; AF, antiferromagnet; AFM, atomic force microscopy; BFO, BiFeO₃; BMO, BiMnO₃; BTO, BaTiO₃; c-AFM, conducting atomic force microscopy; CBD, chemical bath deposition; CFO, CoFe₂O₄; CMR, colossal magnetoresistance; CSD, chemical solution deposition; DSO, DyScO₃; EB, exchange bias; ED, electroless deposition; eV, electron volt; FeRAM, ferroelectric random access memory; FM, ferromagnet; GMR, giant magnetoresistance; GSO, GdScO₃; H, magnetic field; HRTEM, high-resolution transmission electron microscopy; LSMO, La_{0.7}Ca_{0.3}MnO₃; LPD, liquid phase deposition; LSAT, (LaAlO₃)_{0.29}–(Sr_{0.5}Al_{0.5}TaO₃)_{0.71}; MBE, molecular beam epitaxy; MOCVD, metal-organic chemical vapor deposition; MRAM, magnetic random access memory; Oe, Oersted; P_s, saturation polarization; P–E, polarization–electric field; PCD, photochemical deposition; PEEM, photoemission electron microscopy; PFM, piezoresponse force microscopy; PLD, pulsed laser deposition; PMN-PT, Pb(Mg_{0.33}Nb_{0.67})O₃–PbTiO₃; PTO, PbTiO₃; PZT, Pb(Zr_xTi_{1–x})O₃; RF, radio-frequency; RHEED, reflection high-energy electron diffraction; RHEED-TRAXS, reflection high-energy electron diffraction total reflection angle X-ray spectroscopy; SBT, SrBi₂Ta₂O₉; SPES, spin-resolved photoemission spectroscopy; SQUID, superconducting quantum interference device; SRO, SrRuO₃; STO, SrTiO₃; T_c, Curie temperature; T_N, Neel temperature; TEM, transmission electron microscopy; TMR, tunnel magnetoresistance; ToF-ISARS, time-of-flight ion scattering and recoil spectroscopy; XMCD, X-ray magnetic circular dichroism; YMO, YMnO₃.

* Corresponding author at: Department of Materials Science and Engineering, University of Illinois, Urbana-Champaign, Urbana, IL 61801, USA. Tel.: +1 217 244 9162; fax: +1 217 333 2736.

E-mail address: lwmartin@illinois.edu (L.W. Martin).

4.	Ferroelectricity in oxides	98
4.1.	Definition of ferroelectric materials	98
4.2.	Brief history of ferroelectrics	98
4.3.	Thin film ferroelectric phenomena	99
4.3.1.	Size effects in ferroelectrics	99
4.3.2.	Strain effects in ferroelectricity	100
4.3.3.	Artificially engineered ferroelectrics	102
4.3.4.	Controlling ferroelectric domain structures	103
4.4.	Ferroelectric devices and integration	105
4.5.	Ferroelectric tunnel junctions and novel transport phenomena	106
5.	Magnetism in oxides	106
5.1.	Definition of magnetic materials	106
5.2.	Brief history of magnetic oxides	107
5.3.	Common types of magnetism in transition metal oxides	107
5.3.1.	Superexchange	107
5.3.2.	Double exchange	108
5.3.3.	RKKY coupling	108
5.4.	Modern magnetic oxides	108
5.4.1.	Ferrites	108
5.4.2.	Manganites	109
5.5.	Thin film magnetic phenomena	110
5.5.1.	Superlattice effects	110
5.5.2.	Exchange coupling across interfaces	111
6.	Multiferroism and magnetoelectricity	112
6.1.	Scarcity of multiferroics	112
6.2.	Pathways to multiferroism	113
6.3.	Definition of magnetoelectricity	113
6.4.	Thin film multiferroics	113
6.4.1.	Manganite multiferroic thin films	113
6.4.2.	BiMnO ₃ thin films	114
6.4.3.	BiFeO ₃ thin films	115
6.4.4.	Other single phase multiferroic thin films	119
6.4.5.	Horizontal multilayer heterostructures	119
6.4.6.	Vertical nanostructures	121
6.5.	Engineering new functionalities with multiferroics	122
6.5.1.	Electric field versus current control of magnetism	122
6.5.2.	Electric field control of ferromagnetism	123
6.5.3.	Exchange bias with multiferroic antiferromagnets	124
6.6.	Advanced multiferroic-based devices	126
7.	Future directions and conclusions	128
	Acknowledgements	129
	References	129

1. Introduction

Complex oxides represent a vast class of materials encompassing a wide range of crystal structures and functionalities. Among these interesting properties, the study of magnetic, ferroelectric, and more recently multiferroic properties in these oxide materials has driven considerable research over the past few decades. In the past 20 years, driven by the development of new growth techniques – especially for thin film materials – the field of functional oxide materials has experienced unprecedented growth in terms of the discovery of new materials systems, characterization and understanding of the fundamental properties and nature of existing systems, and in the control of properties in these materials through elegant changes in crystal chemistry (i.e., doping), strain, and other variables. In this paper, the recent advances in the growth and characterization of these functional oxide materials will be reviewed. Throughout this review we will investigate the structure, properties, and synthesis of these complex oxide thin films with special attention to understanding the fundamental nature of ferroelectricity, magnetism, and multiferroism. We will investigate a number of prototypical examples of materials within each functional subgroup and delve into the physics of each process. Detailed attention is also given to thin film growth techniques and strain-engineering of oxide

materials. We end with a look to the future of complex oxide materials with special attention given to possible areas of impact for future technology.

2. The wide-world of complex oxides: structures and chemistry

The general field of metal oxide materials has been the focus of much study because of the wide range of structures and properties present in these materials [1,2]. Thus, to begin this treatment, it is important that we investigate first some of the common crystal structures of these oxide materials. The wide array of possible crystal structures for such complex oxides is at first daunting, but careful analysis of these materials reveals a number of common structures, coordinations, and bonding types. One commonality to these materials is that the bonds are typically ionic in nature (although some level of covalency is also expected in these materials and can have significant impact on the physical properties). Thus, with this in mind, we can outline a few common crystal structures for these materials.

Beginning with binary oxide materials (i.e., MO, MO₂, M₂O₃, M = metal cation) common structures include rock salt (Fig. 1(a)), wurtzite (Fig. 1(b)), fluorite (Fig. 1(c)), rutile (Fig. 1(d)), and corundum (Fig. 1(e)). The monoxides (MO) with rock salt structure include such materials as the alkaline earth metal oxides (i.e., MgO)

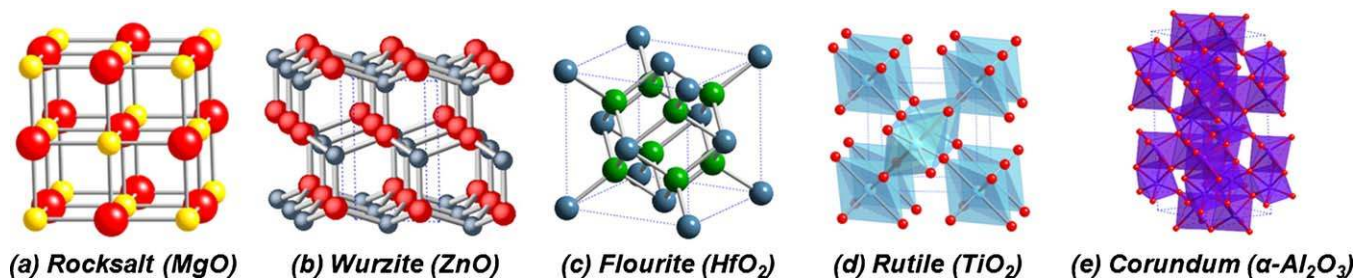


Fig. 1. Common binary oxide crystal structures including (a) rocksalt, (b) wurtzite, (c) fluorite, (d) rutile, and (e) corundum.

and some transition metal oxides (i.e., TiO , VO , CoO , and MnO) and there are a few examples of monoxides with wurtzite structure (i.e., ZnO and BeO). The properties of these monoxides range from insulators (i.e., MgO and CaO) to semiconductors (i.e., MnO and ZnO) to metals (LaO , NdO , and TiO) to superconductors (i.e., NbO) and even magnets (i.e., EuO). As for the binary dioxides (MO_2), the most common structures are the fluorite (i.e., CeO_2 , ThO_2 and ZrO_2) and rutile (i.e., TiO_2 , IrO_2 , MoO_2 , RuO_2 and WO_2) structures. Materials with the fluorite structure are typically insulators (i.e., CeO_2 , HfO_2 and PrO_2) while materials with the rutile structure are typically metallic or semiconducting in nature (i.e., RuO_2 and TiO_2). Finally, for the binary trivalent oxides (M_2O_3), common structures include bixbyite (i.e., Mn_2O_3 , La_2O_3 , and Dy_2O_3), materials with this structure are typically insulating, and corundum (i.e., Al_2O_3 , V_2O_3 , and Cr_2O_3), materials with this structure are typically insulators at room temperature.

Common ternary oxides structures include the ilmenite (Fig. 2(a)), spinel (Fig. 2(b)), perovskite (Fig. 2(c)), and perovskite-derived structures such as the Ruddlesden–Popper series (Fig. 2(d)) and other layered-perovskite structures (Fig. 2(e)). The ilmenite structure, which has chemical formula $(\text{AB})\text{O}_3$ (i.e., FeTiO_3 , MnTiO_3 and LiNbO_3), is closely related to the corundum structure

and has a mixture of trivalent cations on the M-site. Materials with ilmenite structure have been found to be semiconducting and can possess other interesting properties such as piezoelectricity. Yet another ternary oxide structure is the cubic spinel structure, which has chemical formula AB_2O_4 (i.e., MgAl_2O_4 , CoFe_2O_4 and LiTi_2O_4), and is made up of a close-packed fcc array of oxygen ions with one-eighth of the tetrahedral interstices occupied by divalent cations and half of the octahedral interstices occupied by a mixture of divalent and trivalent cations. Properties of the spinels can range from large band gap insulators to magnets to superconductors and more. Another common ternary oxide structure is the perovskite structure, which has chemical formula ABO_3 (i.e., CaTiO_3 , SrRuO_3 and BiFeO_3), and is made up of corner-sharing octahedra with the A-cation coordinated by twelve oxygen ions and the B-cation by six. Typically the ionic radius of the A-cation is somewhat larger than the B-cation. The structure can easily accommodate a wide range of valence states on both the A- and B-site (i.e., $\text{A}^{+1}\text{B}^{+5}\text{O}_3$, $\text{A}^{+2}\text{B}^{+4}\text{O}_3$ and $\text{A}^{+3}\text{B}^{+3}\text{O}_3$) and possesses complex defect chemistry that maintains charge balance in the structure. Similarly, the perovskite structure acts as the parent phase for a wide range of structures including the Ruddlesden–Popper series. The Ruddlesden–Popper series [3] describes the structure that evolves as rock

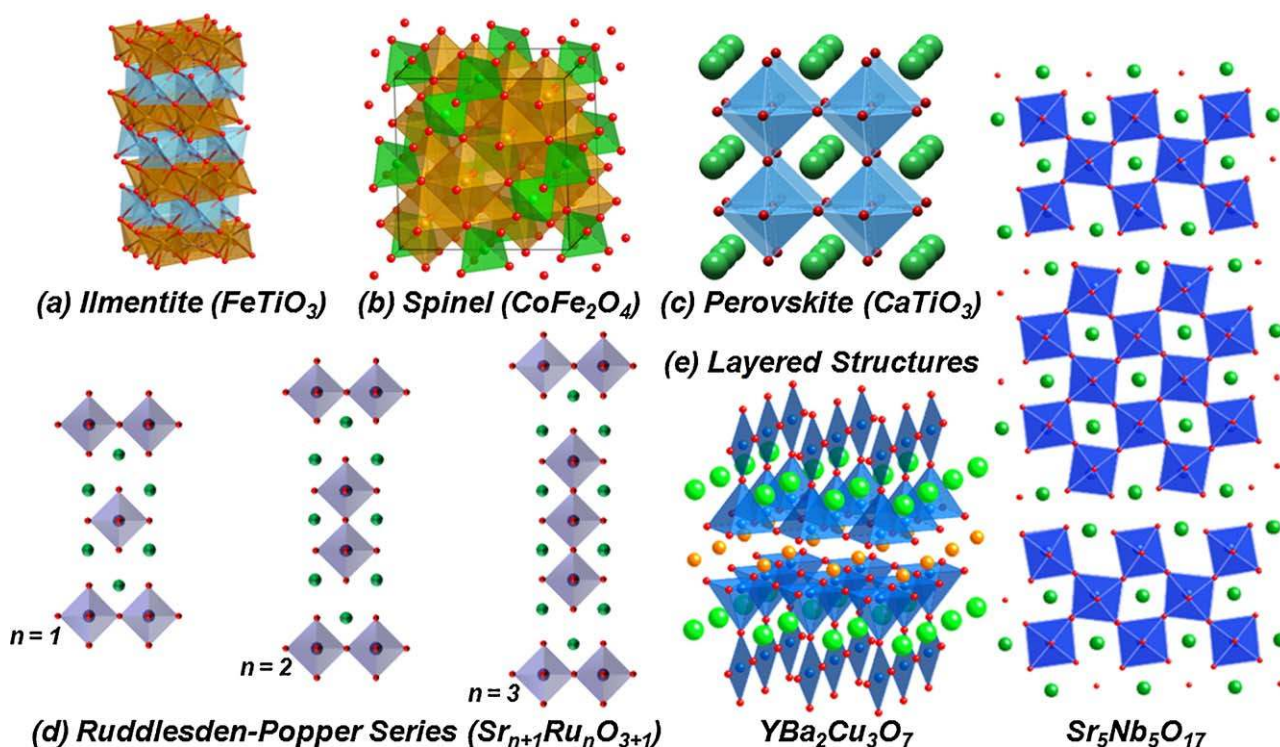


Fig. 2. Common ternary oxide crystal structures including (a) ilmenite, (b) spinel, (c) perovskite, and derivatives of the perovskite such as (d) the Ruddlesden–Popper series and (e) layered perovskites.

salt layers are inserted in the perovskite structure separating (0 0 1) planes and is written as $A_{n+1}B_nO_{3n+1}$ (where $n = \infty$ is the parent perovskite structure). The example shown here is for the Ruddlesden–Popper series based on the widely studied metallic, ferromagnet $SrRuO_3$. As rock salt layers are added to this structure the properties can change quite drastically; the $n = 1$ phase (Sr_2RuO_4) is known to be a superconductor [4] while the $n = 2$ phase ($Sr_3Ru_2O_7$) exhibits complex magnetic structure and interesting changes in resistance at low temperatures [5,6]. Other more complicated layered structures can be derived from the perovskite structure such as those shown in Fig. 2(e) for the high-temperature superconductor $YBa_2Cu_3O_7$. Key to the superconducting properties observed in this material are the square-planar coordinated CuO_4 planes.

At the heart of understanding oxide materials, is recognizing how the chemical structure of the material enables the evolution of the electronic structure. From chemical bonding to chemical doping, the interplay of physics and chemistry in oxide materials is a very rich subject. In the monoxides (MO) like the rock salt materials discussed above both the cation and the O-anion are in octahedral coordination and they possess largely ionic bonds and, therefore, typically have very large band gaps and insulating properties. Monoxides with the wurtzite structure, however, are hexagonal and possess tetrahedral coordination of the cations and anions (very similar to a diamond cubic structure of many traditional semiconductors like Si) and thus typically are more semiconducting in nature. This idea can be extended to a wide range of oxide materials, but is very elegantly described in the richness of properties found in the perovskite-derived oxides.

By far the most interesting aspect of complex oxides, as is exemplified by the perovskites, is the ability to engineer/tune their physical properties simply by replacing the cationic species that are located at the A- and B-sites in and around the oxygen octahedral coordination cage. Thus, the electronic structure and coordination chemistry of the cationic species controls the fundamental physical phenomena. As an example, let us take a look at the prototypical perovskite $SrTiO_3$ which is a good insulator as a consequence of the closed shell electronic structure of both Sr and Ti ($4+$ and d^0): from a band perspective, the valence band is filled while the conduction band is empty. Simply changing the A-site cation from Sr to La makes a dramatic difference in the electronic structure as well as the transport properties. In $LaTiO_3$, the Ti in this compound is in the $+3$ oxidation state and thus in a formal sense has d^1 electronic structure. As such, it is expected to be a good conductor as a consequence; however, the reality is something dramatically different. $LaTiO_3$ is actually a very good insulator; a so-called Mott insulator [7]. This insulating behavior arises due to the interplay between the kinetic energy of the electron and Coulombic repulsion effects at the atomic scale. These two terms trade off of each other and so the manifested transport properties are the result of this competition. Such materials exhibit strong (sometimes *colossal*) changes in their transport properties under external thermodynamic stimuli (i.e., temperature, magnetic field, electric field and chemical potential). If one were to take the $LaTiO_3$ structure and change the cation at the B-site (the transition metal site), for instance by replacing the Ti with Mn, then one will obtain the antiferromagnetic insulator (insulating for the same reason as for $LaTiO_3$) $LaMnO_3$. There are a number of exquisite treatises on the nature of electronic conduction in oxides (see, for example, Refs. [7,8]) and so we will not elaborate further on this subject here, except to note that the entire evolution of the physics and chemistry of these materials and their implementation into next-generation technologies is dependent on the complex interplay between the cationic stereochemistry, electronic structure and the interactions among them.

3. Advances in the growth of oxide thin films

The modern study of complex oxide materials has been driven largely by the development of new growth and characterization techniques that have offered researchers unprecedented access to new phases and insight about these materials. The development of new thin film growth techniques that allow for the production of non-equilibrium phases of materials and strain engineering of existing materials represents a significant step forward in the study of functional complex oxide materials [9]. Epitaxial growth of thin films offers a pathway to the discovery and stabilization of a number of new multiferroics in conjunction with the availability of high quality materials that can be produced with larger lateral sizes than traditionally possible with single crystal samples. Ferroelectric, magnetic, and multiferroic thin films and nanostructures have been produced using a wide variety of growth techniques including sputtering, spin coating, pulsed laser deposition, sol-gel processes, metal-organic chemical vapor deposition, molecular beam epitaxy, and more. In this section we will discuss the details of the growth of oxide thin films as well as recent and future advances in *in situ* characterization and control of the growth of oxide materials. We direct the reader to any of a number of excellent texts on the greater field of thin films growth and characterization for additional information (see, for instance, Refs. [10,11]).

3.1. Thin film growth modes and epitaxy

We begin with a brief overview of thin film growth processes in materials. There are three major thin film growth modes: (1) Volmer–Weber or island growth, (2) Frank–Van der Merwe or layer-by-layer growth, and (3) Stranski–Krastanov growth. These growth mechanisms are illustrated in Fig. 3. Volmer–Weber of island growth (Fig. 3(a)) occurs when the smallest stable clusters nucleate on the substrate and grow into three-dimensional island features. One simplistic explanation for this growth behavior is that the atoms or molecules being deposited are more strongly bonded to each other than to the substrate material. This is often the case when the film and substrate are dissimilar materials. There are a few examples of such behavior in the growth of oxide films on oxide substrates, but this growth mode is typically observed when metal and semiconductor (i.e., Group IV, III–V, etc.) films are grown on oxide substrates. The opposite characteristics, however, are displayed in Frank–Van der Merwe or layer-by-layer growth (Fig. 3(b)) which occurs when the extension of the smallest nucleus occurs in two dimensions resulting in the formation of planar sheets. In layer-by-layer growth the depositing atoms or molecules are more strongly bonded to the substrate than each other and each layer is progressively less strongly bonded than the previous layer. This effect extends continuously until the bulk bonding strength is reached. A typical example of this is the epitaxial growth of semiconductors and oxide materials. The greater field of oxide thin film growth has developed around the ability to control materials through this and other similar growth modes. Such capabilities have ushered in an era of unprecedented control of oxide materials down to the single (or even half-) unit cell level. The final growth mechanism is the Stranski–Krastanov mode (Fig. 3(c)) which is a combination of the layer-by-layer and island growth. In this growth mode, after forming one or more monolayers in a layer-by-layer fashion, continued layer-by-layer growth becomes energetically unfavorable and islands begin to form. This sort of growth is fairly common and has been observed in a number of metal–metal and metal–semiconductor systems [10].

These different growth modes can be described in more detail with simple thermodynamic models for the nucleation and growth

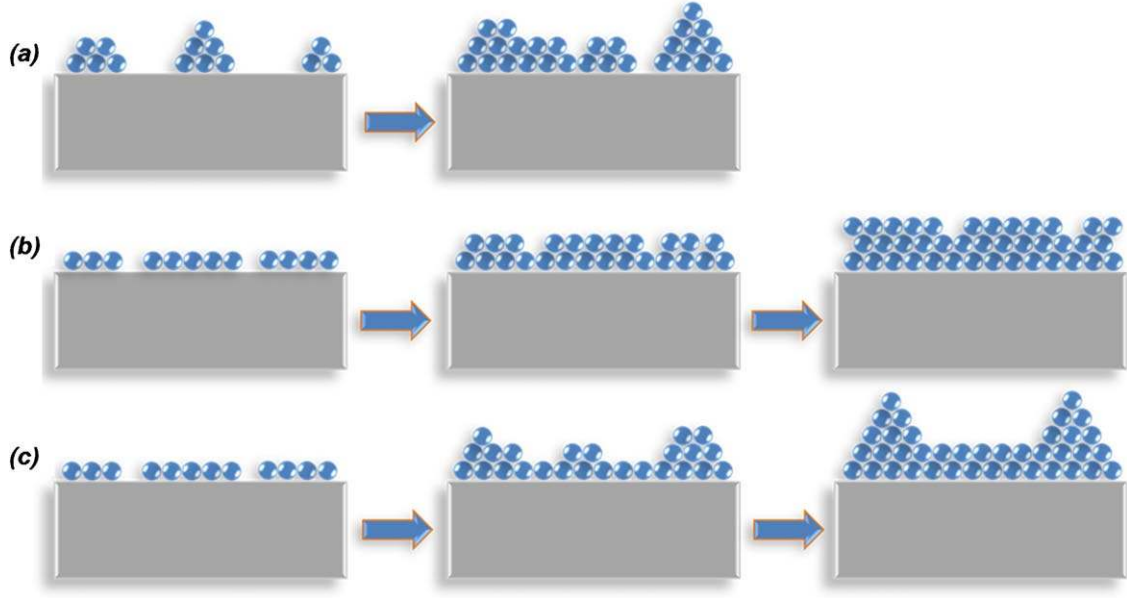


Fig. 3. Illustrations of the basic growth modes including (a) Volmer–Weber (island), (b) Frank–Van der Merwe (layer-by-layer), and (c) Stranski–Krastanov growth.

of film materials. This begins with an understanding of surface energies in materials, or specifically capillarity or droplet theory of heterogeneous nucleation. One can model the atomistic nucleation process on the substrate surface during a vapor deposition like that in Fig. 4. The mechanical equilibrium among the horizontal components of the interfacial tensions between the constitutive phases yields Young's equation:

$$\gamma_{sv} = \gamma_{fs} + \gamma_{fv} \cos \theta \quad \text{or} \quad \cos \theta = \frac{(\gamma_{sv} - \gamma_{fs})}{\gamma_{fv}} \quad (1)$$

where the γ is the interfacial energy, subscripts s, f , and v stand for substrate, film, and vapor respectively, and θ is the contact or wetting angle. One can use Young's equation to better distinguish between the three growth modes. For island growth, $\theta > 0$ therefore $\gamma_{sv} < \gamma_{fs} + \gamma_{fv}$. If γ_{fs} is neglected, this relation suggests that island growth occurs when the surface tension of the film exceeds that of the substrate. Hence this is why metals tend to cluster or ball up on ceramic or semiconducting substrates. On the other hand, in layer-by-layer growth, the film wets the substrate, hence $\theta \sim 0$ and therefore $\gamma_{sv} \geq \gamma_{fs} + \gamma_{fv}$. It should be noted that surface energy values for many oxide are difficult to find in the literature. A special case of this condition is so-called homoepitaxy where the interface between substrate and film essentially vanishes and $\gamma_{fs} = 0$. For high quality layer-by-layer deposition one typically needs a film and substrate with only small differences in surface energy and in general materials with low surface energies will wet surfaces with higher surface energies. In the last case, for Stranski–Krastanov growth initially $\gamma_{sv} \geq \gamma_{fs} + \gamma_{fv}$ is satisfied leading to layer-by-layer growth, but the buildup of

strain energy from lattice mismatch of film and substrate can lead to a transition to island like growth typically after 5–6 monolayers [10].

In the end, film growth becomes much like many processes in materials science, in that it is a nucleation and growth process. As film material deposits on the surface of the substrate, nucleation can occur in a number of ways, at step edges, defects, etc., and once the critical nucleus size is reached the growth of nucleus can occur in many ways. The growth is dependent on the kinetics of the system – the rate of adatom arrival, temperature, pressure, etc., of the system – and these are the tools researchers use to control the growth of their materials.

Epitaxial growth refers to extended single-crystal film formation on top of a crystalline substrate. Epitaxy is of great interest for the work in this manuscript and has been one of the single most important developments in the field of semiconductor processing in the last century and has given rise to our current computing abilities. There are two major types of epitaxy, *homoepitaxy* and *heteroepitaxy*. As the name implies, homoepitaxy refers to the growth of a material on a substrate of that same material, for instance doped-Si on a Si substrate. The film in this case can be of very high quality, free of defects, but have a different doping or functional nature than the substrate. The second type of epitaxy, heteroepitaxy, refers to the case where the film and substrate are different materials, but have similar structures that help guide the growth of the film. This is the growth process used throughout this document. Fig. 5 helps to illustrate the differences between homoepitaxy (Fig. 5(a)) and heteroepitaxy (Fig. 5(b) and (c)). If the film material is exactly the same as the substrate or they are different materials that have very small difference in lattice parameter, interfaces such as that shown in Fig. 5(a) can be achieved where there is little disruption of the structure across the interface. If, however, the film and substrate materials are different and the lattice parameters are slightly more mismatched, it is possible to form one of two types of interfaces. Fig. 5(b) illustrates the so-called strained-layer epitaxy. This sort of structure occurs for most very thin films regardless of substrate mismatch especially if both the substrate and film have the same crystal structure (i.e., perovskite on perovskite, such as is the case for many films in this manuscript). Fig. 5(c) illustrates relaxed epitaxy. In this case the lattice mismatch is somewhat larger and the film

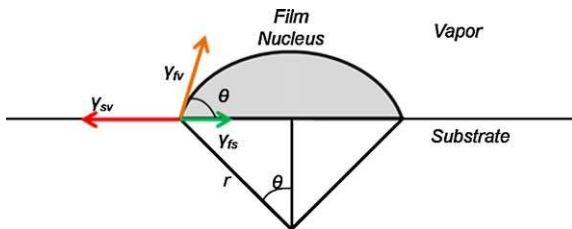


Fig. 4. Schematic of basic atomistic nucleation process during film growth.

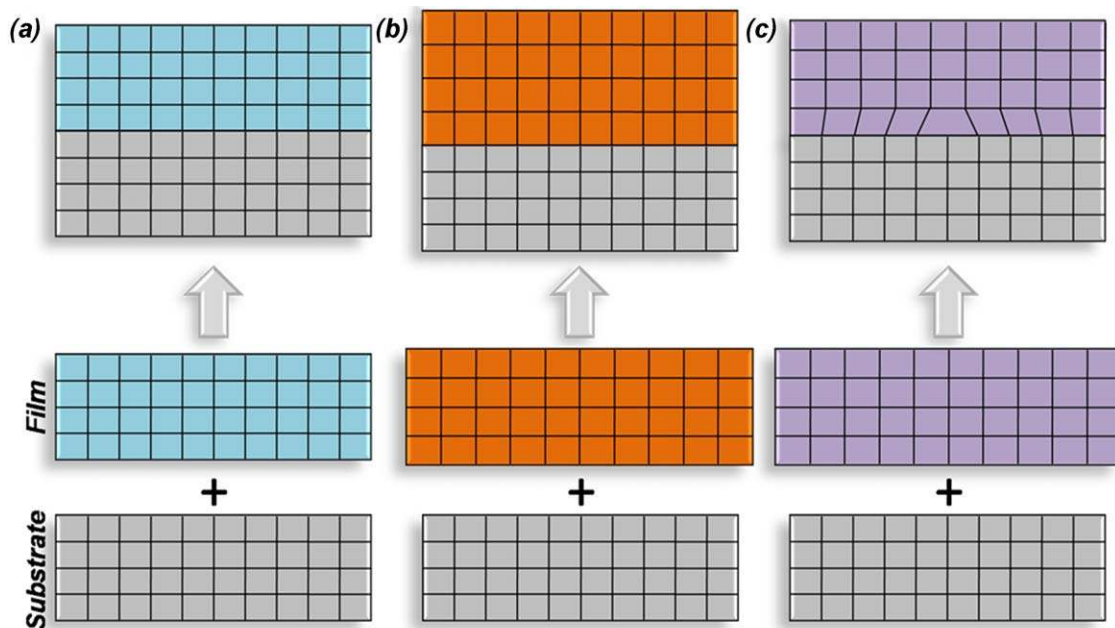


Fig. 5. Schematic illustration of (a) nearly perfectly lattice matched, (b) strained, and (c) relaxed heteroepitaxial film growth.

and substrate materials might even have different crystal structures resulting in a relatively quick relaxation of the film material to its bulk structure through the formation of defects, like dislocations, that accommodate interfacial strain in the system and lead to a relaxed film [10].

One can probe the likelihood that one of these different heteroepitaxial interfaces will form by defining the lattice mismatch f as:

$$f = \frac{2(a_f - a_s)}{a_f + a_s} \sim \frac{a_f - a_s}{a_s} \sim \frac{a_s - a_f}{a_f} \quad (2)$$

and a_f and a_s are the lattice parameters of the film and substrate, respectively. Typically $f < 0.1$ is a requirement for epitaxy because if $f > 0.1$ so few interfacial bonds are well aligned that there is little reduction in the interfacial energy and the film will not grow epitaxially. It should also be noted that f can become a function of temperature if the thermal-expansion coefficients of the film and substrate are vastly different—as is the case of the growth of some oxides on semiconductors like silicon [11].

3.2. Pulsed-laser ablation-based techniques

No other single advance in the creation of oxide materials has had as big an impact as laser-ablation growth techniques. With this in mind, we will focus considerable space to a thorough review of pulsed-laser ablation growth technique. The reader is directed to a number of excellent books and thorough reviews on the history and evolution of this process [12–14]. Throughout much of the 20th century, research into complex oxides was focused on bulk single crystals and powder samples. With the discovery of high T_C superconductors in the late 1980s [15], however, complex oxide materials moved to the forefront of materials research. Just one year after this monumental discovery of high temperature superconductivity, workers at Bell Communications Research triggered a revolution in complex oxide materials research with the growth and characterization of superconducting films via pulsed laser deposition (PLD) [16,17]. PLD itself was used in the growth of semiconductor and dielectric materials [18] and further extended to materials such as SrTiO_3 and BaTiO_3 [19] as early as the

1960s, but did not blossom as the growth technique of choice until the late 1980s. The development of PLD required a number of critical steps including the technical development of the appropriate hardware (i.e., vacuum systems, lasers, etc.) and successful application to new classes of materials (i.e., high T_C superconductivity and colossal magnetoresistance).

PLD is a very simple thin film growth process and is shown schematically in Fig. 6. The system consists of a vacuum chamber equipped with pumps, a target holder and rotator, substrate heater, and is typically equipped with various pressure gauges, controllers, and other instruments to control the deposition environment of the system. Film growth can be carried out in reactive environments, like that for oxides where a partial pressure of oxygen, ozone, or atomic oxygen is carefully controlled. Temperature is controlled with the substrate heater and the combination of reactive gas pressure and temperature offers researchers access to a wide range of thermodynamic conditions. One of the aspects of PLD that makes it such a versatile growth process is that the deposition is achieved by vaporization of materials by an external energy source—the laser. PLD systems are often equipped with a set of optics including apertures, attenuators, mirrors, and lenses to focus and direct the laser beam into the chamber with the right energy density. The rather minimal setup of PLD is just one of a number of advantages of the process over other thin film growth processes. Other advantages include the fact that the process is far from equilibrium and hence is good at preserving complex stoichiometries, it is simple to use multiple materials and easy to replace the targets, it is a cost effective process for exploring a wide range of materials, and it is excellent for rapid prototyping of materials and investigating a wide array of phase space. As with all processes, however, there are some detractors. Historically PLD was said to produce low quality films, although the advent of advanced *in situ* monitoring processes like reflection high energy electron diffraction and increased experience with the process has led some groups to create very high quality films. Another common complaint with PLD is that if one is not careful PLD can lead to non-uniform target erosion, which could result in nonstoichiometry of the growing film. Finally the biggest detractor from PLD has traditionally been macroparticle ejection—in the form of explosive ejection of particles, splashing,

Pulsed Laser Deposition

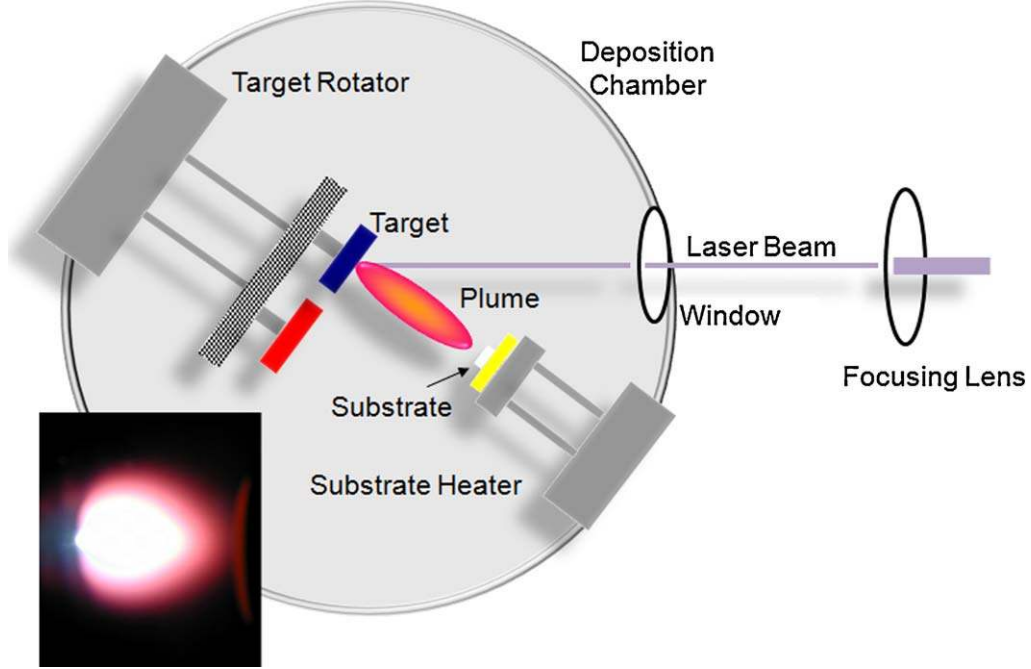


Fig. 6. Schematic of a standard pulsed laser deposition system. The inset picture shows an actual photograph of the plume.

and fragmentation due to thermal shock. In the next section we will investigate how the laser-material interaction can result in such effects.

3.2.1. Laser-material interactions

The mechanisms that lead to laser ablation of materials depend on laser characteristics, as well as optical, topological, and thermodynamic properties of the target material. When the laser radiation is absorbed by a solid surface, electromagnetic energy is converted first into electronic excitation and then into thermal, chemical, and even mechanical energy that cause evaporation, ablation, excitation, plasma formation, and exfoliation. The plume (shown in the inset picture in Fig. 6) consists of a mixture of energetic species including atoms, molecules, electrons, ions, clusters and even micron-sized solid particulates. The plume has a highly directed, dense shape that rapidly expands in the vacuum chamber to create a jet of material directed normal to the target surface. Although this makes PLD ideal for congruent evaporation, maintaining complex stoichiometry and a fast deposition process, it also limits PLD to a research level system that is difficult to scale-up to large wafers due to the directed nature of the plume [12].

Laser ablation and the production of a plume can be described as a flash evaporation process that takes place in the tens of nanosecond time scale (typical pulse length for an excimer laser is 10–30 ns). One can break up the evolution of a plume of materials into a number of steps. The first of which is the photon absorption process. Absorption in a material is defined as

$$I = I_0 \exp(-\alpha x) \quad (3)$$

where $1/\alpha$ is the absorption length which is ~ 100 nm for many oxide materials at the laser wavelengths commonly used in PLD (i.e., < 400 nm). In this process electrons in the target are excited and are thermalized in the picosecond time scale. The next step includes surface melting of the target and conduction of heat into the bulk. The thermal diffusion length is described as

$$\lambda_{th} = 2(\alpha_{th} \Delta t)^{1/2} \quad (4)$$

where α_{th} is the thermal diffusivity which can be written as $K/\rho c$ where K is the thermal diffusivity, ρ is the mass density, and c is the specific heat and Δt is the pulse duration. During this process the temperature rises in the area of the target near the surface as it prepares for the evaporation process. The next step is the actual vaporization of the target material. During this step there is a multiphoton ionization of the gaseous phase creating the characteristic plasma. During this step the temperature at the surface of the target well exceeds the boiling point. The final step of the process is the plasma excitation during which further ionization occurs and free electrons are excited. This results in Bremsstrahlung absorption in which the hot pulse, now at nearly 2000 K, expands in a very directed manner [11].

This analysis can be taken further by discussing the ablation threshold of materials, or the minimum energy density required in a material to create a plume. Let's begin by comparing $1/\alpha$ and λ_{th} . In most oxides the thermal diffusion length is much longer than the absorption length, especially for UV lasers. This arises from the fact that oxide materials are often opaque and good thermal conductors. From this we can calculate an affected volume, which is related to the spot size times λ_{th} . Knowing the volume of affected material, one can then use a simple estimation of the minimum energy needed to raise this volume to the sublimation point as follows:

$$Q_{Heat} = C_S(T_{Melt} - T) + \Delta H_m + C_m(T_{vap} - T_{Melt}) + \Delta H_{vap} \quad (5)$$

where the total energy required (moving left to right) is the sum of the energy needed to bring the target material to the melting temperature plus the heat of melting, plus the energy needed to bring the melted material to the vaporization point plus the heat of vaporization. If this seems like a large amount of energy, it is important to remember that a typical instantaneous power density for a single laser pulse with energy density of ~ 2 J/cm² and 20 ns in length is nearly 10^8 W/cm². This is more than enough energy to ablate nearly all materials [11].

The evaporant distribution or the plume shape can be described with two components. One has a $\cos \theta$ distribution, has considerable

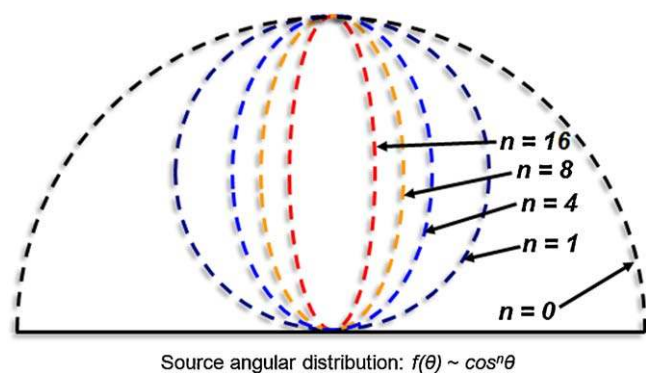


Fig. 7. Schematic illustration of the shape of a plasma plume created by pulsed laser deposition. The angular distribution of the plume is dominated by a $\cos^n \theta$ function.

thermal energy, and tends to be nonstoichiometric as in conventional thermal evaporation. The other component has a sharply lobed $\cos^n \theta$ distribution, with n values reported in the range of 4–14. This lobed component shown schematically as a function of n in Fig. 7, is closely stoichiometric and has velocity of $\sim 10^4$ m/s which is well above thermal velocity and gives particle energies of ~ 40 eV. This large kinetic energy is a key feature of PLD where the large energy can help to modify film structures, activate reactions – such as the dissociation of gas molecule like O_2 , and helps to accelerate the stoichiometric vapor and remove some of the nonstoichiometric thermal components [11].

Historically, the biggest drawback of PLD has been the ejection of large particles that can end up in the film. One such effect is known as “splashing,” or the presence of surface particulates from the target. Splashing can occur for a number of reasons including something known as subsurface boiling or as a consequence of low target densities. It occurs if the time required to transfer energy into heat is shorter than that needed to evaporate a surface layer with a thickness on the order of the skin depth. In such a situation a subsurface layer is superheated before the surface has become a vapor and micron sized molten globules can be expelled from the system. Another cause for splashing is the expulsion of the liquid layer by the shock wave recoil pressure. In other words the force that causes the liquid to splash comes from the pressure shock wave produced by the plume. It results in nearly identical globules to that from the subsurface boiling. Finally, another cause of the formation of large particles in the PLD process is something known as exfoliation. This process is dependent on laser energy and the surface morphology of the target and refers to the ejection of small features that form on an ablated target with time. Thermal shock can jar the features loose and they can be carried towards the substrate with the plume [12].

3.2.2. Recent advances in pulsed laser deposition

Great strides have been made in utilizing the unique features of PLD to create novel new materials and structures. This includes automation of systems to enable alloy formation from multiple targets. This builds on the idea that each laser pulse results in significantly less material than is needed to create a full monolayer, thus alternating shots between different targets can be used to build up a wide range of chemical compositions. This sort of concept has been used to make materials such as $KTa_{1-x}Nb_xO_3$ [20] and $Bi(Fe_{1-x}Cr_x)O_3$ [21]. A natural evolution of this compositional mixing is to combine it with lateral translation of the substrate to achieve spatial variations in composition in a single film. This is highly desirable in that it allows researchers to create a wide array of samples in a short time period and builds off the ideas of combinatorial materials science. Application of this technique, however, has been limited due to difficulty in analyzing the

resulting materials. Regardless, elegant processes to enable laterally varying compositional spreads have been developed, including utilization of the directed nature of PLD growth via synchronized substrate motion and laser firing [22] or the introduction of an aperture between target and substrate [23]. Other studies have focused on temperature – one of the most critical parameters in PLD film growth – and ways to cover large thermodynamic phase spaces in relatively short times. This has lead researchers to investigate multiple-sample approaches. One elegant technique, which has been used in the optimization of ferroelectric properties in $Sr_xBa_{1-x}Nb_2O_6$ [24] and in the determination of crystallization temperatures for a series of rare earth scandates [25], utilizes a specially designed substrate heater engineered to possess a lateral range in temperatures from 200 to 800 °C.

With the advent of new technologies to aid the PLD process, researchers today can also create precisely controlled interfaces in materials that rival the capabilities of molecular beam epitaxy (MBE) (see Section 3.3). One major advance has been the incorporation of reflection high energy electron diffraction (RHEED) into the PLD process prompting the term “laser-MBE” to be coined. RHEED works on the principle that a beam of electrons are accelerated at a glancing angle towards the surface of the substrate, laser-MBE refers to the ability to monitor *in situ* the oscillations of this intensity thereby obtaining information about the growth of oxide materials. This process has blossomed with the development of differentially pumped RHEED systems, that have allowed researchers to monitor growth processes in high partial pressures of gases (in some cases well in excess of 300 mTorr) [26,27] and has enabled sequential growth of binary oxide materials (akin to a classic MBE process) [28], intercalation of layers in oxides [29], and highly controlled layer-by-layer growth of complex oxide materials [30–32]. This has lead, in part, to the rise of a strong research component focused on interfacial properties and interactions in complex oxides and has proved to be one of the most important enabling technologies in the last decade. For a more complete review of real-time growth monitoring and high-pressure RHEED capabilities see Ref. [26]. It should also be mentioned that techniques such as RHEED-TRAXS (total-reflection-angle X-ray spectroscopy) [33] are also being used in preliminary studies of oxide materials. In this process, incident RHEED electrons collide with the atoms in the sample, knocking secondary electrons out of their shells. Electrons in the outer shells drop into the empty inner shells, emitting X-rays whose energies are characteristic of the species of atoms in the growing film. The RHEED beam that strikes the sample thus creates a spectrum of X-rays detailing the surface stoichiometry.

Yet another development in *in situ* characterization of oxide materials is time-of-flight ion scattering and recoil spectroscopy (ToF-ISARS) [34–37]. ToF-ISARS is a non-destructive, *in situ*, real-time probe of thin film composition and structure which does not interfere with the growth process. An excellent review of the technique is given in Ref. [34], but briefly it utilizes a low-energy (5–15 keV) pulsed ion beam surface analysis process that can give information on surface composition, the atomic structure of the first few monolayers, trace element detection, lattice defect density, mean vibrational amplitude, and information on thickness and lateral distribution of the growth region.

There has also been a recent push to integrate other emerging characterization techniques into pulsed laser ablation growth systems. This includes introduction of X-ray photoelectron spectroscopy (XPS), scanning probe measurements systems (including atomic force microscopy, piezoresponse force microscopy, magnetic force microscopy, scanning tunneling microscopy, etc.), and many more including synchrotron-based techniques. At the Photon Factory in Tsukuba, Japan researchers have created a

high-resolution synchrotron-radiation angle-resolved photoemission spectrometer (ARPES) combined with a combinatorial laser-MBE growth system to investigate the electronic structure of transition metal oxide thin films [38]. Around this same time, time-resolved X-ray diffraction studies of the PLD process were completed at the UNICAT undulator beamline at the Advanced Photon Source located at Argonne National Laboratory [39]. A similar system has since been constructed at the European Synchrotron Radiation Facility in Grenoble, France [40]. At the Cornell High Energy Synchrotron Source (CHESS), researchers have developed a laser-ablation growth system equipped with *in situ* X-ray reflectivity capabilities that enable careful studies of thin film growth morphology [41].

3.3. Molecular beam epitaxy

Long the standard of comparison for high-precision growth, molecular beam epitaxy (MBE), has a strong history in the growth of complex oxide materials, beginning with work in the late 1980s in pursuit of better high- T_c superconductor phases [42,43]. Within years, again driven by the search for higher and higher T_c in complex oxide superconductors, numerous reports on the growth of superconducting materials using molecular beam epitaxy drove new innovations—including growth in ozone [44]. A number of recent reviews cover the developments and use of MBE in the growth of oxide materials in some detail (see, for instance, Refs. [45–47]). In contrast to PLD, MBE involves the generation of low energy (~ 1 eV) thermal atomic beams for each of the constituent materials desired in the film (both cations such as transition metals and anions such as oxygen). Beams of metal atoms can be created using either radiatively heated sources (i.e., Knudsen or effusion cells) or from electron beam evaporators. Oxygen is typically supplied either as molecular oxygen (O_2), ozone (O_3), or atomic oxygen (O)—due to greatly enhanced oxidizing potentials ozone and atomic oxygen are commonly used today to assure growth of a fully oxidized film. The high purity of commercially available metal and O_2 materials means that MBE techniques can be used to produce extremely pure and defect-free films of complex oxides [47]. Although the quality of materials created by MBE is very good, widespread usage of this technique is limited due to a number of factors including high system, component, and materials prices (a good MBE system can cost well in excess of \$1 million), the requirement of UHV background pressures, and limited materials flexibility compared to other growth processes. Regardless, MBE and MBE-like systems (i.e., systems possessing near UHV background vacuum levels, and load-lock assemblies) stand to make serious impact in next generation materials science. By combining cutting-edge thin film growth techniques together with a wide-range of materials characterization methods, major stumbling blocks in the pursuit of science will be overcome.

3.4. Sputtering

The basic sputtering process has been known and used for many years since the development of “conventional” magnetrons in the early 1970s, was greatly improved with the development of unbalanced magnetrons in the 1980s, and with the incorporation of multi-source “closed-field” systems in the 1990s [48]. The term sputtering, typically refers to the process known as magnetron sputtering where a target (or cathode) plate is bombarded by energetic ions generated in a glow discharge plasma situated in front of the target. This is a classic physical deposition process whereby the bombardment process ejects atoms from the target as a result of a collision cascade that subsequently deposit the film [49]. For a detailed description of recent advances in sputtering technology, the reader is directed to the review by Kelly and Arnell

[48]. For the sake of space, here we will focus on sputter growth of oxide thin films. Over the years, a wide range of oxide materials has been grown via sputter deposition processes. Although pulsed laser ablation techniques are good at maintaining complex stoichiometries in oxides, such processes are not scalable. Sputtering, on the other hand, is a widely used deposition technique for large-scale production. With the advent of multi-source deposition, significant advances in sputtering of complex chemical composition materials have been obtained. Thus, sputtering has been used to make semiconductor, dielectric, insulating, magnetic, and superconducting oxide materials as well as catalysts, protective coatings, and more [50]. Key to the ability to create high quality oxide thin films is intimate knowledge of sputtering yields of the various chemical species in a material (as different elements are sputtered at different rates from targets, starting composition may need to be carefully tuned to give stoichiometric final films), deposition rate is key for controlling the crystal phase, temperatures for microstructure, sputtering atmosphere is important in controlling surface structure, and substrate position or bias voltage is key in determining the types and density of defects in these films. Several sputter deposition techniques have been used in the growth of oxide thin films including on-axis dc magnetron sputtering [51], cylindrical magnetron sputtering [52], ion-beam sputtering [53], and off-axis sputtering [54]. Of particular interest for the growth of oxide thin films is the use of a reactive gas – such as pure O_2 or Ar/ O_2 mixtures – which helps assure oxygen stoichiometry is close to the desired level. For a more detailed discussion of the evolution of sputtering growth (especially in terms of work on ferroelectric materials) see the review by Schwarzkopf and Fornari [55].

3.5. Metal-organic chemical vapor deposition

Metal-organic chemical vapor deposition (MOCVD) is of great importance for large-scale production of oxide thin films [56]. It is routinely used in the electronics industry, has excellent film uniformity over large areas, is capable of conformal coating of arbitrary geometries, can be done at relatively high partial pressures of oxygen, has easy and reproducible control of film stoichiometry, has relatively high deposition rates, and allows for multilayer growth, superlattices, and graded compositions [2,55]. MOCVD works on the principle that one can create a complex organic molecule decorated with the material desired for thin film growth. By passing an inert gas through a bubbler of a liquid precursor, these molecules are transported to the reaction chamber and passed over a substrate at high temperature. The heat helps to break the molecules and deposits the desired material on the surface. One of the biggest challenges for MOCVD growth of oxide materials is identification of the appropriate metal-organic precursors. Precursors for materials with high atomic number typically have limited vapor pressure at room temperature and thus it is essential to heat the bubblers and all the lines in the system to avoid clogging. This requires careful attention so as to avoid hot spots where premature deposition might occur as well as cool spots where condensation of the precursor can occur. In the end, very high quality thin films of oxide materials can be created using this technique. Again, for a more thorough review of the MOCVD process, precursors, and specific details in reference to ferroelectric materials please see Ref. [55].

3.6. Solution-based thin film deposition techniques

There are a variety of solution-based approaches for the creation of complex oxide materials including sol–gel, chelate, and metalorganic decomposition (for good reviews, see Refs. [57,58]). Very briefly, solution deposition usually involves four steps: (1)

synthesis of the precursor solution, (2) deposition by spin-casting or dip-coating, (3) low-temperature heat treatment for drying and/or pyrolysis of organics, and formation of amorphous films (typically 300–400 °C), (4) high temperature heat treatment for densification and crystallization (anywhere from 600 to 1100 °C). Such processes are highly scalable, cheap, and very quick. Great strides have been made in utilizing such techniques to make high quality and highly oriented films for devices.

3.7. Low-temperature aqueous solution depositions

In stark contrast to the previously reported growth techniques, there is a set of aqueous solution-based deposition techniques that enable the creation of films at lower temperatures (25–100 °C). Processes such as chemical bath deposition (CBD), successive ion layer adsorption and reaction (SILAR), liquid phase deposition (LPD), electroless deposition (ED), as well as more modern variants such as photochemical deposition (PCD), deposition assisted by applied fields, ferrite plating, liquid flow deposition, and more can be used to create films of oxide materials at low temperatures. For a detailed review see Ref. [59].

4. Ferroelectricity in oxides

4.1. Definition of ferroelectric materials

Of the 32 crystal classes of materials, 11 possess centers of symmetry and hence possess no polar properties. Of the remaining 21, all but one exhibit electrical polarity when subjected to a stress and are called *piezoelectric*. Of the 20 piezoelectric crystal classes, 10 show a unique polar axis. These crystals are called *polar* because they possess a spontaneous polarization [60]. Typically such a spontaneous polarization cannot be detected by the presence of charge on the surface of the crystal as free charge within the crystal flows to screen or compensate the polarization. One can, however, often detect the presence of a spontaneous polarization by studying the temperature dependent changes in polarization which results in the flow of charge to and from the surfaces. This is known as the *pyroelectric effect* and these 10 polar crystal classes are often referred to as the *pyroelectric classes*. A material is said to be *ferroelectric* when it has two or more orientational states in the absence of an electric field and can be shifted from one to another of these states by an electric field. Any two of the orientational states are identical in crystal structure and differ only in electric polarization at zero applied field [61]. Ferroelectric materials are invariant under time reversal symmetry, but must break spatial inversion symmetry. Ferroelectrics are materials that undergo a phase transition from a high-temperature phase that behaves as an ordinary dielectric to a low temperature phase that has a spontaneous polarization whose direction can be switched by an applied electric field. Any lattice of oppositely signed point charges is inherently unstable and relies on short-range interactions between adjacent electron clouds in the material to stabilize the structure. In ferroelectric materials these interactions result in the formation of a double-well potential that stabilizes a distorted structure over the symmetric structure. In the case of classic perovskite ferroelectrics like PbTiO_3 and BaTiO_3 the Ti 3d – O 2p orbital hybridization is essential for stabilizing the ferroelectric distortion. It has also been found that most perovskite ferroelectrics have B-site ions that are formally d^0 in nature and thus the lowest unoccupied energy levels are the d states and they tend to hybridize with the O 2p orbitals resulting in the double well potential [62]. A material is said to be a *ferroelastic* when it has two or more orientation states in the absence of mechanical stress (and electric field) and can be shifted from one to another of these states by mechanical stress. It is imperative that two of the orientational

states are identical or enantiomorphous in crystal structure and different in mechanical strain tensor at null mechanical stress (and electric field) [61].

4.2. Brief history of ferroelectrics

The modern field of ferroelectrics finds its roots over 150 years ago in studies of pyroelectric effects in materials completed during the mid-1850s [63]. By the late 1800s, the Curies had discovered piezoelectricity [64], but the idea of ferroelectricity remained somewhat elusive until the 1920s when researchers working on Rochelle salt ($\text{NaKC}_4\text{H}_4\text{O}_6 \cdot 4\text{H}_2\text{O}$) discovered that the polarization of this material could be switched by an external electric field and quickly drew comparisons with ferromagnetic materials such as iron [65]. Despite early use of terms such as “Curie point,” the term ferroelectricity did not come into wide spread use until the 1940s [66]. The late 1930s and 1940s, however, ushered in new life for the field of ferroelectrics. Busch and Scherrer in Zurich produced the first series of ferroelectric crystals [67,68]. These crystals, based on the phosphates (such as KH_2PO_4) and arsenates, proved that ferroelectricity was not a fluke discovery. Significant world events quickly forced these materials into service in devices – $(\text{NH}_4)\text{H}_2\text{PO}_4$ became the principal underwater sound transducer and submarine detector in World War II [61]. Around the same time, the first microscopic model of ferroelectricity was developed by Slater and it has withstood the test of time quite well [69].

The modern field of oxide ferroelectrics was jumped started in 1945 when BaTiO_3 ceramics were found to possess dielectric constants between 1000 and 3000 at room temperature [70]. Lines and Glass mark this event with some significance as it represented the first ferroelectric without hydrogen bonds, the first with more than one ferroelectric phase, the first with a non-piezoelectric prototype or paraelectric phase, and the most chemically simple of all ferroelectrics discovered to date [61]. This material represented the first of what has become the largest single class of ferroelectrics. By 1950, ferroelectricity had been discovered in KNbO_3 and KTaO_3 [71], LiNbO_3 and LiTaO_3 [72], and PbTiO_3 [73]. From 1945 to 1960, great strides were made in understanding the fundamental mechanisms for ferroelectricity. Starting from the macroscopic level, Ginzburg [74] and Devonshire [75] developed groundbreaking work that assumed that the same energy function is capable of describing both polar and non-polar phases and this was extended to antiferroelectrics soon after by Kittel [76]. On the microscopic level, Slater developed the fundamental framework for displacive transitions in 1950 and Anderson [77] and Cochran [78] developed the idea of a “rattling” ion within the framework of lattice dynamics, especially soft modes in materials. But the field of oxide ferroelectrics really came into its own in the 1960s and 1970s. With advances in theoretical pictures for the behavior, in synthesis of materials, and new characterization methods, ferroelectrics were thrust to the forefront of solid state physics research. It is this era that has built up much of the fundamental understanding and knowledge that has enabled modern advances in ferroelectric materials. For a wonderful jaunt through the history of ferroelectrics the reader is directed to the excellent book by Lines and Glass [61] and a delightful perspective by Ginzburg [79].

What has been discovered, is that although most ferroelectric materials are not oxides, it is the oxide ferroelectrics that possess the robust properties and great potential for practical applications. Ferroelectric perovskites, such as $\text{Pb}(\text{Zr}_x\text{Ti}_{1-x})\text{O}_3$ (PZT), BaTiO_3 (BTO), and BiFeO_3 (BFO), have attracted a lot of attention with respect to potential application in ultrahigh density memory devices [80]. The magnitude and stability of the switchable ferroelectric polarization are the central figures of merit for such devices. However, in general it is necessary to stabilize local

polarization with a critical polarized volume to break the symmetry. Such an expectation results from the screening of the depolarization field, which becomes much stronger when the film thickness is reduced. This intriguing phenomenon plays a key role in the area of thin film and nanostructured ferroelectrics.

4.3. Thin film ferroelectric phenomena

Using thin film epitaxy it is possible to dramatically engineer and control ferroelectric materials. This includes the observation of a number of intriguing phenomena including size effects, strain enhancement of and driven ferroelectricity, engineered ferroelectricity through superlattice growth, as well as deterministic control of ferroelectric domain structures in materials. In this section, we examine the developments of such work in thin film ferroelectrics.

4.3.1. Size effects in ferroelectrics

As early as 1999, Tybell et al. [81] had demonstrated that ferroelectricity in perovskite thin films could exist down to only 10 unit cells and early calculations suggested the limit could be pushed even further or that there might not be a critical size in some materials [82,83]. In 2003, Junquera and Ghosez [84] used

first principle calculations to simulate the behavior of a realistic ferroelectric structure made of an ultra-thin BaTiO₃ film between two metallic SrRuO₃ electrodes grown epitaxially on a SrTiO₃ substrate (Fig. 8(a)). These calculations took into consideration the influence of the finite screening length of the electrode, the interface chemistry and the strain conditions imposed by the substrate to understand both the atomic relaxation and polarization. They showed that the reason for the disappearance of the ferroelectric instability is the depolarizing electrostatic field resulting from dipoles at the ferroelectric–metal interfaces. They predicted that the BaTiO₃ thin films would lose their ferroelectric properties below a critical thickness of about six unit cells (Fig. 8(b)). This work showed the powerful nature of modern theoretical approaches to simulate and guide experimental investigations. Soon after, in 2004, Fong et al. [85] used synchrotron-based X-ray techniques to study PbTiO₃ films as a function of temperature and film thickness. With the careful control of growth, they were able to verify the film thickness from one to four unit cells directly on insulating SrTiO₃ substrates. It was observed that ferroelectric domains of alternating polarity were formed to reduce the electrostatic energy from the depolarization field (Fig. 8(c)). Additionally, it was reported that at room temperature the ferroelectric phase was stable down to thick-

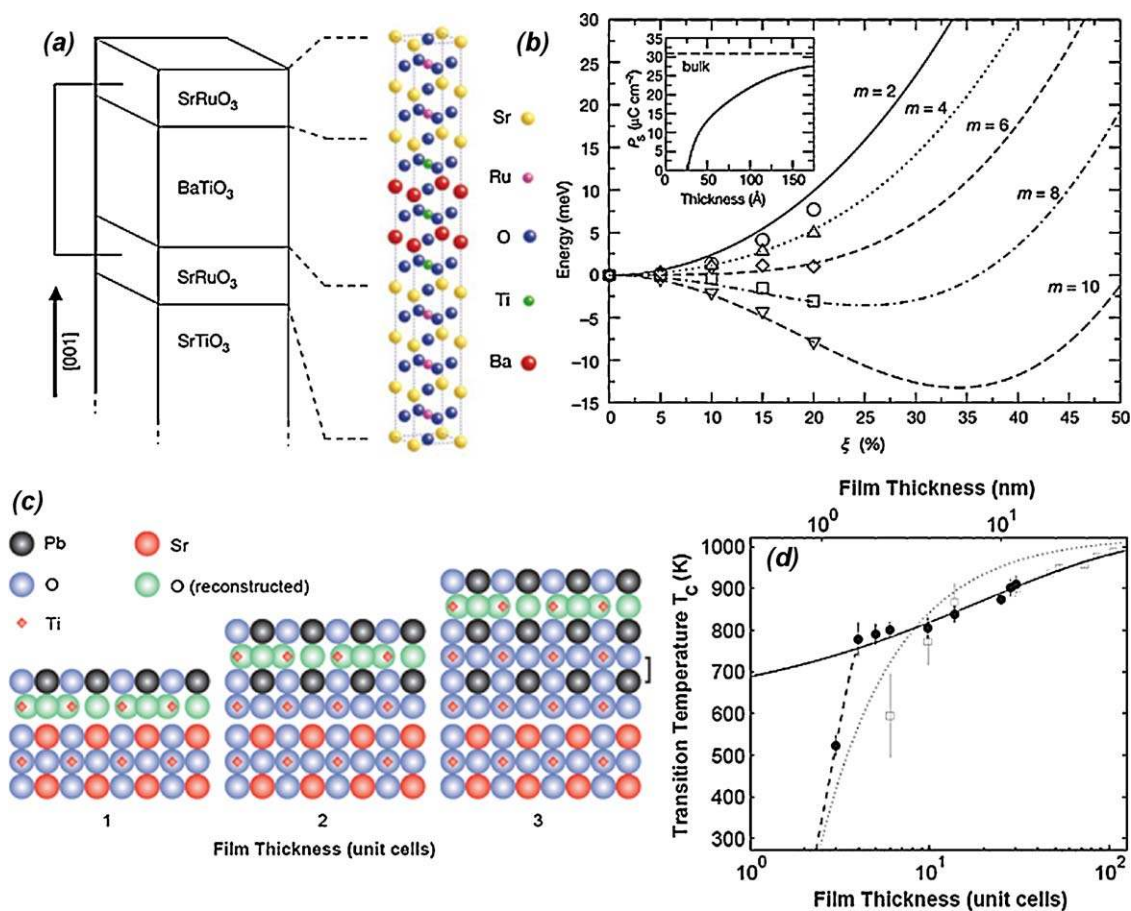


Fig. 8. Size effects in ferroelectrics. (a) Schematic view of the system considered in Ref. [84] where they studied fully epitaxial SRO/BTO/SRO/STO (0 0 1) heterostructures with short-circuited electrode layers. (b) Atomic representation of the related supercell that was simulated. (c) Evolution of the energy as a function of the soft-mode distortion ξ . First principles results are shown in the symbols and electrostatic model results are shown as lines for different thicknesses (m is the number of unit cells) of the ferroelectric thin film [$m = 2$ (circles, full line), $m = 4$ (upward-pointing triangles, dotted), $m = 6$ (diamonds, short-dashed), $m = 8$ (squares, dot-dashed), and $m = 10$ (downward-pointing triangles, long-dashed)]. Reveals a critical thickness of ~ 6 unit cells (adapted from Ref. [84]). (d) Schematic of PTO films 1–3 unit cells thick with the top unit cell reconstructed. The 3-unit cell film is the thinnest film having PbO and TiO₂ layers with the nearest-neighbor environment of bulk PTO (indicated by bracket). (e) Ferroelectric transition temperature, T_c , versus film thickness, determined from satellite intensities (circles). Also shown (squares) is T_c determined from the lattice parameter, which becomes inaccurate at low thicknesses. Dotted curve is Landau theory fit to all data; solid curve and dashed guide to the eye are described in the text. This work reveals a critical thickness of only 3 unit cells. (Adapted from Ref. [85]).

nesses of just 3 unit cells (Fig. 8(d)), which implies that, for all practical matters, there is no size limit for the creation of a ferroelectric material.

Over the coming years, however, the suppression of ferroelectricity in ultra-thin films with electrodes was widely observed [86]. The argument comes from the idea that as films are reduced in thickness, finite screening occurring at both electrodes can begin to overlap and can adversely affect ferroelectric order in a material. Such interface related problems have been addressed in some studies, but direct observation and understanding of this effect was not obtained until 2007 when Jia et al. [87] used high resolution transmission electron microscopy to probe this problem by looking at the detailed atomic structure at ferroelectric–electrode ($\text{PbZr}_{0.2}\text{Ti}_{0.8}\text{O}_3$ – SrRuO_3) interface (Fig. 9(a) and (b)). A systematic reduction of the atomic displacements was observed, suggesting that interface-induced suppression of the ferroelectric polarization plays a key role in the size limit of ferroelectric films (Fig. 9(c)). This study provided direct evidence for the fact that the electrical boundary conditions play a dominant role in the stabilization of the ferroelectric polarization for ultra-thin films. Based on these studies, it is clear that imperfect screening of the depolarization field is still a key factor in determining the ferroelectric size limit of a material and, in turn, two possibilities can occur in ultra-thin films: (1) that the material will form a self-compensated periodic domain structure to reduce the depolarization field or (2) that the material will decrease the magnitude of polarization (by locally changing atomic displacements), which lessens the depolarization field. In conclusion, what can be taken away from these studies is that the interface between the ferroelectric and the metal contact plays a critical role in determining the ferroelectric properties. It is this interface, in fact, that is responsible for the critical thickness in ferroelectrics (i.e., the idea of a so-called “dead layer”). So where does this leave us for development of ultra-thin ferroelectric capacitors for memory applications? In an attempt to shed light on these challenges, Stengel et al. [88] have used density functional theory to calculate the properties of ultra-thin BaTiO_3 and PbTiO_3 layers in contact with electrodes. They have shown that the local chemical environment, through the force constant of the metal oxide bonds, has a strong influence on interfacial effects. This includes a novel mechanism of interfacial ferroelectricity that produces and overall enhancement of the ferroelectric instability of the film and, therefore, might lead to new possibilities in ferroelectric devices based on ultra-thin films.

Other recent exciting studies that have pushed the boundaries of size effects in ferroelectrics include the work of Lee et al. [89] who utilized anodized aluminum oxide (AAO) nanotemplates [90]

as a shadow mask to create arrays of $\text{Pb}(\text{Zr}_{0.2}\text{Ti}_{0.8})\text{O}_3$ individually addressable metal/ferroelectric/metal nanocapacitors with a density of 176 Gb/in^2 . The process, which consists of only a few steps, requires the creation of the AAO template, adhesion of the template to the growth surface, vapor phase growth of the nano-features, and removal of the template. Although the AAO-based process is very simple, at very small pore diameters it is possible to choke-off the pores with vapor phase growth techniques. Although this was just the first demonstration of such a process to produce nano-scale features of ferroelectric materials, it offers a wonderfully simple way to reduce the sizes of ferroelectric materials not only as thin films, but as nano-features.

4.3.2. Strain effects in ferroelectricity

Another great advantage given to researchers and engineers utilizing epitaxial growth is that one can manipulate the strain state in thin films, through selection of the appropriate substrate, to engineer the physical properties of thin films. This includes both strain enhanced ferroelectric order in materials, controlling Curie temperatures in ferroelectric oxides, and inducing room temperature ferroelectricity in non-ferroelectric materials. For a detailed treatment of strain tuning in ferroelectric thin films, see the work by Schlom et al. [91]. Let us begin this section by investigating how strain can be used to enhance ferroelectricity in thin films. Much of the recent success in strain engineering of oxide ferroelectrics has arisen from the development of new oxide substrate materials. Techniques and materials developed during the intense study of high-temperature superconductors in the 1980s and 1990s have led to a wide variety of oxide substrates (Fig. 10). For ferroelectric perovskite (such as those listed in red in Fig. 10), chemically and structurally compatible perovskite substrates are needed (shown in blue, purple, and green in Fig. 10) [91]. These substrates include YAlO_3 , LaSrAlO_4 , LaAlO_3 , LaSrGaO_4 , NdGaO_3 , $(\text{LaAlO}_3)_{0.29}-(\text{Sr}_{0.5}\text{Al}_{0.5}\text{TaO}_3)_{0.71}$ (LSAT), LaGaO_3 , SrTiO_3 , DyScO_3 , GdScO_3 , SmScO_3 , KTaO_3 , and NdScO_3 that give quality starting materials with lattice parameters from as low as ~ 3.70 to ~ 4.0 Å.

In turn, researchers are given a broad capacity to tune and engineer the properties of ferroelectrics with epitaxial thin film strain. One example from Haeni et al. [92] used epitaxial strain to shift the ferroelectric transition temperature of SrTiO_3 by *hundreds of degrees* to make a new room temperature ferroelectric phase (Fig. 11(a)). This report marked the largest-ever reported strain-induced enhancement of T_C . Soon after, Choi et al. [93] reported the use of biaxial compressive strain to markedly enhance the ferroelectric properties of BaTiO_3 . By growing BaTiO_3 films on rare-earth scandate substrates, the researchers demonstrated that

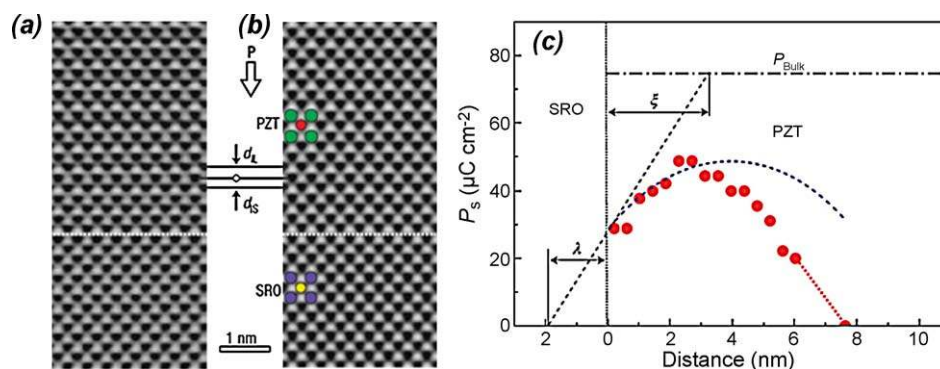


Fig. 9. Interface effects on ferroelectrics. (a) Experimental and (b) calculated images of the PZT/SRO interface. The polarization direction of the PZT film is shown by an arrow, pointing from the film interior to the interface of PZT/SRO. White dotted lines mark the SRO/PZT interface. The cation positions are indicated: Pb (green), Zr/Ti (red), Sr (violet), Ru (yellow). (c) The spontaneous polarization, P_s , calculated on the basis of the atomic displacements determined from the images. The blue dashed curve is calculated for a system of an 8 nm ferroelectric layer sandwiched between metallic electrodes based on the Kretschmer–Binder model. (Adapted from Ref. [87].) (For interpretation of the references to colour in this figure legend, the reader is referred to the web version of the article.)

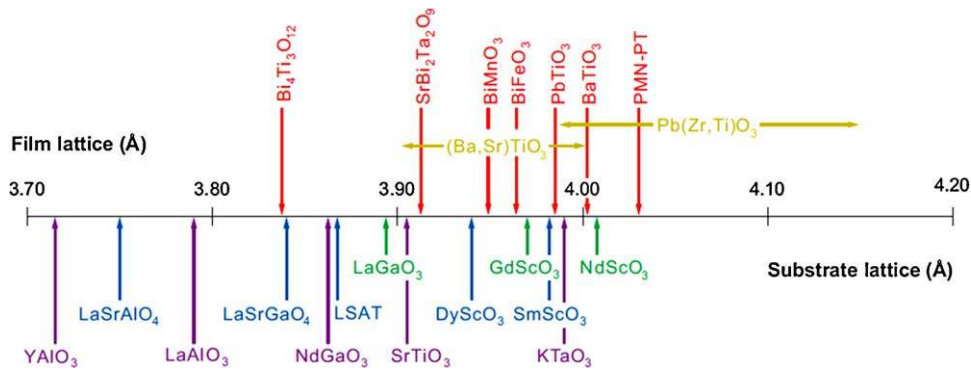


Fig. 10. Strain engineering. A number line showing the pseudotetragonal or pseudocubic a -axis lattice constants (in Å) of some ferroelectric perovskites of current interest (above the number line) and of some of the perovskite and perovskite-related substrates that are available commercially (below the number line). (Adapted from Ref. [91].)

the T_C could be enhanced by nearly 500 °C and that the remnant polarization could be increased by almost 250% compared to bulk BaTiO_3 single crystals (Fig. 11(b) and (c)). This, in turn, made the properties comparable to those of unstrained $\text{Pb}(\text{Zr}_x\text{Ti}_{1-x})\text{O}_3$, but in a material not based on toxic materials such as Pb. Such behavior, however, does not occur for all ferroelectrics. It depends on the mechanism that drives ferroelectric-order in the material. For some ferroelectric materials, such as BaTiO_3 and PbTiO_3 , the d^0 configuration of the Ti cation plays a crucial role in the formation of a ferroelectric instability; in turn, ferroelectric properties in these materials are strongly influenced by strain state. For the materials, such as BiFeO_3 , where the ferroelectricity is driven primarily by the presence of the Bi 6s lone pair electrons, the ferroelectric state is relatively insensitive to strain [94].

Yet another exciting manifestation of the power of thin film strain in effecting the nature of ferroelectric materials was recently reported in the multiferroic material BiFeO_3 . Through the growth of thin films of BiFeO_3 on a wide range of substrates (including SrTiO_3 , LaAlO_3 , and YAlO_3), Zeches et al. [95] were able to demonstrate the formation of a strain-driven morphotropic (or isosymmetric) phase boundary in the BiFeO_3 . A morphotropic phase boundary [96] is a boundary between phases with different structural symmetry (typically tetragonal and rhombohedral) present in complex materials (for instance near 52% PbZrO_3 and 48% PbTiO_3 in $\text{Pb}(\text{Zr}_x\text{Ti}_{1-x})\text{O}_3$) [97]. It is the presence of such boundaries in materials like PZT and PMN-PT that are responsible for the huge piezoelectric strains observed in these materials and behind the use of these materials in modern actuator and other

device applications. In the bulk, BiFeO_3 is a rhombohedrally distorted perovskite, however, previous reports, both theoretical [98,99] and experimental [100,101], suggested that a tetragonal version of this film might exist. Growth of BiFeO_3 on substrates with lattice mismatches in excess of ~4.5% resulted in the growth of the tetragonal phase of BiFeO_3 . Upon increasing the film thickness, however, the films exhibited mixtures of the tetragonal-like and rhombohedral-like versions of BiFeO_3 (Fig. 12(a)). Close inspection of this morphotropic-like phase boundary revealed that there was nearly a 13% change in the out-of-plane lattice parameter across this boundary in just over 10 unit cells without the formation of any misfit dislocations (Fig. 12(b)). Furthermore, consistent with previous observations of Pb-based systems like PZT and PMN-PT, films possessing these morphotropic-like phase boundaries exhibited strong piezoelectric responses – on the order of 1–2% vertical surface strains (Fig. 12(c)). This represents a significant advancement in the field of piezoelectrics in that it demonstrates a new pathway, other than chemical alloying, with which one can induce a morphotropic phase boundary and represents the first Pb-free example of this behavior.

These experimental advances have been aided significantly by advances in theory and simulations including the development of first principles approaches, effective Hamiltonian methods, molecular dynamic simulations, phenomenological models based on Ginzburg–Landau theory, and phase-field and finite-element models. The work of Zeches et al. [95] represents a recent example of the close interaction of experimental and theoretical approaches to understand emergent behavior in these complex materials. For

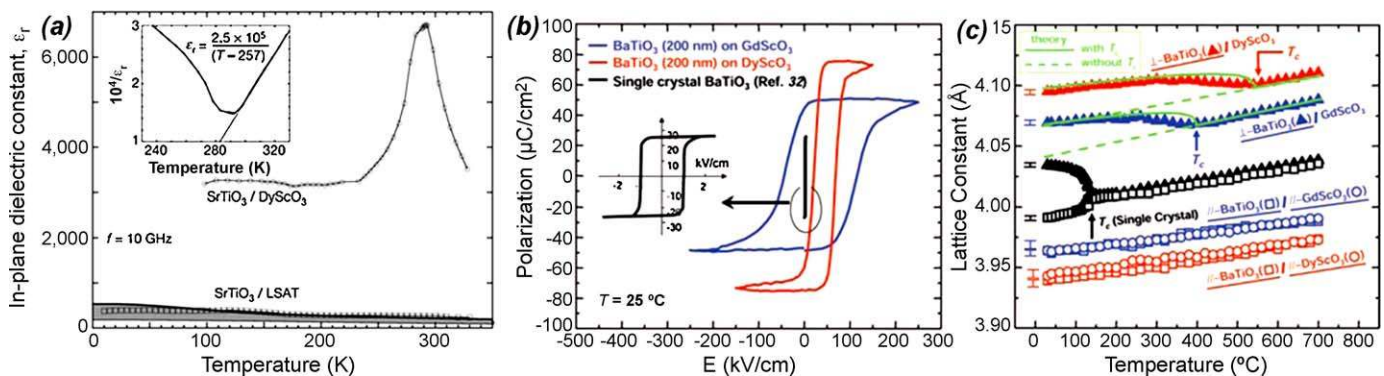


Fig. 11. Strain engineering of ferroelectrics. (a) In-plane dielectric constant in and strained (tensile, STO/DSO) and (compressive, STO/LSAT) epitaxial STO films as a function of temperature and film thickness at a measurement frequency of 10 GHz. This data shows that the phase transition for STO can be enhanced by hundreds of degrees in temperature. (Adapted from Ref. [92].) (b) Polarization–electric field hysteresis loops for strained BTO thin film capacitors with SRO top and bottom electrodes grown on DSO and GSO substrates. The inset shows the hysteresis loop of an unstrained bulk BTO single crystal for comparison. (c) Temperature dependence of the lattice parameters of these same strained SRO/BTO/SRO capacitor structures. The in-plane (\parallel) and out-of-plane (\perp) lattice constants of the BTO thin films, SRO bottom electrode, and underlying substrates are shown. The lattice parameters of the SRO film on DSO could not be resolved because SRO and DSO are isostructural with very similar lattice parameters. The change in slope at high temperature indicates that the phase transition. (Adapted from Ref. [93].)

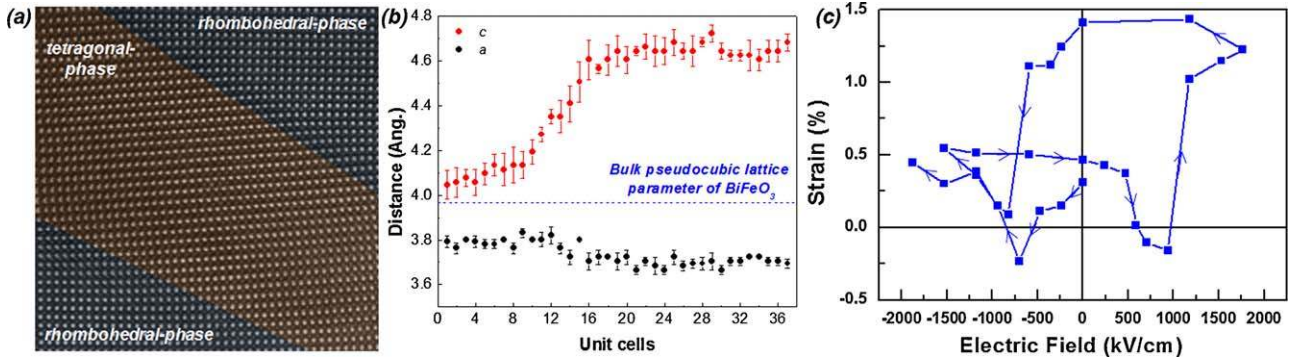


Fig. 12. Strain induced morphotropic phase boundary. (a) A high-resolution transmission electron microscopy image of the strain-driven morphotropic phase boundary in BFO. Areas of both the rhombohedral and tetragonal phase are shown. (b) Detailed analysis of the image in (a) reveals nearly at 13% change in the out-of-plane lattice parameter in just over 10 unit cells across the boundary. (c) Surface strain as a function of applied electric field reveals large piezoelectric responses in films possessing mixed rhombohedral–tetragonal phases. This represents an exciting step forward in the production of a high-performance lead-free piezoelectric. (Adapted from Ref. [95].)

instance, first principles calculations can give insight into the evolution of atomic arrangements and, therefore, polarization, which allows investigators to arbitrarily set boundary conditions (i.e., structure strain) and investigate the resulting change in structure and properties. Nowadays such first principles density functional theory methods can accommodate up to 100 atoms (or about 20 unit cells for perovskites) [91]. This can be extended to longer length- and time-scales using interatomic potentials and effective Hamiltonians constructed from first-principles input that allow researchers to tackle supercells of many thousands of atoms [102–105]. Progression to phenomenological macroscopic approaches such as Landau–Devonshire theory can give insight into non-equilibrium properties and parameters where experimental information is not available [106]. Of special interest to this section is the application of the phase-field method based on time-dependent Ginzburg–Landau equations, which makes it possible to predict domain structures and properties of ferroelectric thin films as a function of substrate, temperature, electrical boundary conditions, thickness, and inhomogeneous defect distribution [91]. The powerful nature of this modeling technique is demonstrated for the case of BaTiO₃ where a phase diagram as a function

of strain state and temperature (Fig. 13(a)) and equilibrium ferroelectric domain structures at different temperatures and strain values (Fig. 13(b)) are shown [107]. For a more detailed description of the phase-field model and its capabilities see the review by Chen [108].

4.3.3. Artificially engineered ferroelectrics

Recently, epitaxial growth with unit cell control has encouraged theoretical investigations that have led to the predictions of new artificial ferroelectric materials including enhancement of ferroelectric properties in two- [109,110] and three-component [111–113] heterostructures. Using such unit cell growth control, researchers have, in turn, built up superlattice structures with exciting new properties. One fantastic example of this work is the report by Lee et al. [114] in which so-called “tri-color” superlattice structures consisting of BaTiO₃, SrTiO₃, and CaTiO₃ were fabricated on conducting, atomically smooth SrRuO₃ layers. By preserving full strain in the BaTiO₃ layer and combining heterointerfacial coupling, the researchers found a 50% enhancement in ferroelectric polarization of the tri-color superlattice in comparison to similarly grown pure BaTiO₃. The most intriguing part in this study is that

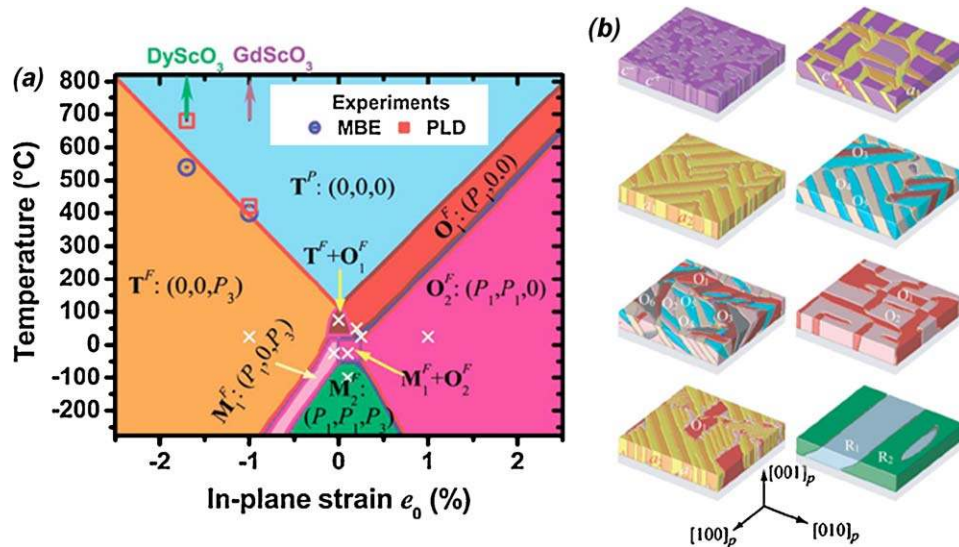


Fig. 13. Phase field models of ferroelectrics. (a) Phase diagram of the evolution of the structure of BTO films as a function of temperature and substrate in-plane strain. The scattered circles and squares denote the ferroelectric transition temperatures measured from experiments on BTO films commensurately grown on DSO and GSO. The X's indicates the locations of the domain structures shown in (b). (b) various domain morphologies in BTO films as a function of temperature and substrate strain. (Adapted from Ref. [107].)

even superlattices containing only single-unit-cell layers of BaTiO₃ in a paraelectric matrix remained ferroelectric. This suggests that specific interfacial structure and local asymmetries play an important role in the polarization enhancement. Additional studies of such artificially designed heterostructures have reported enhanced ferroelectric properties in two-component heterostructures [115–121], three-component heterostructures [122], and relaxor-based, two-component heterostructures [123].

4.3.4. Controlling ferroelectric domain structures

The formation of domain structures is a consequence of minimizing the elastic and electrostatic energy of a ferroelectric system. It is especially important to study such domain formation in ferroelectrics since it has a profound influence on the physical properties of these materials. Controlling the domain structures to obtain periodic domain patterns, which can be used for nanolithography and nonlinear optics, has garnered much attention in recent years [124,125]. To illustrate the advances in the use of thin film epitaxy to control ferroelectric domain structures in materials, we focus in this section on two important ferroelectric materials, tetragonal PZT and rhombohedral BFO that have been studied extensively. Let us begin by investigating, briefly, the work done on the prototypical tetragonal ferroelectric PZT. Polydomain formation in the lead zirconate titanate family of ferroelectric perovskites has been a subject of extensive research for decades [126]. Monodomain PZT thin films have been grown on STO substrates; however, when the thickness is increased, multi-domain structures have typically been observed. The formation of domain structures in tetragonal ferroelectric films is a mechanism of strain and electrostatic energy relaxation. Tetragonal PZT thin films show the *c/a/c/a* polydomain pattern that consists of alternating *c*-domains with the tetragonal axis perpendicular to the film–substrate interface (typically for (001)-oriented substrates), and *a* domains (90° domains) with the *c* axis of the tetragonal film along either 100- or 010-directions of the substrate. The head–tail alignment of polarization vectors at the interface of *a* and *c* domains occurs so as to prevent charge building up at the boundary [127]. Theoretical models have predicted that one could control the ferroelectric domain structure of PZT through careful control of thin film heteroepitaxial growth constraints [128]. Additionally, periodic domain patterns in PZT can be controlled through the use of vicinal (001)-oriented STO substrates [129]. In this case, there is a preferential nucleation of the *a*-domains along the step edges of the underlying substrate. Using piezoresponse force microscopy (PFM), it has been found that all *a* domains have their polarization aligned along the same direction. This result is in contrast to non-vicinal substrates where fourfold symmetry of *a*-domains is observed. A model based on minimization of elastic energy to describe the effect of localized stresses at step edges on the formation of *a*-domains in the ferroelectric layer has also been developed.

To further illustrate the advances in the use of thin film epitaxy to control ferroelectric domain structures in materials, we now proceed to focus on the widely studied ferroelectric, multiferroic BFO. In recent years, much attention has been given to a new class of ferroelectric materials that are lead-free, have strong intrinsic polarizations, high ordering temperatures, and many other properties that make them of interest for a wide variety of applications. The material BFO is a fine example of this new generation of ferroelectric material. Before addressing how one can control domain structures in rhombohedral BFO, it is essential that we first understand what kinds of domain patterns can be obtained in rhombohedral ferroelectrics. Several theoretical studies have been published that provide equilibrium domain patterns of rhombohedral ferroelectrics such as BFO. On the (001)_c perovskite surface, there are eight possible ferroelectric polarization direc-

tions corresponding to four structural variants of the rhombohedral ferroelectric. Early work published by Streiffer et al. [130] found that domain patterns can develop with either {100}_c or {101}_c boundaries for (001)_c oriented rhombohedral films. In both cases, the individual domains in the patterns are energetically degenerate and thus equal width stripe patterns are theoretically predicted. Zhang et al. [131] have gone on to use phase field simulations to understand how the strain state can affect the polarization variants and to predict the domain structures in epitaxial BFO thin films with different orientations. In these models, long range elastic and electrostatic interactions were taken into account as were the effects of various types of substrate constraints on the domain patterns. These findings suggest that the domain structure of BFO thin films can be controlled by selecting proper film orientations and strain constraints. Moreover, these phenomenological analyses reveal that both the depolarization energy and the elastic energy play a key role in determining the equilibrium domain structures. For instance, in the case of an asymmetrical electrostatic boundary condition (i.e., the presence of a bottom electrode) the dominant domain scaling mechanism changes from electrostatic-driven to elastic-driven. Therefore, the domain size scaling law in epitaxial BFO films is predicted to show a different behavior from the conventional elastic domains: the 101-type or so-called 71° domains are expected to be much wider than the 100-type so-called 109° domains despite the fact that these {100} boundaries possess a larger domain wall energy.

Experimental demonstration of similar ideas has progressed in recent years. In 2006, Chu et al. [132] demonstrated an approach to create one-dimensional nanoscale arrays of domain walls in epitaxial BFO films. Focusing on heterostructures like those shown in Fig. 14(a), the authors took advantage of the close lattice matching between BFO, SRO, and DyScO₃ (DSO) (110) and the anisotropic in-plane lattice parameters of DSO (*a*₁ = 3.951 and *a*₂ = 3.946 Å) to pin the structure of the SRO layer and, in turn, the ferroelectric domain structure of BFO. This anisotropic in-plane strain condition leads to the exclusion of two of the possible structural variants. Phase-field modeling of the ferroelectric domain structure in such heterostructures (Fig. 14(b)) predicted stripe-like ferroelectric domain structures which were confirmed in the final BFO films (Fig. 14(c) and (d)). The growth mechanism of the underlying SRO layer was found to be important in determining the final ferroelectric domain structure of the BFO films. SRO layers grown via step-bunching and step-flow growth mechanisms resulted in ferroelectric domain structures with 4-polarization variants (Fig. 14(c)) and 2-polarization variants (Fig. 14(d)), respectively. These films have been shown to exhibit excellent ferroelectric properties with room temperature *2P_r* = 120–130 μC cm^{−2} and strong intrinsic ferroelectric properties [133].

In 2007, Chu et al. [134] further demonstrated the ability to create different domain structures in epitaxial BFO films on (001), (110), and (111) SrTiO₃ substrates that were consistent with phase field models. Such a result made a connection between the theoretical predictions and experiments and offered one pathway for researchers to simplify the complex domain structure of the BFO films. What was discovered was that one must induce a break in the symmetry of the various ferroelectric variants. One avenue to accomplish this is through the use of vicinal SrTiO₃ substrates (Fig. 15(a)). Beginning with a (001) oriented substrate, one can progressively tilt the crystal along different directions to end up with different orientations. For instance, by tilting 45° along the 010-direction one can obtain a (110) oriented substrate, while tilting by another 45° along the 110-direction gives rise to a (111) oriented substrate. Through the use of carefully controlled, vicinally cut (001) SrTiO₃ substrates (Fig. 15(b)–(e)) researchers were able to demonstrate fine control of the ferroelectric domain

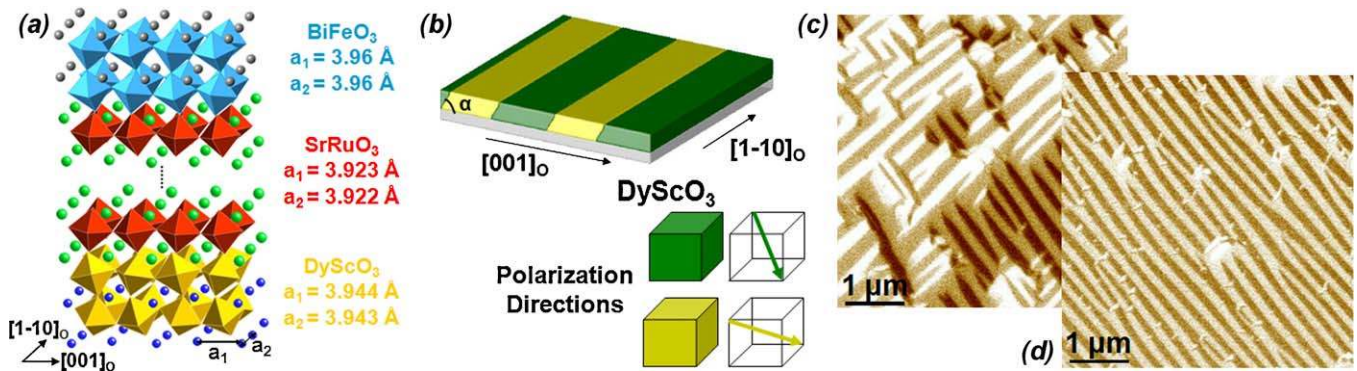


Fig. 14. Controlling ferroelectric domain structures. (a) Schematic of the BFO/SRO/DSO heterostructures and (b) domain structure of the BFO film as predicted by phase-field simulations. In-plane PFM images of the ferroelectric domain structure in BFO films showing (c) 4-polarization variants (left) and 2-polarization variants (right). (Adapted from Ref. [132].)

structure in BiFeO₃. This includes evolving the domain structure from possessing 4-variants (Fig. 15(f)), 2-variants (Fig. 15(g) and (h)), and 1-variant (Fig. 15(i)). Added control comes from the use of asymmetric boundary conditions including the use of SRO bottom electrodes, that drives the out-of-plane component of polarization to be preferentially downward pointing. These films represent an important step forward in that they provide a set of model thin films that can be used to further explore the magnetoelectric properties of this system as well as its interactions with other layers. Additionally, multiferroic materials with electrically controllable periodic domain structures such as these, could be of great interest for applications in photonic devices.

Finally, in 2009, Chu et al. [135] through the careful control of electrostatic boundary conditions, such as the thickness of the underlying SRO bottom electrode, were able to demonstrate the creation of ordered arrays of the prototypical domain structures as predicted by Streiffer et al. nearly 10 years earlier [130] (Fig. 16(a) and (b)). Fig. 16(a) represents a series of 71° domain walls located on 1 0 1-type planes and Fig. 16(b) represents a series of 109° domain walls located on 1 0 0-type planes. When the bottom electrode layer is thick (typically > 10 nm and thus a good metal) the presence of an asymmetric boundary condition results in the formation of a film that is fully out-of-plane polarized downward towards the SRO layer and elastic energy is the dominate energy in the system. On the other hand, when the SRO layer is very thin, electrostatic energy becomes the dominant energy and drives the film to have domains alternatively pointing up and down. The

surface morphology of the resulting films with 71° (Fig. 16(c)) and 109° (Fig. 16(d)) is consistent with the theoretically predicted structure. The corresponding out-of-plane (Fig. 16(e) and (f)) and in-plane (Fig. 16(g) and (h)) PFM images confirm the presence of the periodic, equilibrium domain structures.

In addition to epitaxial growth control of ferroelectric domain structures, recent advances in scanning probe-based manipulation of ferroelectric domain structures have opened up the next level of control. Zavaliche et al. [136] have developed a standard procedure to use PFM to characterize and understand the domain structure of such ferroelectric materials. These studies have identified locally three possible polarization switching mechanisms namely 71°, 109°, and 180° rotations of the polarization direction. 180° polarization reversals appear to be the most favorable switching mechanism in epitaxial films under an applied bias along [0 0 1]. A combination of phase field modeling and scanning force microscopy of carefully controlled, epitaxial [1 1 0] BFO films with a simplified domain structure revealed that the polarization state can be switched by all three primary switching events by selecting the direction and magnitude of the applied voltage [137]. Moreover, the instability of certain ferroelastic switching processes and domains can be dramatically altered through a judicious selection of neighboring domain walls. The symmetry breaking of the rotationally invariant tip field by tip motion enables deterministic control of non-180° switching in rhombohedral ferroelectrics. The authors also demonstrated the controlled creation of a ferrotorroidal order parameter. The ability to control

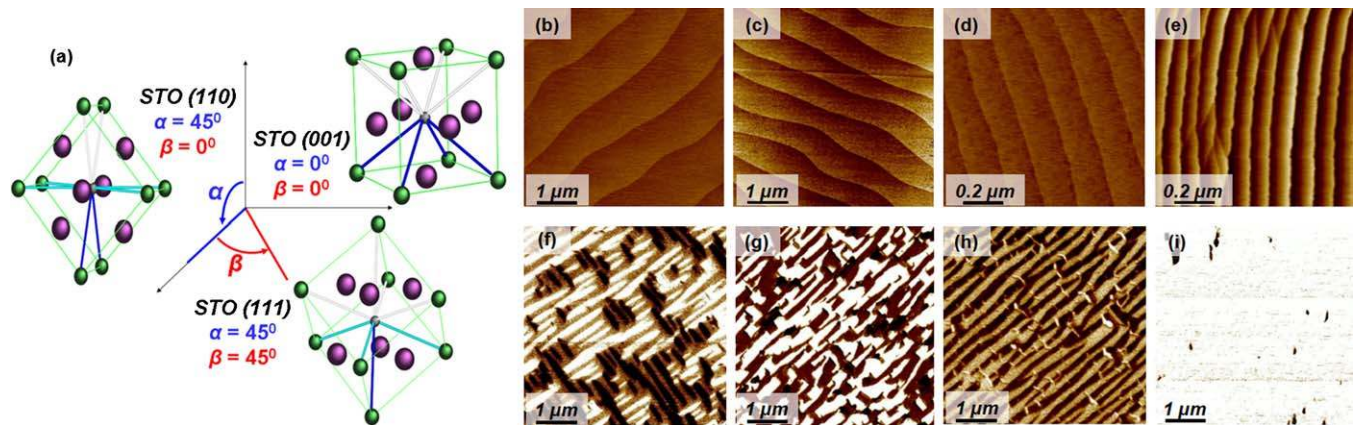


Fig. 15. Vicinal control of ferroelectric domain structures. (a) Schematic illustration of vicinal STO substrates and corresponding predicted polarization variants on STO (0 0 1), (1 1 0), and (1 1 1) substrates. AFM images of typical vicinal STO substrates with different miscut angles, (b) a = 0° and b = 0°, (c) a = 0.5° and b = 0°, (d) a = 1° and b = 0°, and (e) a = 3° and b = 0°, as well as the corresponding IP-PFM images of the resulting BFO films, (f) a = 0° and b = 0°, (g) a = 0.5° and b = 0°, (h) a = 1° and b = 0°, and (i) a = 3° and b = 45°. (Adapted from Ref. [134].)

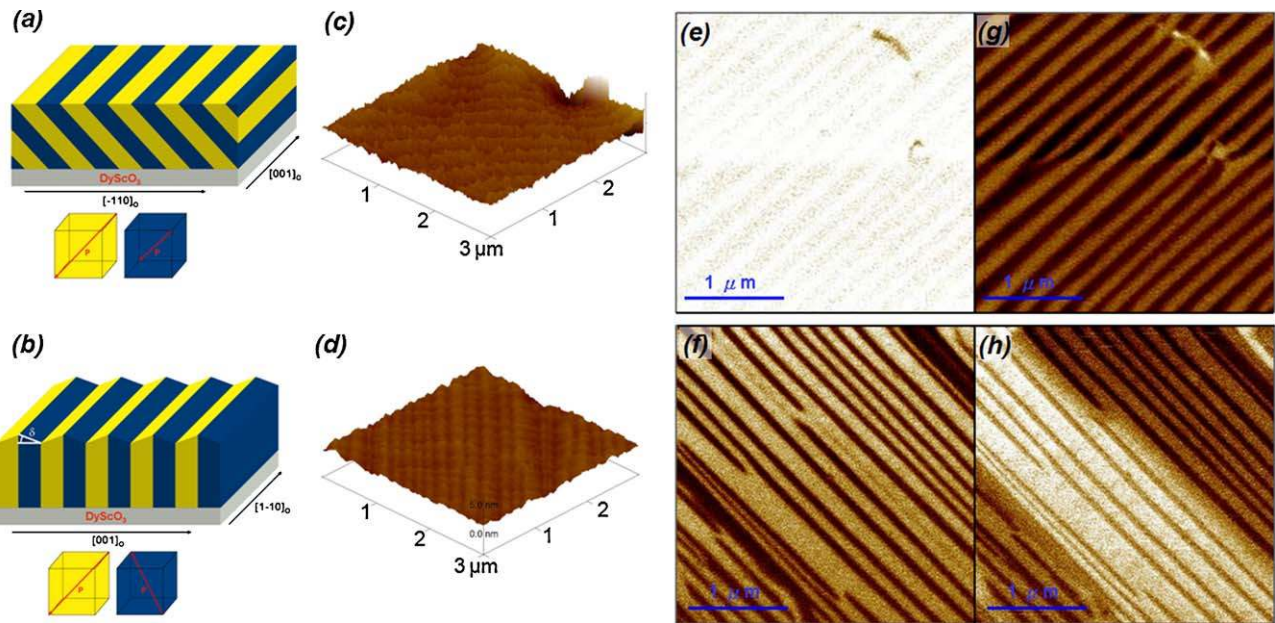


Fig. 16. Ordered arrays of ferroelectric domains and domain walls. (a) and (b) Schematics of equilibrium structure of an ordered array of 71° and 109° domain walls, respectively. (c) and (d) Surface topography as measured by AFM of 71° and 109° domain walls samples, respectively. Out-of-plane (e) and (f) as well as in-plane (g) and (h) PFM images for samples possessing ordered arrays of 71° and 109° domain walls. (Adapted from Ref. [135].)

local elastic, magnetic and torroidal order parameters with an electric field will make it possible to probe local strain and magnetic ordering, and engineer various magnetoelectric, domain-wall-based and strain-coupled devices.

For eventual device applications, the use of a coplanar epitaxial electrode geometry has been proposed to aid in controlling multiferroic switching in BFO [138]. PFM has been used to detect and manipulate the striped ferroelectric domain structure of a BFO thin film grown on DSO (1 1 0) substrates. Time-resolved imaging revealed ferroelastic switching of domains in a needle-like region that grew from one electrode toward the other. Purely ferroelectric switching was suppressed by the geometry of the electrodes. Such results demonstrate the capability to control the ferroelectric order parameter and domain structures in a device architecture.

4.4. Ferroelectric devices and integration

Beginning in the late 1990s extensive efforts were directed at trying to find an alternative oxide material to SiO₂ in semiconductor field-effect transistors – the push for the development of the so-called high-*k* gate oxides for next generation CMOS technology had begun. In 1996, Hubbard and Schlom [139], used tabulated thermodynamic data to complete a comprehensive study of the thermodynamic stability of binary oxides in contact with Si at 1000 K. This work has been extremely influential in the development and integration of oxides on Si and eventually led to the integration of HfO₂ on Intel's Penryn line of processors in late 2007. However, in the late 1990s, a wide range of oxides such as Ta₂O₅ [140], TiO₂ [141], Al₂O₃ [142], HfSi_xO_y [143], Gd₂O₃ [144], and perovskite materials such as SrTiO₃ [145] and others possessing high dielectric constants, were being actively considered to use in next generation MOSFET devices.

This early work represents the foundation of the maturing field of epitaxial growth of complex oxide materials on semiconductor substrates. Essential to this work was the development of ways to grow high quality layers of materials such as SrTiO₃ on Si. SrTiO₃ is expected to growth epitaxially on Si (1 0 0) with a lattice mismatch of 1.7% and the unit cell of the SrTiO₃ rotated 45° in-plane. Early work resulted in rough surfaces as the result of island-like growth

[146,147]. A number of approaches were eventually developed to overcome this limitation. These include processes based on metallic Sr deoxidation of the Si surface followed by deposition of thick SrO buffer layers [148,149], complete thermal desorption of the native oxide followed by metallic Sr reaction with the Si surface at high temperatures to form a stable strontium silicide that acts as a buffer layer [150], and finally the development of direct MBE growth techniques at Motorola Labs and Oak Ridge National Laboratory that produced high quality SrTiO₃ films on Si (1 0 0) [145]. It is this last technique based on MBE growth that has enabled many of the recent studies of complex oxides on Si substrates. Similar techniques have also been used to create high quality layers of LaAlO₃ [151] and other perovskites. Taking this concept further, recent studies suggest that by using the strain effects, ultra-thin SrTiO₃ films on Si can be engineered to exhibit ferroelectric properties at room temperature, which could lead to the creation of a metal–ferroelectric–semiconductor field-effect transistor with nonvolatile characteristics [152]. More recently, similar techniques have also been used to integrated complex oxide materials (such as ferroelectric and multiferroic materials) on other semiconducting substrates such as GaN [153,154].

Around the same time, considerable effort was underway to utilize ferroelectric oxides – in which information can be stored in the electrical polarization state – as a new generation of data storage device. Early work focused on making thin films (i.e., <1 μm) of ferroelectrics in hopes of bringing down coercive voltages to levels that were compatible with CMOS technologies (typically ≤5 V). The development of new growth techniques has greatly enabled the development of these materials and today high-density arrays of non-volatile ferroelectric memories are commercially available. The integration of ferroelectric oxides (such as PZT and SrBi₂Ta₂O₉ (SBT)) on Si for nonvolatile memory applications (FRAM's) preceded the studies of oxide heteroepitaxy (Fig. 17); however, the key materials innovations in the field of ferroelectric capacitors directly benefited from the concepts of heteroepitaxy. It is fair to state that the critical roadblocks to the implementation of a commercial FRAM technology were overcome by the fundamental studies that involved the use of conducting perovskite electrodes to contact the ferroelectric layers. This

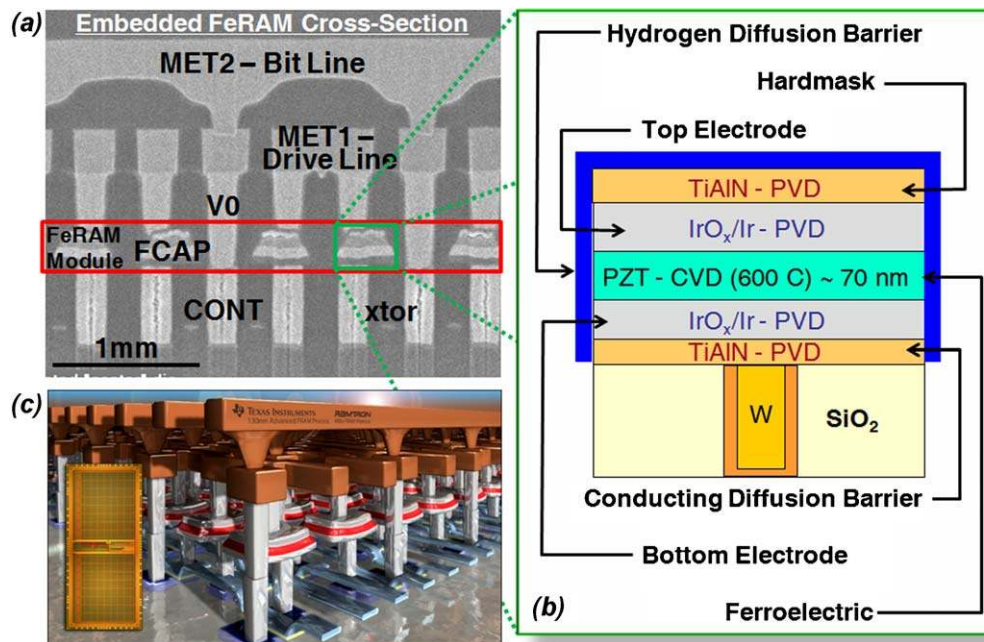


Fig. 17. Ferroelectric memories. (a) Cross-sectional scanning electron microscopy image of an actual ferroelectric memory device. (b) Schematic illustration of the FeRAM module showing all the layers needed for the creation of this device. (c) Artist's depiction of a FeRAM device, courtesy of Texas Instruments and Ramtron.

approach led to the elimination of interface related degradation mechanisms such as polarization fatigue and imprint. It is important to note, however, that such epitaxial heterostructure synthesis approaches are not easily transferrable to the FRAM manufacturing process. Indeed, currently manufactured FRAM's use oxide electrodes and PZT, albeit in polycrystalline form. More recent efforts have also focused on the implementation of epitaxial PZT films in a probe-based data storage concept (based on the Millipede idea developed by IBM). This approach, aimed at creating memory elements with lateral dimensions in the 20–50 nm range, requires exquisite control over the surface quality of the ferroelectric layer, thus automatically requiring an epitaxial PZT layer. A proof of concept of this was demonstrated using STO/Si as the substrate that enabled the heteroepitaxial growth of PZT with a conducting perovskite bottom electrode (SrRuO₃).

4.5. Ferroelectric tunnel junctions and novel transport phenomena

Previously we discussed size effects in ferroelectric materials and the study of how ferroelectricity can be sustained down to just a few unit cells. This has led to research on using high quality ultra-thin films of these ferroelectric materials as adjustable tunnel barriers for various applications [155]. The phenomenon of tunneling has been known since the advent of quantum mechanics. A typical tunneling junction is built up with two conducting electrodes separated by a very thin insulating barrier. New types of tunneling junctions can be very useful for future technological applications. For example, magnetic tunneling junctions have shown the potential application in spintronic devices [156]. The idea is to use ferroelectric tunneling junctions to replace the insulating barrier in traditional tunnel junction devices, and because the direction of the spontaneous polarization can be controlled via applied electric fields, this construction could enable new functionality. The polarization reversal of a ferroelectric barrier layer is predicted to show a giant resistive switching effect [157] because the sign of the polarization charges at the interface has been altered. Using this effect to our advantage, it may be possible to build up memories with nondestructive resistive

readouts. Recently, Garcia et al. [158] showed robust ferroelectricity in films down to only 1 nm in highly strained BaTiO₃ thin films. The researchers used conductive atomic force microscopy to measure the tunneling current and demonstrated resistive readout of the polarization states, which may pave the way towards high-density ferroelectric memories with simple device structures. Another recent study demonstrated tunneling based on high quality thin film surfaces. Maksymovych et al. [159] used atomic force microscopy to inject electrons from the tip of an atomic force microscope into a thin film of Pb(Zr_{0.2}Ti_{0.8})O₃. The key concept demonstrated in this study was the use of the surface polarization as an electric field source to extract electrons. The tunneling current exhibits a pronounced hysteresis with abrupt switching events that coincide with the local switching of ferroelectric polarization. They have shown 500-fold amplification of the tunneling current upon ferroelectric switching. This also opens an avenue to possible applications in high-density data storage.

5. Magnetism in oxides

5.1. Definition of magnetic materials

The symmetry concerns for magnetism are slightly more complex than those for ferroelectricity. Magnetic materials violate time reversal symmetry, but are invariant under spatial inversion, in other words, when magnetic moments are present in a crystal the antisymmetry operator must also be present. The 32 classical crystallographic point groups do not have the antisymmetry operator and hence cannot fully describe the symmetry of magnetic crystals. Symmetry analysis reveals 122 total magnetic space groups of which only 31 can support ferromagnetism [60,160]. A material is said to be a ferromagnet when there is long range, parallel alignment of the atomic moments resulting in a spontaneous net magnetization even in the absence of an external field. Ferromagnetic materials undergo a phase transition from a high-temperature phase that does not have a macroscopic magnetization (atomic moments are randomly aligned resulting in a *paramagnetic* phase) to a low-temperature phase that does.

There are other types of magnetism including antiferromagnetism (atomic moments are aligned antiparallel) and ferrimagnetism (dipoles align antiparallel, but one subset of dipoles is larger than the other resulting in a net moment). The theory of magnetism is a rich field, the details of which are beyond the scope of this treatment, but is built upon the idea of the quantum mechanical exchange energy which causes electrons with parallel spins and therefore parallel moments to have lower energy than spins with antiparallel spin. Inherent to this concept is the presence of unpaired electrons in a material. Thus a requirement for magnetism in transition metals is a partially filled *d* (or *f*) orbital [62]. Magnetic materials find pervasive use in all walks of life, from information technologies (storage, sensing and communications) to health sciences (e.g., cancer treatment) and beyond.

5.2. Brief history of magnetic oxides

Unfortunately, a brief history of the role of oxide materials in the development of the greater field of magnetism is a rather difficult undertaking. In fact, the Greek philosopher Thales of Miletus, who was alive from approximately 634 to 546 BC, is thought to be the first person to describe magnetism after observing the attraction of iron by the mineral magnetite (Fe_3O_4). From that day forward, magnetic oxides were an essential key to the advances in many fields, including navigation, power production, and more. For a complete history of magnetism in materials see Ref. [161]. For the sake of brevity, we focus here solely on magnetic oxides. According to Pliny the Elder's (23–79 AD) *Historia Naturalis* the name “magnet” came from a shepherd called Magnes, who likely originated from a town called Magnesia in the Greek Empire where nearby ore deposits were naturally magnetized and found that iron nailed shoes or iron-tipped canes stuck to the ground [162]. Beginning in the 1500s, the name lodestone (in old English “lode” is the word for lead) began being used to describe such iron-oxide (Fe_3O_4) based magnetic ore and also saw these materials make significant impact in the realm of navigation (although the earliest reports of lodestone-based direction pointers come from China between 221 and 206 BC and the earliest use of such pointers for navigation come from late 11th or early 12th century China and in Europe sometime in the late 12th century) [162]. Scholarly pursuit of the field of magnetism also began in 1269 when French crusader and scholar Peter Peregrinus (Pierre Pèlerin de Maricourt) wrote a lengthy letter describing lodestone and how one could create useful devices from it. But real systematic studies of magnetism came only in 1600 with the publication of William Gilbert's *De Magnete* – in which Gilbert proposed the presence of magnetic poles on the Earth which would only be confirmed in Carl Friedrich Gauss in 1835 [161]. Through 1819, only magnetization produced by lodestone was known, but the work of Hans Christian Oersted, Jean-Baptiste Biot, Felix Savart, and André Marie Ampère in the late

1700s and early 1800s lead to the delineation of classical electromagnetism and the work of Michael Faraday and James Clerk Maxwell to the field of modern magnetism [162].

The early 20th century saw much work on the development of an atom-based model for magnetic phenomena including the work of Pierre Weiss who introduced the theory of ferromagnetism based on a molecular field concept [163] and Paul Langevin who explained the ferromagnetic-paramagnetic transition observed by Pierre Curie. In 1928, Heisenberg formulated a spin-dependent model for the exchange interaction that allowed Weiss' molecular field to be interpreted as having its origin in the exchange interaction [164] and marked the birth of modern magnetism theory. This, in turn, made it possible for the field of magnetic oxides to develop at a feverish pace. Of fundamental importance to this early work was a series of publications by Lois Néel who developed the idea of antiferromagnetism [165]. By the late 1950s a rapid expansion of technology, especially high-frequency devices, stimulated rapid research in ferromagnetic oxides and Smit and Wijn in their book on ferrites note that in 1959 the properties of magnetic oxides were better understood than the properties of metallic ferromagnets [166].

5.3. Common types of magnetism in transition metal oxides

Throughout the 20th century a number of fundamental ideas of coupling in oxide materials were developed that explained how indirect exchange – mediated through non-magnetic ions like oxygen – give rise to the effects seen in oxide materials including superexchange, double exchange, and RKKY coupling.

5.3.1. Superexchange

Superexchange gets its name from the fact that it extends the normally very short-range exchange interaction to a longer range [162]. The idea that exchange could be mediated by an intermediate, non-magnetic atom was put forth in 1934 [167] and the theory was formally developed by Anderson in 1950 [168]. Superexchange is an important effect in ionic solids where 3*d* and 2*p* orbitals of transition metals and oxygen or fluorine atoms interact and it describes, through a simple valence bonding argument, how antiferromagnetic ordering occurs. Fig. 18(a) shows a schematic illustration of the superexchange effect in LaMnO_3 . Each of the Mn^{3+} ions contains four 3*d* electrons and when these atoms bond, with some degree of covalency, with a mediating O^{2-} anion the only way hybridization can take place is with the donation of electrons from the oxygen to the manganese ions. By Hund's rule, the spin of the electron donated to the left Mn-ion must be the same as the spins in the Mn-ion, which leaves an electron of the opposite spin in the oxygen *p*-orbital to be donated to the right Mn-ion. By the same argument, this bonding can only take place if the spins of the right Mn-ion are opposite to the left Mn-ion. What occurs in the end is that the

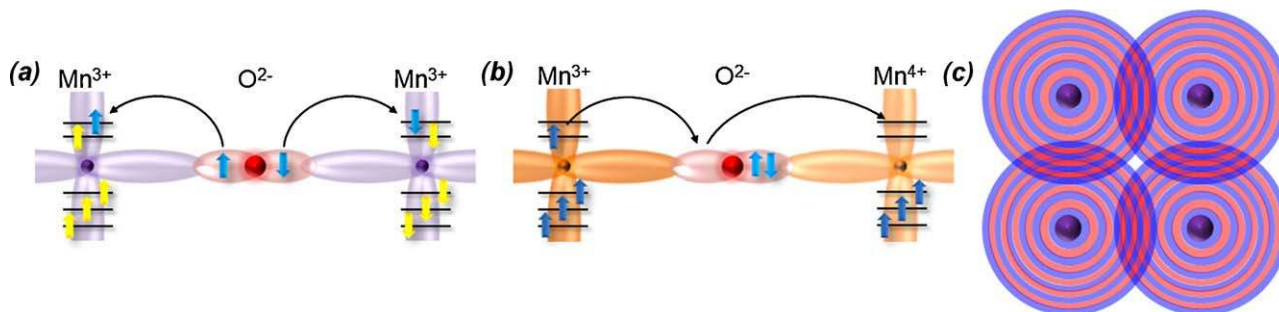


Fig. 18. Magnetic coupling in oxides. Schematic illustrations of (a) superexchange, (b) double exchange, and (c) RKKY coupling.

oxygen-mediate bonding leads to a collective antiparallel spin alignment of nearest neighbor Mn-ions.

5.3.2. Double exchange

Double exchange, which was first proposed by Zener in 1951 [169], begins to change the nature of magnetic coupling in materials like LaMnO_3 if one dopes in materials like Sr or Ca on the La-site, creating a mixed valence compound. Double exchange describes the magneto-conductive properties of these mixed valence compounds and delineates the mechanism for hopping of an electron from one site to another through the mediating oxygen atom. Again, because the O^{2-} ion has full p -orbitals, the movement from one ion through O^{2-} to another ion is done in two steps. Let us explore this idea for the case of the widely studied oxide ferromagnet $\text{La}_{0.7}\text{Sr}_{0.3}\text{MnO}_3$ which has Mn^{3+} and Mn^{4+} ions (Fig. 18(b)). Assuming the ligand field is relatively small and we fill the 3d orbitals following Hund's rules the Mn^{3+} and Mn^{4+} ions are filled with electrons as shown with the dark blue arrows. In such materials, electron conduction proceeds by this double step process by which one of the electrons on the Mn-sites jumps back and forth across the oxygen. The electron is thus delocalized over the entire M–O–M group and the metal atoms are said to be of mixed valency. This is aided by the fact that spin-flips are not allowed in electron hopping processes and thus it is more energetically favorable if the magnetic structure of the two Mn-ions is identical; therefore, ferromagnetic alignment of moments is achieved.

5.3.3. RKKY coupling

The final type of exchange we will discuss here is RKKY exchange. Unlike the previous two examples, RKKY exchange (named after the work of Ruderman and Kittel [170], Kasuya [171], and Yosida [172]) is not based on the relationship between bonding and magnetism, but instead is the concept that a local moment can induce a spin polarization in a surrounding conduction electron sea. Such studies showed that the spin polarization of the conduction electrons oscillates in sign as a function of distance from the localized moment and this spin information can be carried over relatively long distances (Fig. 18(c)). Such coupling has been proposed to explain coupling in dilute magnetic semiconductor systems where magnetic ions are too far apart to interact with each other directly and the sign of this coupling depends on the distance between magnetic ions.

5.4. Modern magnetic oxides

Since 1950 a number of magnetic oxides have dominated the landscape of solid state physics research. In this section we will investigate two of these systems: ferrites and manganites.

5.4.1. Ferrites

The ferrites include the entire family of Fe-containing oxides such as the spinels (AFe_2O_4), garnets ($\text{AFe}_5\text{O}_{12}$), hexaferrites ($\text{AFe}_{12}\text{O}_{19}$), and orthoferrites (RFeO_3 , where R is one or more of the rare-earth elements). In the past, ferrites have been used in applications as diverse as transformer cores [173] and microwave magnetic devices [174] to magneto-optic data storage materials [175] and flux guides and sensors [176]. In this section we will focus primarily on spinel ferrites as they have received much recent attention. The recent push with these materials has been to create high quality thin films of these complex materials to enable better understanding of structure–property relationships and to enable the creation of novel new devices based on the intriguing properties of these materials. Considerable effort has been undertaken to achieve bulk-like properties in ferrite thin films and because of the rather complex chemical nature of these

materials careful control of strain effects, growth conditions, and post-annealing treatments are needed to achieve high quality samples. In fact, recent theoretical studies of the spinel materials in particular point to the delicate nature of these materials as the electronic structure is strongly dependent on cationic order/disorder in these materials [177]. In some cases, a half-metallic character is expected and this, combined with the high Curie temperatures of these materials, makes them of great interest as electrodes in magnetic tunnel junctions [178] and spintronic devices. Additionally, the spinel ferrites have become quite popular in the study of composite multiferroic heterostructures. Here we will investigate briefly the work on epitaxial films of the materials Fe_3O_4 , NiFe_2O_4 , and CoFe_2O_4 . For a detailed review of spinel ferrite thin films see Ref. [179].

5.4.1.1. Fe_3O_4 . Fe_3O_4 or magnetite is one of the oldest known magnetic materials and has been extensively studied over the years [180], yet it has enjoyed a rejuvenation in interest driven by the possibility of utilizing the half-metallic nature of the material in magnetic multilayer devices. Band structure calculations suggest that the majority spin electrons in Fe_3O_4 are semiconducting with a sizable energy-gap and that the minority spins are metallic in nature [181]. Magnetite is the half-metal with the highest known Curie temperature (~ 858 K). Fe_3O_4 has also been studied because it undergoes an interesting first-order metal–insulator phase transition known as the Verwey transition [182] at 120 K where the Fe_3O_4 undergoes a structural transition from cubic to monoclinic [183] structure that is accompanied by a dramatic increase in resistivity [184] and decrease in magnetic moment. Strong debate about the fundamental mechanisms for this transition are still ongoing – especially discussion of the localized or delocalized nature of 3d electrons in this system [162].

Driven by the desire to incorporate this material into magnetic devices, epitaxial growth of Fe_3O_4 has been achieved on (0 0 1) MgO substrates using a wide variety of deposition techniques. Pulsed laser deposition growth with substrate temperature between 200 and 500 °C has yielded good, bulk-like properties [185–190]. A comparison of magnetic properties for bulk Fe_3O_4 and various thin films is shown in Fig. 19(a) and shows that careful attention must be given to materials synthesis to achieve bulk-like properties in these films. Detailed studies of magnetoresistance [187,191,192] as well as the study of magnetic devices, such as magnetic tunnel junctions based on Fe_3O_4 [193–196] have also been completed.

5.4.1.2. NiFe_2O_4 . Nickel ferrite or NiFe_2O_4 , unlike Fe_3O_4 , has a sizeable gap in the majority spins and a smaller one in the minority spins resulting in an insulating state. Epitaxial films of NiFe_2O_4 have been grown via pulsed laser deposition on c -plane sapphire at 900 °C and high oxygen pressures [197]. Other routes to create high quality films of NiFe_2O_4 include the use of buffered spinel substrates [198]. Studies of such epitaxial films, however, revealed anomalous magnetic behavior including diminished magnetization and an anomalous approach to saturation for films grown in the range of 400–700 °C [199]. Over the years it has been shown that post-growth anneals at 1000 °C reduced the anomalous magnetic behavior of these NiFe_2O_4 films (Fig. 19(b)). More recent investigations into ultrathin films of NiFe_2O_4 on SrTiO_3 (0 0 1) substrates has shown that, under the appropriate growth conditions, epitaxial stabilization leads to the formation of a spinel phase with distinctly different magnetic and electronic properties – including magnetic moments that are enhanced by nearly 250% and metallic character – that results from an anomalous distribution of Fe and Ni cations among the A and B sites that occurs during non-equilibrium growth [200].

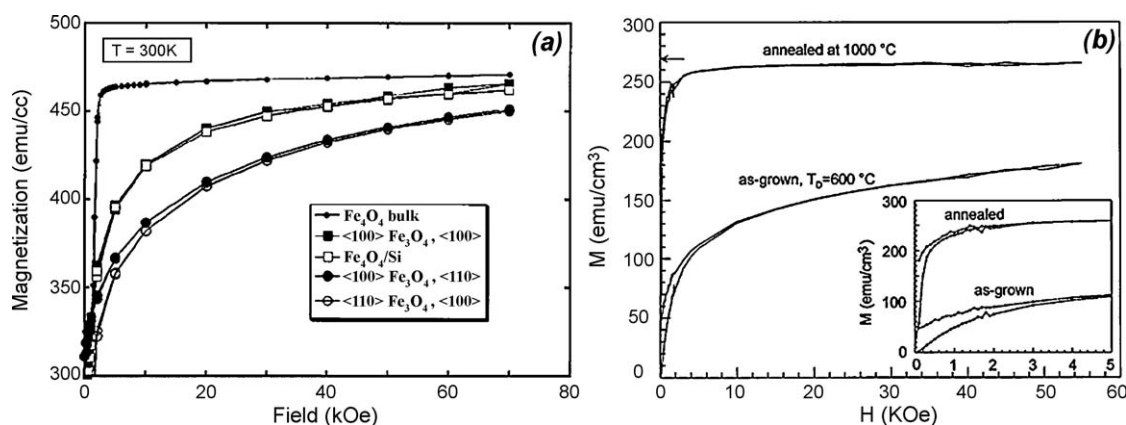


Fig. 19. Magnetism in spinel thin films. (a) Magnetization measured in the film plane for Fe_3O_4 films grown on Si (1 0 0) and MgO (1 0 0) and (1 1 0). The crystallographic direction along which the field is applied is indicated beside each film in the figure. The magnetization axis is offset to facilitate observation of the high field data. (Adapted from Ref. [186].) (b) Magnetization of as-grown and post-annealed NiFe_2O_4 thin films demonstrates the lengths to which one must go to achieve bulk-like properties in spinel films. (Adapted from Ref. [199].)

5.4.1.3. CoFe_2O_4 . As is typically the case with these spinel ferrites, the properties of CoFe_2O_4 thin films were found to be quite different from bulk properties. Studies have found that the microstructure of the film significantly impacts the magnetic properties. Thin films have been grown on a wide array of substrates, including MgO (1 0 0) [201,202] and spinel structure substrates such as MgAl_2O_4 (1 1 0) and CoCr_2O_4 -buffered MgAl_2O_4 substrates which allowed researchers to create films free of anti-phase boundaries and led to the connection of cation distribution and lattice distortions to anomalous magnetic behavior [203]. More recently CoFe_2O_4 has also been used a tunnel barrier layer in conjunction with a Fe_3O_4 electrode and interesting exchange spring magnet behavior arises at the interface between these two materials [204].

5.4.1.4. $\text{BaFe}_{12}\text{O}_{19}$. Barium hexaferrite is by far the most widely studied hexaferrite material. It is an attractive material for use in non-reciprocal devices that operate at microwave and millimeter wavelengths, it possesses a relatively high dielectric constant and a large uniaxial magnetocrystalline anisotropy. Thin films of $\text{BaFe}_{12}\text{O}_{19}$ have been studied for nearly 30 years and have been grown via sputtering [205], metal-organic chemical vapor deposition [206], liquid phase epitaxy [207], pulsed laser deposition [208,209] and more. The effect of epitaxial thin film strain on the structural and magnetic properties of $\text{BaFe}_{12}\text{O}_{19}$ thin films has also been studied [210]. With appropriate thin film strain conditions and annealing procedures, narrow line widths of only 37 Oe were measured in ferromagnetic resonance (FMR)—the presence of strain was found to broaden the resonance absorption. More recently, the most narrow FMR line-widths of only 27 Oe at 60.3 GHz have been measured in PLD grown films [211], exotic domain wall superconductivity has been observed in superconductor- $\text{BaFe}_{12}\text{O}_{19}$ heterostructures [212], epitaxial thin films have been achieved on SiC substrates [213], and much more. The hexaferrites continue to remain an exciting, technologically relevant materials system worthy of future study.

5.4.1.5. RFeO_3 . The rare-earth orthoferrites (RFeO_3 , including $R = \text{La, Nd, Sm, Gd, Dy, Er, Yb, and Y}$) have a crystalline structure which is close to that of the perovskites. In general the orthoferrites are antiferromagnetic due to the antiparallel alignment of the magnetic moments of the Fe sublattices; however, weak ferromagnetism due to canting has been observed in some phases [214,215]. The rare-earth orthoferrites show strong uniaxial anisotropy and, beginning in the 1960s, were studied as candidate

materials for bubble memories [216]. Future development of these materials, however, was hindered because it was difficult to make high quality thin films of these materials. In the 1990s work on thin films of these materials accelerated as thin films of YFeO_3 [217], DyFeO_3 , GdFeO_3 , SmFeO_3 [218], and others were produced. In recent years, interesting new properties have been reported in these materials, including relaxor-like dielectric behavior and weak ferromagnetism in YFeO_3 materials [219]. In the end, the orthoferrites stand to experience a renewed period of interest as the search for magneto-optically active materials used in the near infrared that can be directly grown on Si or InP becomes increasingly important. The current standard materials, the garnets, possess a lattice parameter more than twice that of Si [220] rendering growth difficult.

5.4.2. Manganites

In the last 20 years, two classes of materials have defined and dominated the landscape of condensed matter physics study of oxide materials – high-temperature superconductivity in doped cuprates and, the focus of this section, colossal magnetoresistance (CMR) materials like doped manganites. As there exist a number of excellent and detailed reviews on CMR materials (see Refs. [221–225]), and in the essence of space, we give here only a limited overview of these intriguing materials and thin film aspects of this rich field.

5.4.2.1. Manganite physics. Although present in many metal oxides, the manganite materials are especially interesting since they present large electronic correlations leading to a strong competition between lattice, charge, spin, and orbital degrees of freedom. These manganese-based perovskite oxides exhibit half-metallic character and CMR response rendering them as the ideal materials to develop novel concepts of oxide-electronic devices and for the study of fundamental physical interactions. Due to the close similarity between kinetic energy of charge carriers and Coulomb repulsion, tiny perturbations caused by small changes in temperature, magnetic or electric fields, strain and so forth may drastically modify the magnetic and transport properties of these materials.

5.4.2.2. Thin film manganites. In 1993, the modern rejuvenation of interest in manganite materials came with the discovery of the so-called CMR effect in thin films of $\text{La}_{0.67}\text{Ca}_{0.33}\text{MnO}_3$ where a magnetoresistance effect gave rise to a change in resistance of the material 3 orders of magnitude larger than that observed in giant

magnetoresistance (GMR) materials [226]. Since that time, thin film strain has been shown to be very important in determining the properties of manganite thin films.

Despite nearly 15 years of intensive study on these materials, continued research brings to light new insights on the physics of these complex materials. In this section, we will attempt to give a brief overview of a select few highlights – by no means is this an exhaustive list of the excellent work done in this field. In 2002, Zhang et al. [227] were able to shed some light on the origin of the magnetoresistance in these CMR materials by imaging the percolation of ferromagnetic, metallic domains in a $\text{La}_{0.33}\text{Pr}_{0.34}\text{Ca}_{0.33}\text{MnO}_3$ thin film with magnetic force microscopy. This work helped solidify prior experimental and theoretical work that suggested that such doped manganites were inhomogeneous and that phase separation was common in these materials. In 2006, however, Moshnyaga et al. [228] found that in epitaxial $\text{La}_{0.67}\text{Ca}_{0.33}\text{MnO}_3$ films on MgO (1 0 0) substrates an unusual rhombohedral ($R\bar{3}c$) structure occurred as a result of a unique ordering of La and Ca and that such A-site ordered films were electronically homogeneous down to the 1 nm scale as studied by scanning tunneling microscopy/spectroscopy. The La and Ca ordering was found to compensate the cation mismatch stress and to enhance homogeneity and, despite the lack of observable phase separation, large magnetoresistance values of $\sim 500\%$ were measured in the A-site order films. And by 2008, Cox et al. [229] reported that the widely observed so-called stripe phases, which were long thought to be caused by localization of charge on atomic sites [230–233], were, in reality, caused by a charge-density wave that undergoes collective transport. The charge-density wave exists in the presence of a high density of impurities and this leads to the observation of hysteresis effects in the resistance.

Building on earlier work on the effects of thin film strain on CMR materials (see Refs. [234–244]), Adamo et al. [245] have recently studied the effect of biaxial strain on thin films of $\text{La}_{0.7}\text{Sr}_{0.3}\text{MnO}_3$ with biaxial strains ranging from -2.3% to $+3.2\%$. Biaxial strain was thought to influence the Jahn–Teller effect in this phase and as early as 1998 Millis et al. [246] had proposed an analytical model to describe the effects of biaxial strain on the properties of CMR materials. This study brings together a wide range of work and confirms many of the previous findings and predictions including how the Curie temperature and saturation magnetization varies with strain. Among the more interesting aspects of thin film control of properties of such manganite materials is the idea that thin film strain could enable the control and modification of orbitals in materials. Having been first demonstrated in semiconductors, [247] in 2007 Abad et al. [248] suggested that similar control could be achieved in the manganites. In $\text{La}_{0.67}\text{Ca}_{0.33}\text{MnO}_3$ films grown on STO and NdGaO_3 (0 0 1) substrates it was demonstrated that the structural strain was strong enough to modify the electronic structure of the Mn in that it could split the e_g and t_{2g} levels which leads to a pseudocubic structure in which the $3z^2-r^2$ orbitals order along the strain axis and the x^2-y^2 orbitals order within the plane of the biaxial strain. This strain, in turn, enhances the Jahn–Teller like distortions thus promoting selective orbital occupancy and charge localization and gives rise to interesting orbital glass insulating states.

In recent years, increasing attention has been given to combining these CMR materials into artificial heterostructures. In 2002, Tanaka et al. [249] showed that they could modulate the metal–insulator transition, corresponding to the ferromagnetic transition temperature, by over 50 K with application of just +1 to +1.8 V to a $\text{La}_{0.9}\text{Ba}_{0.1}\text{MnO}_3/\text{Nb:STO}$ p – n junction. Building on this work, in 2005 Nakagawa et al. [250] showed that in rectifying $\text{La}_{0.7}\text{Sr}_{0.3}\text{MnO}_3/\text{Nb:STO}$ junctions one can use a magnetic field to tune the depletion layer thereby creating a large positive magnetocapacitance. At the same time, the corresponding reduc-

tion in the barrier results in an exponentially enhanced differential magnetoresistance despite the absence of a spin filter. More recently, in 2009 Hoppler et al. [251] demonstrated a rather large superconductivity-driven modulation of the vertical ferromagnetic magnetization profile in superconductor/ $\text{La}_{0.67}\text{Ca}_{0.33}\text{MnO}_3$ superlattices.

5.5. Thin film magnetic phenomena

The greater field of magnetism is rich with thin film phenomena. As one might suspect, there are similar size effects to those discussed previously for ferroelectric materials. Developments and understanding of the greater field of thin film magnetism, however, is beyond the scope of this manuscript and the reader is directed to Ref. [252] and for a more general treatment. Much like traditional metallic magnets, oxide magnets experience magnetic size effects including diminished magnetization in ultrathin films, decreased magnetocrystalline anisotropy, and more. Classic examples of thin film effects on magnetism have been described above, including diminished magnetization in as-grown spinels. Additionally, it has been observed that thin film strain (i.e., tensile or compressive) can change the easy magnetization direction in materials like the manganites. For instance, growth of $\text{La}_{0.7}\text{Sr}_{0.3}\text{MnO}_3$ on SrTiO_3 (0 0 1) (tensile strain) substrates results in in-plane magnetization while growth on LaAlO_3 (0 0 1) (compressive strain) substrates results in out-of-plane magnetization [253–255]. Furthermore, studies using a combination of spin-resolved photoemission spectroscopy (SPES), SQUID magnetometry, and X-ray magnetic circular dichroism (XMCD) have shown that there is diminished magnetism at the surface boundary of $\text{La}_{0.7}\text{Sr}_{0.3}\text{MnO}_3$ thin films [256] and this begs the question as to what happens in ultrathin films where the substrate–film interface and surface boundary come close together. Recent work has demonstrated that careful growth of such materials can extend the critical thickness for the observation of ferromagnetic-like properties down to thicknesses of only 3 unit cells in materials like $\text{La}_{0.7}\text{Sr}_{0.3}\text{MnO}_3$, and that bulk-like properties occur in films with only 13 unit cells or more [27]. In this section we will discuss the development of exciting new areas of magnetic oxide studies that focus on ultrathin films and the development of properties at interfaces.

5.5.1. Superlattice effects

The current fascination with interfacial magnetism arose from the pioneering work of Takahashi et al. in 2001 [257]. They created oxide superlattices of the antiferromagnetic insulator CaMnO_3 (10 unit cells) and the paramagnetic metal CaRuO_3 (n unit cells) on LaAlO_3 substrates via PLD. The resulting superlattices showed ferromagnetic transitions at $T_C \sim 95$ K and negative magnetoresistance below T_C . These results ushered in the idea that coupling across these heteroepitaxial interfaces could give rise to novel new magnetic states and physics. Building off of this work, researchers moved to study highly controlled artificial heterostructures of similar materials – with large pieces of the work focusing on heterostructures of LaMnO_3 and SrMnO_3 – both antiferromagnetic insulators and the parent compounds for the classic CMR materials. Work suggested again that superlattices with small repeat distances (less than or equal to 2 unit cells) behaved as ferromagnetic metals and that as the thickness of the layers increased the magnetism became dominated by the LaMnO_3 , but electronic transport continued to be dominated by the interfaces [258]. Further studies of similar heterostructures demonstrated a metal-to-insulator transition as a function of the repeat thickness [259]. Metallic states occurred for $n \leq 2$ and insulating states for $n \geq 3$. Detailed polarized neutron reflectivity studies of these interfaces also revealed enhanced magnetization at certain

interfaces and the formation of an asymmetric magnetization across the LaMnO_3 layers [260]. Additionally, this work has also demonstrated that cation-ordered superlattices possess higher T_N values than randomly mixed materials [261]. This work has spawned a number of theoretical treatments [262,263,264], including the proposal that a spin-polarized two-dimensional electron gas could be formed at such interfaces [265].

5.5.2. Exchange coupling across interfaces

It is possible that exchange bias, more than any other single effect, has played the biggest role in the development of modern magnetic materials. When heterostructures with a ferromagnet are placed in contact with an antiferromagnet and are cooled through the Néel temperature (T_N) of the antiferromagnet (with the Curie temperature, T_C , of the ferromagnet larger than T_N) in the presence of an applied magnetic field, an anisotropy is induced in the ferromagnetic layer. Exchange bias is one of a number of phenomena observed at the interface between an antiferromagnet and a ferromagnet [266]. First discovered in 1956 by Meiklejohn and Bean [267,268] during a study of Co-nanoparticles coated with their native antiferromagnetic oxide (CoO), exchange bias has since spawned countless scientific reports and multi-billion dollar technologies. Exchange bias has been observed in many different systems containing ferromagnet–antiferromagnet interfaces in small particles, inhomogeneous materials, ferromagnetic films on antiferromagnetic crystals, as well as all thin film heterostructures [266]. Exchange bias has found a home in applications as varied as permanent magnets [269], magnetic recording media [270,271], domain stabilizers in recording heads based on anisotropic magnetoresistance [272], and as a means to reduce saturation fields to observe giant magnetoresistance (GMR) as compared to standard GMR systems [273]. It was this last finding that made exchange bias a major focus of the magnetic recording industry and placed it firmly as one of the most important technological discoveries of the computer age [274].

Exchange bias can be qualitatively understood by assuming an exchange interaction occurs at an antiferromagnet–ferromagnet interface. Traditionally, an exchange bias interaction is produced when a magnetic field, H , is applied to an antiferromagnet–ferromagnet heterostructure in a temperature range $T_N < T < T_C$ causing the ferromagnetic spins to line up along the applied field

direction while the antiferromagnetic spins remain (predominantly) in a random state above the ordering temperature (Fig. 20(a)). While maintaining the external magnetic field, the temperature is lowered to $T < T_N$. Due to the exchange interaction across the interface, the top layer of the antiferromagnet spins align parallel to the spins in the ferromagnet in order to minimize the exchange energy of the system. Once this has occurred the remaining spins in the antiferromagnet follow suit and align in order to produce a zero net magnetization for the antiferromagnetic material (Fig. 20(b)). Upon application of a magnetic field opposite the direction of the cooling field, the spins in the ferromagnet attempt to rotate, however, for sufficiently large antiferromagnetic anisotropy the antiferromagnet spin structure remains unchanged (Fig. 20(c)). This, in turn, leads to the formation of an interfacial interaction between the pinned spins in the antiferromagnet and the spins in the ferromagnet that tries to maintain the parallel alignment of the different spin systems across the interface. In other words, one can think of this as an additional internal field preventing the ferromagnet spins from rotating freely. This interaction acts as a torque in the opposite direction to the applied field thereby creating only one stable configuration of spins in the system—in other words, the anisotropy is unidirectional. This means a larger magnetic field must be applied in the direction opposite to the cooling field direction in order to completely switch the ferromagnet when it is in contact with an antiferromagnet (Fig. 20(d)). If one then attempted to complete the magnetic hysteresis loop and apply a field parallel to the original cooling field, the spins in the ferromagnet will begin to rotate at a smaller field because of the same internal field from the antiferromagnet (Fig. 20(e)). The interaction in this case acts as a torque in the same direction as the applied magnetic field causing the spins in the ferromagnet to rotate at lower fields than one would expect. This combination of interactions across the interface between an antiferromagnet and a ferromagnet gives rise to the classic shifted exchange bias magnetic hysteresis loop [266]. Although this simple phenomenological model is quite intuitive and simple to understand, as with most topics, there is much more to this effect. To date efforts to quantitatively understand these phenomena have continually been met with difficulties. It has been found that exchange bias is affected by factors ranging from surface/interface spin structure

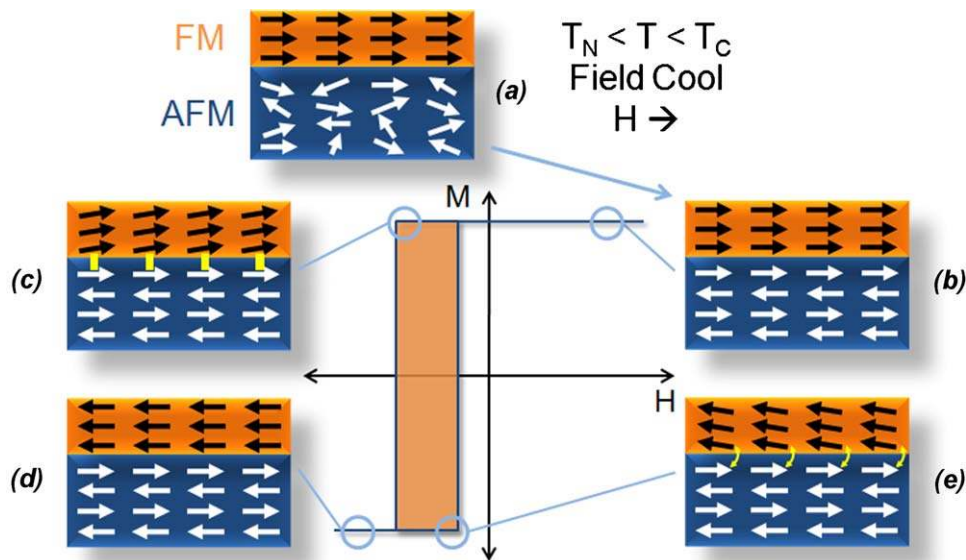


Fig. 20. Exchange bias. Schematic diagram illustrating the various stages of spin configuration in an exchange bias heterostructure being magnetically cycled. The diagrams show the spin configuration (a) above T_N under an applied magnetic field H , (b)–(e) below T_N at different applied magnetic fields. (Adapted from Ref. [266].)

and alignment, to ferromagnet and antiferromagnet thickness, sample orientation, interfacial disorder (roughness, crystallinity, etc.), antiferromagnet anisotropy, domain structures, and much more. Regardless many researchers have attempted to understand the nature of these antiferromagnet–ferromagnet heterostructures using a wide range of characterization techniques from traditional magnetization measurements to torque magnetometry, ferromagnetic resonance, neutron diffraction, magnetoresistance, AC-susceptibility, domain observation, Brillouin scattering, magnetic dichroism, and Mössbauer spectroscopy. For a full discussion of the nomenclature and history of exchange bias studies, please see any of the excellent references on exchange bias [266,275–278,279].

The current understanding of exchange bias builds on the vast experimental and theoretical work that has taken place over more than 50 years. The idea of this classic picture of a fully uncompensated spin surface giving rise to very large exchange bias interactions has been found to be a poor representation of reality—where defects such as domain walls and roughness, give rise to a fraction of pinned uncompensated spins that lead to the actual exchange bias interaction. We will discuss in later sections, modern manifestations of exchange bias structures designed to allow for new functionalities in materials. Regardless, it is clear that exchange bias will continue to play an important role as it is applied to new materials like complex oxides.

6. Multiferroism and magnetoelectricity

In the last decade there has been a flurry of research focused on multiferroic and magnetoelectric materials (see Ref. [280] and the articles therein). From the investigation of bulk single crystals to novel characterization techniques that probe order parameters, coupling, and spin dynamics this is truly a diverse field, rich with experimental and theoretical complexity. By definition, a single-phase multiferroic [281] is a material that simultaneously possesses two or more of the so-called “ferroic” order parameters—ferroelectricity, ferromagnetism, and ferroelasticity. Magnetoelectric coupling typically refers to the linear magnetoelectric effect or the induction of magnetization by an electric field or polarization by a magnetic field [282]. The promise of coupling between magnetic and electronic order parameters and the potential to manipulate one through the other has captured the imagination of researchers worldwide. The ultimate goal for device functionality would be a single-phase multiferroic with strong coupling between ferroelectric and ferromagnetic order parameters making for simple control over the magnetic nature of the material with an applied electric field at room temperature.

One aspect of fundamental interest to the study of multiferroics is the production of high quality samples of such materials for detailed study. In this section we will focus on the growth and characterization of thin film multiferroics (both single-phase and composite) as an example of a pathway to high quality, controllable multiferroics. We will discuss the basics of and fundamental nature of order parameters in multiferroics, the coupling between order parameters in single phase and composite multiferroics, and finally the current status of state-of-the-art thin film multiferroic materials. For other reviews on thin film multiferroics see Refs. [283–285].

6.1. Scarcity of multiferroics

Multiferroism describes materials in which two or all three of the properties ferroelectricity, ferromagnetism, and ferroelasticity occur in the same phase. The overlap required of ferroic materials to be classified as multiferroic is shown schematically in Fig. 21(a). Only a small subgroup of all magnetically and electrically polarizable materials are either ferromagnetic or ferroelectric and fewer still simultaneously exhibit both order parameters. In these select materials, however, there is the possibility that electric fields can not only reorient the polarization but also control magnetization; similarly, a magnetic field can change electric polarization. This functionality offers an extra degree of freedom and hence we refer to such materials as magnetoelectrics (Fig. 21(b)). Magnetoelectricity is an independent phenomenon that can arise in any material with both magnetic and electronic polarizability, regardless of whether it is multiferroic or not. By definition, a magnetoelectric multiferroic must be simultaneously both ferromagnetic and ferroelectric [286]. It should be noted, however, that the current trend is to extend the definition of multiferroics to include materials possessing two or more of any of the ferroic or corresponding antiferroic properties such as antiferroelectricity and antiferromagnetism.

The scarcity of magnetoelectric multiferroics can be understood by investigating a number of factors including symmetry, electronic properties, and chemistry. We note that there are only 13 point groups that can give rise to multiferroic behavior. Additionally, ferroelectrics by definition are insulators (and in 3d transition metal based oxides, typically possess ions that have a formal d^0 electronic state), while itinerant ferromagnets need conduction electrons; even in double exchange ferromagnets such as the manganites, magnetism is mediated by incompletely filled 3d shells. Thus there exists a seeming contradiction between the conventional mechanism of off-centering in a ferroelectric and the formation of magnetic order which explains the scarcity of

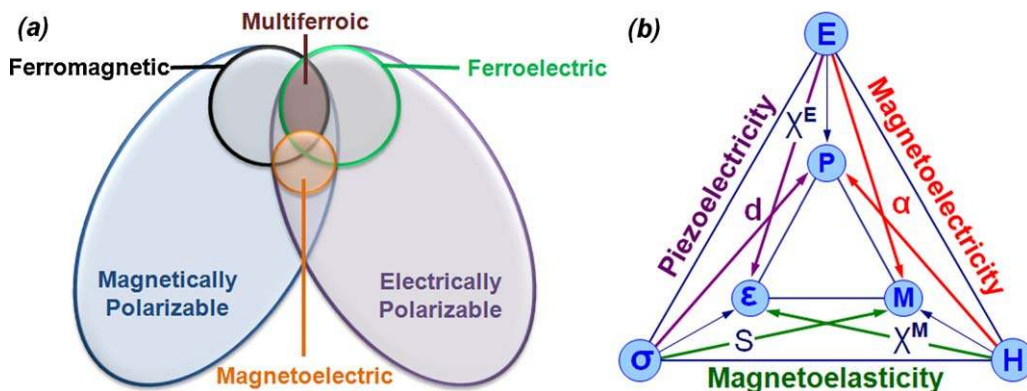


Fig. 21. Multiferroic and magnetoelectric materials. (a) Relationship between multiferroic and magnetoelectric materials. Illustrates the requirements to achieve both in a material. (Adapted from Ref. [286].) (b) Schematic illustrating different types of coupling present in materials. Much attention has been given to materials where electric and magnetic order is coupled. These materials are known as magnetoelectric materials. (Adapted from Ref. [285].)

ferromagnetic–ferroelectric multiferroics [62]. The focus of many researchers, therefore, has been in designing and identifying new mechanisms that lead to magnetoelectric coupling and multiferroic behavior. In the following section we will investigate a number of these pathways.

6.2. Pathways to multiferroism

There are a number of pathways with which one can achieve multiferroism in materials that can be broken down into one of two types as elegantly described by Khomskii [287]. Type I multiferroics are materials in which ferroelectricity and magnetism have different sources and appear largely independent of one another. One can create a Type I multiferroic by engineering the functionality on a site-by-site basis in model systems like the perovskites (ABO_3) where one can make use of the stereochemical activity of an A-site cation with a lone pair (i.e., 6s electrons in Bi or Pb) to induce a structural distortion and ferroelectricity while inducing magnetism with the B-site cation. This is the case in one of the most widely studied single phase multiferroics—the antiferromagnetic, ferroelectric $BiFeO_3$ [288]. Another way to achieve such Type I multiferroics is through geometrically driven effects where long-range dipole–dipole interactions and anion rotations drive the system towards a stable ferroelectric state. This is thought to drive multiferroism in materials like $YMnO_3$ [289]. Finally there can also be charge ordering driven multiferroics where non-centrosymmetric charge ordering arrangements result in ferroelectricity in magnetic materials as is found in $LuFe_2O_4$ [290]. On the other hand, Type II multiferroics are materials in which magnetism causes ferroelectricity—implying a strong coupling between the two order parameters. The prototypical examples of this sort of behavior are $TbMnO_3$ [291] and $TbMn_2O_5$ [292] where ferroelectricity is induced by the formation of a symmetry-lowering magnetic ground state that lacks inversion symmetry.

6.3. Definition of magnetoelectricity

From an applications standpoint, the real interest in multiferroic materials lies in the possibility of strong magnetoelectric coupling and the possibility to create new functionalities in materials. The magnetoelectric effect was proposed as early as 1894 by Curie [293], but experimental confirmation of the effect remained elusive until work on Cr_2O_3 in the 1960s [294,295]. As early as the 1970s a wide range of devices, including devices for the modulation of amplitudes, polarizations, and phases of optical waves, magnetoelectric data storage and switching, optical diodes, spin-wave generation, amplification, and frequency conversion had been proposed that would take advantage of magnetoelectric materials [296]. The magnetoelectric effect in its most general definition delineates the coupling between electric and magnetic fields in matter. A better understanding of magnetoelectric coupling arises from expansion of the free energy of a material, i.e.

$$F(\vec{E}, \vec{H}) = F_0 - P_i^S E_i - M_i^S H_i - \frac{1}{2} \epsilon_0 \epsilon_{ij} E_i E_j - \frac{1}{2} \mu_0 \mu_{ij} H_i H_j - \frac{1}{2} \beta_{ijk} E_i H_j H_k - \frac{1}{2} \gamma_{ijk} H_i E_j E_k - \dots \quad (6)$$

with \vec{E} and \vec{H} as the electric field and magnetic field, respectively. Differentiation leads to the constitutive order parameters polarization

$$P_i = (\vec{E}, \vec{H}) = - \frac{\partial F}{\partial E_i} = P_i^S + \epsilon_0 \epsilon_{ij} E_j + \alpha_{ij} H_j + \frac{1}{2} \beta_{ijk} H_j H_k + \gamma_{ijk} H_i E_j + \dots \quad (7)$$

and magnetization

$$M_i = (\vec{E}, \vec{H}) = - \frac{\partial F}{\partial H_i} = M_i^S + \mu_0 \mu_{ij} H_j + \alpha_{ij} E_j + \beta_{ijk} E_i H_j + \frac{1}{2} \gamma_{ijk} E_j E_k + \dots \quad (8)$$

where ϵ and μ are the electric and magnetic susceptibilities respectively and α represents the induction of polarization by a magnetic field or magnetization by electric field and is designated the linear magnetoelectric effect. It should be noted that higher order magnetoelectric effects like β and γ are possible, however, they are often much smaller in magnitude than the lower order terms. Furthermore, it can be shown that the magnetoelectric response is limited by the relation $\alpha_{ij}^2 < \epsilon_{ii} \mu_{jj}$ or more rigorously $\alpha_{ij}^2 < \chi_{ii}^e \chi_{jj}^m$ where χ^e and χ^m are the electric and magnetic susceptibilities. This means that the magnetoelectric effect can only be large in ferroelectric and/or ferromagnetic materials. To date the largest magnetoelectric responses have been identified in composite materials where the magnetoelectric effect is the product property of a magnetostrictive and a piezoelectric material and in multiferroic materials [297].

6.4. Thin film multiferroics

The re-emergence of interest in multiferroics has been driven, in part, by the development of thin film growth techniques that allow for the production of non-equilibrium phases of materials and strain engineering of existing materials [9]. Thin films offer a pathway to the discovery and stabilization of a number of new multiferroics in conjunction with the availability of high quality materials that can be produced in larger lateral sizes than single crystal samples. Multiferroic thin films and nanostructures have been produced using a wide variety of growth techniques including sputtering, spin coating, pulsed laser deposition, sol–gel processes, metal-organic chemical vapor deposition, molecular beam epitaxy, and more.

Despite the fact that there are a number of algorithms with which one can create multiferroism in materials, to date the only single-phase multiferroics produced as thin films include the hexagonal manganites and Bi- and Pb-based perovskites. In this section we will investigate these single-phase thin film multiferroics in more detail.

6.4.1. Manganite multiferroic thin films

The rare-earth manganites ($REMnO_3$) are an intriguing materials system and depending on the size of the RE ion the structure takes on an equilibrium orthorhombic ($RE = La-Dy$) or hexagonal ($RE = Ho-Lu$, as well as Y) structure [298]. All of the hexagonal rare-earth manganites are known to show multiferroic behavior with relatively high ferroelectric ordering temperatures (typically in excess of 590 K) and relatively low magnetic ordering temperatures (typically between 70 and 120 K) [299]. In these hexagonal phases, the ferroelectric ordering is related to the tilting of the rigid MnO_5 trigonal bipyramid [289]. On the other hand, only the orthorhombic phases with $RE = Dy, Tb$, and Gd are multiferroic in nature and have very low ($\sim 20-30$ K) ferroelectric ordering temperatures [300,301]. In these materials the ferroelectricity arises from magnetic ordering induced lattice modulations.

One of the earliest thin film multiferroic manganites to be produced was the hexagonal manganite $YMnO_3$ (YMO) (Fig. 22(a)) [302]. Work on YMO in the 1960s suggested that it was both a ferroelectric [303] and an A-type antiferromagnet [304]; however, it was not until sometime later that the true nature of ferroelectricity in this material was understood to arise from long range dipole–dipole interactions and oxygen rotations working together to drive the system towards a stable ferroelectric state

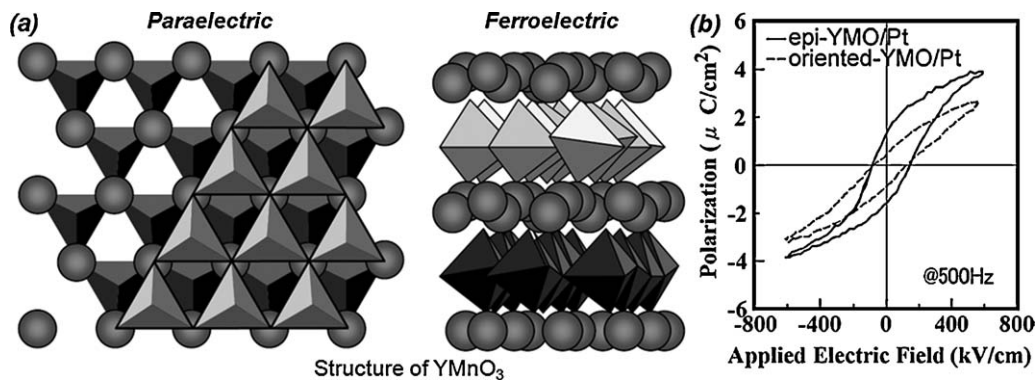


Fig. 22. YMnO₃. (a) The crystal structure of YMnO₃ in the paraelectric and ferroelectric phases. The trigonal bipyramids depict MnO₅ polyhedra and the spheres represent Y ions. (Adapted from Ref. [289].) (b) *P*–*E* hysteresis of the epitaxial-YMO/Pt and the oriented-YMO/Pt. (Adapted from Ref. [315].)

[289]. The first films [302] were grown via radio-frequency magnetron sputtering and obtained epitaxial (0001) films on MgO (111) and ZnO (0001)/sapphire (0001) and polycrystalline films on Pt (111)/MgO (111). It was soon shown that using the epitaxial strain intrinsic to such thin films, one could drive the hexagonal phase of YMO to a metastable, non-ferroelectric orthorhombic perovskite phase by growth on the appropriate oxide substrates including SrTiO₃ (001) and NdGaO₃ (101) [305]. This work was of great interest because it was the first evidence for a competition between hexagonal and orthorhombic YMO phases and how epitaxial thin film strain could be used to influence the structure of this material. This is a perfect example of the power of epitaxial thin film growth and how it can give researchers access to high pressure and temperature phases that are not easily accessible by traditional bulk synthesis techniques. Since this time YMO has been grown on a number of other substrates including Si (001), [302,306] Pt/TiO_x/SiO₂/Si (001), [307] Y-stabilized ZrO₂ (111) [308], and GaN/sapphire (0001) [309,310] and with a wide range of deposition techniques including sputtering [306,309], spin coating [307], sol–gel processes [311], pulsed laser deposition [312,313], metal-organic chemical vapor deposition [314] and molecular beam epitaxy [309].

Although thin films of YMO typically exhibit a reduction in the ferroelectric polarization as compared to bulk single crystals [302], high quality epitaxial films of YMO have also been shown to possess better ferroelectric properties than oriented-polycrystalline films (Fig. 22(b)) [315]. Polarization–electric field (*P*–*E*) hysteresis loops for YMO films have revealed that the saturation polarization in YMO is rather small (just a few μC/cm²) and that films can have a retention time of 10⁴ s at ±15 V applied voltages. Such results have led some to suggest that YMO films could be a suitable material for ferroelectric gate field-effect transistors, [315] but the high growth temperatures (800 °C [315,316] 850 °C [317]) make it impractical for integration into current applications. Work has also shown that doping the A-site with more than 5%–Bi can decrease the deposition temperatures to under 700 °C without detrimentally affecting the electric properties of the material [317]. Like many other manganites, however, A-site doping can also have strong effects on the properties of YMO [318]. A-site doping with Zr has been shown to decrease leakage currents, while doping with Li and Mg has been found to lead to increases in leakage currents, and finally Li-doping can also drive the antiferromagnetic YMO to become a weak ferromagnet [316]. The weak ferromagnetic moment is thought to have arisen from a small canting of the Mn spins. The hope that by controlling the carrier concentration researchers could make the normally antiferromagnetic YMO a robust ferromagnet has not been realized. Additionally, doping on the B-site has been shown to enhance the magnetoelectric coupling in the form of changes in the magnetocapacitance by two orders of magnitude [319].

Over the last few years thin films of a wide range of hexagonal-REMnO₃ materials have been grown. This includes studies of films with RE = Nd, Ho, Tm, Lu [320], Yb [321], and more recently Tb [322], Dy, Gd, and Sm [323]. Despite all of this focus, researchers have yet to find a REMnO₃ compound that exhibits both room temperature ferroelectricity and magnetism, but hexagonal manganites remain a diverse system with intriguing scientific implications for multiferroic materials. Recent work by Lee et al. [322] has shown that a hexagonal thin film form of TbMnO₃ can be stabilized that shows 20 times larger remnant polarization and an increase in the ferroelectric ordering temperature to near 60 K. Regardless, these hexagonal/orthorhombic manganites serve as a model system in the study of the power of thin film epitaxy to engineer new phases and properties—and the role of epitaxial strain in stabilizing the hexagonal-REMnO₃ phases is paramount in creating high quality samples of these materials for further study. More recently the REMn₂O₅ (RE = rare earth, Y, and Bi) family of materials has been studied extensively and have been shown to possess intriguing fundamental physics including coinciding transition temperatures for magnetism and ferroelectricity as well as strong coupling between these order parameters [292]. Prior to 2010, most studies focused on these materials were centered on bulk or single crystal samples and only recently have thin films for these materials been created [324].

6.4.2. BiMnO₃ thin films

Conventional growth of bulk samples of the ferromagnetic, ferroelectric [325] BiMnO₃ (BMO) required high temperatures and pressures [326] because the phase is not normally stable at atmospheric pressure. Such phases lend themselves well to thin film growth where epitaxial strain stabilization of metastable phases can be achieved. The first growth of BMO thin films was on SrTiO₃ (001) single crystal substrates using pulsed laser deposition [327] and was quickly confirmed in other studies [328]. Films of BMO have been found to be ferroelectric below ~450 K and undergo an unusual orbital ordering leading to ferromagnetism at ~105 K (Fig. 23(a)) [329].

Temperature dependent magnetic measurements have also shown that the ferromagnetic transition temperature varies depending on the substrate and can be as low as 50 K on LaAlO₃ [330]. This depression in Curie temperature has been attributed to concepts as varied as stoichiometry issues, strain, and size effects. The ferromagnetic nature of BMO has led some to study it as a potential barrier layer in magnetically and electrically controlled tunnel junctions [331] and eventually led to the production of a four-state memory concept based on La-doped BMO multiferroics [332]. Gajek et al. reported La-doped BMO films that retained their multiferroic character down to thicknesses less than 2 nm and

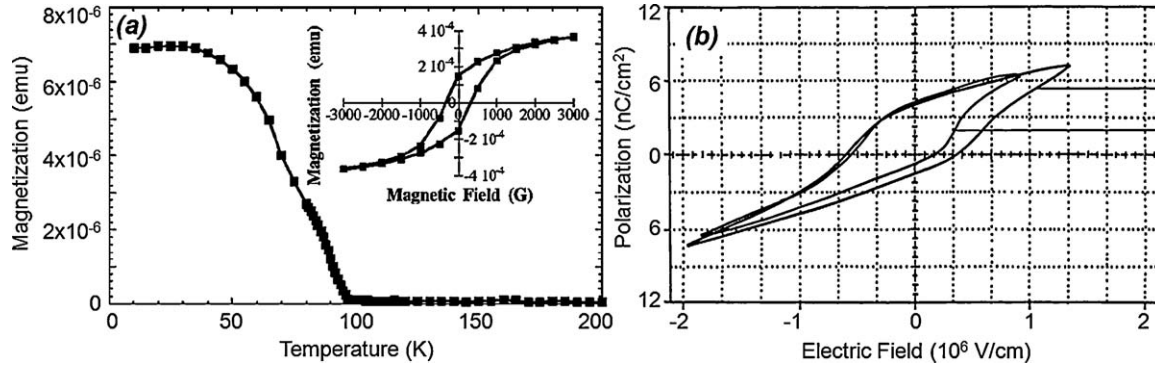


Fig. 23. BiMnO₃. (a) Magnetization curve of a BiMnO₃ film cooled under no applied magnetic field. The inset shows the ferromagnetic hysteresis loop at 5 K. (Adapted from Ref. [327].) (b) *P*–*E* hysteresis loop of a thin film of BiMnO₃ on Si (1 0 0) above and below the ferromagnetic *T*_C. (Adapted from Ref. [325].)

proved that multiferroic materials could be used to create new memories by demonstrating the possibility of spin-dependent tunneling using multiferroic barrier layers in magnetic tunnel junctions. More recently, significantly La-doped BMO films have been shown to exhibit a 70-fold increase in the magnetodielectric effect compared to pure BMO [333]. Unfortunately, it coincides with a decrease in the ferroelectric Curie temperature to ~ 150 K and is observed only at applied magnetic fields of 9 T. Additionally, optical second-harmonic measurements with applied electric fields [328], as well as Kelvin force microscopy techniques [330], have been used to confirm the presence of ferroelectric polarization in BMO films. High levels of leakage, however, have limited direct *P*–*E* hysteresis loop measurements (Fig. 23(b)) on thin film samples and recently the reanalysis of diffraction data [334] and first principles calculations [335] have called into question the ferroelectricity in BMO. Some calculations have predicted a small polar canting of an otherwise antiferroelectric structure (weak ferroelectricity) that could be used to explain the experimental findings [336]. Regardless, recent studies of dielectric properties of BMO thin films done using impedance spectroscopy between 55 and 155 K reveal that there is a large peak in the dielectric permittivity in thin films at the paramagnetic–ferromagnetic transition that could point to indirect coupling effects via the lattice in this material [337].

6.4.3. BiFeO₃ thin films

No other single-phase multiferroic has experienced the same level of attention as BiFeO₃ (BFO) in the last seven years and because of this we will discuss the evolution of this material in more length.

6.4.3.1. Historical perspective. The perovskite BFO was first produced in the late 1950s [338] and many of the early studies were focused on the same concepts important today—the potential for magnetoelectric coupling [339]. Throughout the 1960s and 1970s much controversy surrounded the true physical and structural properties of BFO, but as early as the 1960s BFO was suspected to be an antiferromagnetic, ferroelectric multiferroic [340,341]. The true ferroelectric nature of BFO, however, remained somewhat in question until ferroelectric measurements made at 77 K in 1970 [341] revealed a spontaneous polarization of $\sim 6.1 \mu\text{C}/\text{cm}^2$ along the 1 1 1-direction which was found to be consistent with the rhombohedral polar space group *R*3c determined from single crystal X-ray diffraction [342] and neutron diffraction studies [343]. These findings were at last confirmed by detailed structural characterization of ferroelectric/ferroelastic monodomain single crystal samples of BFO in the late 1980s [339]. Chemical etching experiments on ferroelastic single domains later proved without a doubt that the BFO was indeed polar, putting to rest the hypothesis

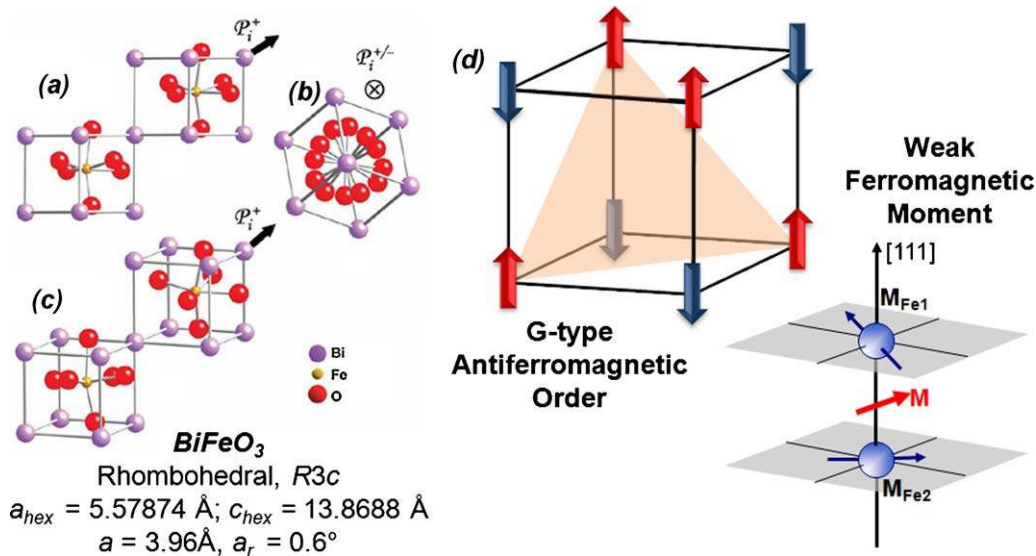


Fig. 24. BiFeO₃. (a) Structure of BiFeO₃ shown looking (a) down the pseudocubic-[1 1 0], (b) down the pseudocubic-[1 1 1] polarization direction, and (c) a general three-dimensional view of the structure. (d) The magnetic structure of BiFeO₃ is shown including G-type antiferromagnetic ordering and the formation of the weak ferromagnetic moment. (Adapted from Ref. [285].)

that BFO might be antiferroelectric, and proved that the ferroelectric/ferroelastic phase was stable from 4 to ~ 1103 K [344]. The structure of BFO can be characterized by two distorted perovskite blocks connected along their body diagonal or the pseudocubic $\langle 111 \rangle$, to build a rhombohedral unit cell (Fig. 24(a)). In this structure the two oxygen octahedra of the cells connected along the $\langle 111 \rangle$ are rotated clockwise and counterclockwise around the $\langle 111 \rangle$ by $\pm 13.8(3)^\circ$ and the Fe-ion is shifted by 0.135 \AA along the same axis away from the oxygen octahedron center position. The ferroelectric state is realized by a large displacement of the Bi-ions relative to the FeO_6 octahedra (Fig. 24(a)–(c)) [339,345].

During the 1980s, the magnetic nature of BFO was studied in detail. Early studies indicated that BFO was a G-type antiferromagnet (G-type antiferromagnetic order is shown schematically in Fig. 24(d)) with a Néel temperature of ~ 673 K [346] and possessed a cycloidal spin structure with a period of $\sim 620 \text{ \AA}$ [347]. This spin structure was found to be incommensurate with the structural lattice and was superimposed on the antiferromagnetic order. It was also noted that if the moments were oriented perpendicular to the $\langle 111 \rangle$ -polarization direction the symmetry also permits a small canting of the moments in the structure resulting in a weak ferromagnetic moment of the Dzyaloshinskii–Moriya type (Fig. 24(d)) [348,349].

In 2003 a paper focusing on the growth and properties of thin films of BFO spawned a hailstorm of research into thin films of BFO that continues to the present day. The paper reported enhancements of polarization and related properties in heteroepitaxially constrained thin films of BFO [288]. Structural analysis of the films suggested differences between films (with a monoclinic structure) and bulk single crystals (with a rhombohedral structure) as well as enhancement of the polarization up to $\sim 90 \mu\text{C}/\text{cm}^2$ at room temperature and enhanced thickness-dependent magnetism compared to bulk samples. In reality, the high values of polarization observed actually represented the intrinsic polarization of BFO. Limitations in the quality of bulk crystals had kept researchers from observing such high polarization values until much later in bulk samples [350]. More importantly this report indicated a magnetoelectric coupling coefficient as high as $3 \text{ V}/\text{cm Oe}$ at zero applied field [288]. A series of detailed first principles calculations utilizing the local spin-density approximation (LSDA) and LSDA + U methods helped shed light on the findings in this paper. Calculations of the spontaneous polarization in BFO suggested a value between 90 and $100 \mu\text{C}/\text{cm}^2$ (consistent with those measured in 2003) [351] which have since been confirmed by many other experimental reports. Other theoretical treatments attempted to understand the nature of magnetism and coupling between order parameters in BFO. Such calculations confirmed the possibility of weak ferromagnetism arising from a canting of the antiferromagnetic moments in BFO. The canting angle was calculated to be $\sim 1^\circ$ and would result in a small, but measurable, magnetization of $\sim 0.05 \mu_B$ per unit cell [352]. It was also found that the magnetization should be confined to an energetically degenerate easy $\{111\}$ perpendicular to the polarization direction in BFO. These same calculations further discussed the connection of the weak ferromagnetism and the structure (and therefore ferroelectric nature) of BFO. This allowed the authors to extract three conditions necessary to achieve electric-field-induced magnetization reversal: (i) the rotational and polar distortions must be coupled; (ii) the degeneracy between different configurations of polarization and magnetization alignment must be broken; (iii) there must be only one easy magnetization axis in the $\langle 111 \rangle$ which could be easily achieved by straining the material [352].

Nonetheless, the true nature of magnetism in thin film BFO continues to be a contentious subject. The original work of Wang et al. presented an anomalously large value of magnetic moment (of the order of $70 \text{ emu}/\text{cm}^3$) [288], which is significantly higher than the expected canted moment of $\sim 8 \text{ emu}/\text{cm}^3$. There have been

several studies aimed at clarifying the origins of this anomalous magnetism. Eerenstein et al. [353] proposed that the excess magnetism was associated with magnetic second phases (such as $\gamma\text{-Fe}_2\text{O}_3$); this was supported by the studies of Béa et al. [354] who showed that BFO films, when grown under reducing conditions (for example under oxygen pressures lower than 1×10^{-3} Torr) showed enhanced magnetism as a consequence of the formation of magnetic second phases. It is, however, important to note that low oxygen pressure during growth is not the cause for the enhanced moment in the 2003 report by Wang et al. where films were grown in oxygen pressures between 100 and 200 mTorr and cooled in 760 Torr rendering formation of such secondary magnetic phases thermodynamically unlikely and there was no evidence (despite extensive study of samples with X-ray diffraction and transmission electron microscopy techniques) for such second phases. Furthermore, subsequent X-ray magnetic circular dichroism studies supported the assertion that this magnetism is *not* from a magnetic $\gamma\text{-Fe}_2\text{O}_3$ impurity phase [355]. To date, additional mixed reports—including reports of enhanced magnetism in nanoparticles of BFO [356] as well as the observation of samples exhibiting no such enhancement—have been presented. It is thus fair to say that this one issue that remains unresolved in a rigorous sense.

6.4.3.2. Growth of BiFeO_3 films. Today, much progress has been made in understanding the structure, properties, and growth of thin films of BFO. High quality epitaxial BFO films have been grown via pulsed laser deposition [288,357], radio-frequency (RF) sputtering [358,359], metalorganic chemical vapor deposition (MOCVD) [360,361], and chemical solution deposition (CSD) [362] on a wide range of substrates including traditional oxide substrates as well as Si [357,363] and GaN [364]. This work has shown that high quality films, like those shown in Fig. 25 can be produced. Typical XRD $\theta - 2\theta$ measurements (Fig. 25(a)) show the ability of researchers to produce high quality, fully epitaxial, single phase films of BFO (data here is for a BFO/SRO/STO (001) heterostructure). Detailed XRD analysis has shown that films possess a monoclinic distortion of the bulk rhombohedral structure over a wide range of thicknesses, but the true structure of very thin films ($< 15 \text{ nm}$) remains unclear [365]. The quality of such heterostructures as produced by pulsed laser deposition can be probed further by transmission electron microscopy (TEM) (Fig. 25(b)). TEM imaging reveals films that are uniform over large areas and with the use of high resolution TEM we can examine the atomically abrupt, smooth, and coherent interface between BFO and a commonly used bottom electrode material SRO.

In Section 4.3.4, we discussed the advances that have been made in controlling ferroelectric domain structures of thin films of BFO. This work, in turn, has enabled significant progress in the understanding of this complex multiferroic material. In addition to being of great interest for photonic devices, nanolithography, and more, fine control of the domain structures and the ability to create extremely high quality thin films of these materials make it possible to probe a number of important questions related to this material. This includes, the evolution of magnetism in thin films (i.e., variations from the bulk picture and the mechanism of enhanced magnetism in thin films), the role of domain walls in determining macroscopic properties, doping effects in BFO, the nature of magnetoelectric coupling in these materials, and more. In the next few sections, we will address these different questions in detail.

6.4.3.3. Evolution of antiferromagnetism in BiFeO_3 thin films. As was discussed in Section 6.4.3.1, the structure of BFO can be characterized by two distorted perovskite blocks connected along their body diagonal or the pseudocubic $\langle 111 \rangle$ to build a rhombohedral unit cell, possesses G-type antiferromagnet order with the moments confined to a plane perpendicular to the $\langle 111 \rangle$ -polarization

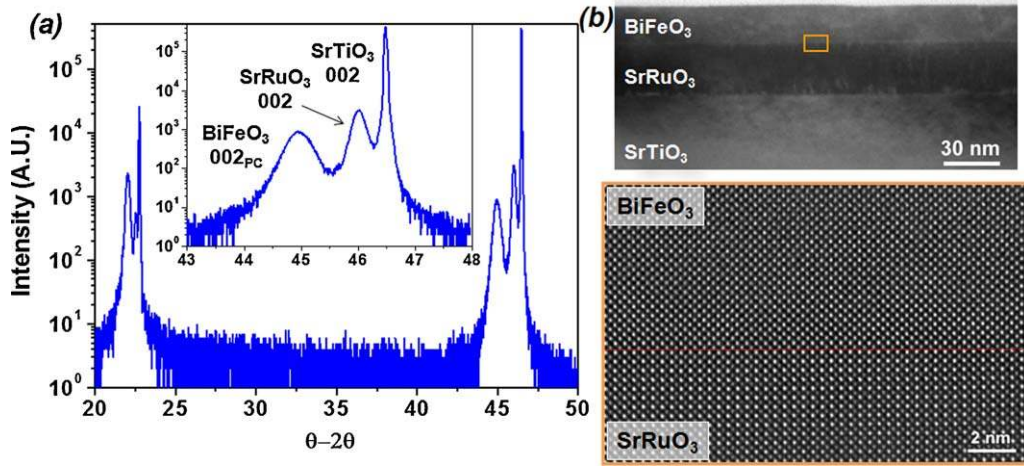


Fig. 25. Thin films of BiFeO_3 . (a) X-ray diffraction results from a fully epitaxial, single phase BFO/SRO/STO(0 0 1) heterostructure. (b) Low (top) and high (bottom) resolution transmission electron microscopy images of BFO/SRO/STO(0 0 1) heterostructure. (Adapted from Ref. [285].)

directions, and possesses symmetry that permits a small canting of the moments in the structure resulting in a weak ferromagnetic moment of the Dzyaloshinskii–Moriya type [348,349]. Also recall that Ederer and Spaldin suggested that only one easy magnetization axis in the energetically degenerate 1 1 1-plane might be selected when one was to strain the material [352]. Thus, one critical question concerning magnetism in multiferroics such as BFO that is of both fundamental and technological importance is how this order parameter develops with strain and size effects?

Using angle and temperature dependent dichroic measurements and photoemission spectromicroscopy, Holcomb et al. [366] have discovered that the antiferromagnetic order in BFO evolves and changes systematically as a function of thickness and strain. Lattice mismatch induced strain is found to break the easy-plane magnetic symmetry of the bulk and leads to an easy axis of magnetization which can be controlled via the sign of the strain—1 1 0-type for tensile strain and 1 1 2-type for compressive strain. This understanding of the evolution of magnetic structure and the ability to manipulate the magnetism in this model multiferroic has significant implications for eventual utilization of such magnetoelectric materials in applications.

6.4.3.4. Role of domain walls in BiFeO_3 . A number of recent findings are poised to definitively answer the questions surrounding the wide array of magnetic properties observed in BFO thin films. There is now a growing consensus that epitaxial films (with a thickness less than ~ 100 nm) are highly strained and thus the crystal structure is more akin to a monoclinic phase rather than the bulk rhombohedral structure. Furthermore, a systematic dependence of the ferroelectric domain structure in the film as a function of the growth rate has been observed [367]. Films grown very slowly (for example by MBE, laser-MBE, or off-axis sputtering) exhibit a classical stripe-like domain structure that is similar to ferroelastic domains in tetragonal $\text{Pb}(\text{Zr}_x\text{Ti}_{1-x})\text{O}_3$ films. Due to symmetry considerations, two sets of such twins are observed. These twins are made up of 71° ferroelastic walls, that form on the {1 0 1}-type planes (which is a symmetry plane). In contrast, if the films are grown rapidly (as was done in the original work of Wang et al. [288]) the domain structure is dramatically different. It now resembles a mosaic-like ensemble that consists of a dense distribution of 71° , 109° , and 180° domain walls. It should be noted that 109° domain walls form on {0 0 1}-type planes (which is not a symmetry plane for this structure). Preliminary measurements reveal a systematic difference in magnetic moment between samples possessing different types and distributions of domain

walls. The work of Martin et al. [367] suggests that such domain walls could play a key role in the many observations of enhanced magnetic moment in BFO thin films.

This suggestion builds off of the work of Přivratská and Janovec [368,369], where detailed symmetry analyses were used to make the conclusion that magnetoelectric coupling could lead to the appearance of a net magnetization in the middle of antiferromagnetic domain walls. Specifically, they showed that this effect is allowed for materials with the $R3c$ space group (i.e., that observed for BFO). Although such analysis raises the possibility of such an effect, the group-symmetry arguments do not allow for any quantitative estimate of that moment. The idea that novel properties could occur at domain walls in materials presented by Přivratská and Janovec is part of a larger field of study of the morphology and properties of domains and their walls that has taken place over the last 50 years with increasing recent attention given to the study novel functionality at domain walls [370–372]. For instance, recent work has demonstrated that spin rotations across ferromagnetic domain walls in insulating ferromagnets can induce a local polarization in the walls of otherwise non-polar materials [372,373], preferential doping along domain walls has been reported to induce 2D superconductivity in WO_{3-x} [374] and enhanced resistivity in phosphates [375], while in paraelectric (non-polar) SrTiO_3 the ferroelastic domain walls appear to be ferroelectrically polarized [376]. Taking this idea one step further, Daraktchiev et al. [377,378] have proposed a thermodynamic (Landau-type) model with the aim of quantitatively estimating whether the walls of BFO can be magnetic and, if so, to what extent they might contribute to the observed enhancement of magnetization in ultrathin films. One can develop a simple thermodynamic potential incorporating two order parameters expanded up to P^6 and M^6 terms (the transitions in BFO are found experimentally to be first order, and the low-symmetry ($\pm P_0, 0$) phase is described here) with biquadratic coupling between the two order parameters (biquadratic coupling is always allowed by symmetry, and therefore always present in any system with two order parameters). Because biquadratic free energy terms such as P^2M^2 are scalars in any symmetry group, this potential can be written thusly:

$$\begin{aligned}
 G_{MP} &= G_0 + \frac{\kappa}{2}(\nabla P)^2 + \frac{\lambda}{2}(\nabla M)^2 + L_{MP}(P, M) \\
 &= G_0 + \frac{\kappa}{2}(\nabla P)^2 + \frac{\lambda}{2}(\nabla M)^2 + \frac{\alpha}{2}P^2 + \frac{\beta}{4}P^4 + \frac{\eta}{6}P^6 + \frac{a}{2}M^2 \\
 &\quad + \frac{b}{4}M^4 + \frac{n}{6}M^6 + \frac{\gamma}{2}P^2M^2
 \end{aligned} \tag{9}$$

When one goes from $+P$ to $-P$, it is energetically more favorable for the domain wall energy trajectory not to go through the centre of the landscape ($P = 0, M = 0$), but to take a diversion through the saddle points at $M_0 \neq 0$, thus giving rise to a finite magnetization (Fig. 26). The absolute values of the magnetic moment at the domain wall will depend on the values of the Landau coefficients as well as the boundary conditions imposed on the system, namely whether the material is magnetically ordered or not. Analysis of the phase space of this thermodynamic potential shows that it is possible for net magnetization to appear in the middle of ferroelectric walls even when the domains themselves are not ferromagnetic (Fig. 26(b)). The authors of this model note, however, that it is presently only a “toy model” which does not take into account the exact symmetry of BFO, so it cannot yet quantitatively estimate how much domain walls can contribute to the magnetization. The exact theory of magnetoelectric coupling at the domain walls of BFO also remains to be formulated.

Recently, a holistic picture of the connection between processing, structure, and properties has brought to light the role of magnetism at ferroelectric domain walls in determining the magnetic properties in BFO thin films. By controlling domain structures through epitaxial growth constraints and probing these domain walls with exchange bias studies, X-ray magnetic dichroism based spectromicroscopy, and high resolution transmission electron microscopy He et al. [379] have demonstrated that the formation of certain types of ferroelectric domain walls (i.e., 109° walls) can lead to enhanced magnetic moments in BFO. Building off the work of Martin et al. [367], the authors of this study were able to demonstrate that samples possessing 109° domain walls show significantly enhanced circular dichroism that is consistent with collective magnetic correlations, while samples with only 71° domain walls show no circular dichroism. In summary, it appears certain domain walls can give rise to enhanced magnetic behavior in BFO thin films.

It is also important to note that Seidel et al. [380], motivated by the desire to understand similar magnetic properties at domain walls in BFO, undertook a detailed scanning probe-based study of these materials and discovered a new and previously unanticipated finding: the observation of room temperature electronic conductivity at certain ferroelectric domain walls. The origin of the observed conductivity was explored using high-resolution transmission electron microscopy and first-principles density functional computations. The results showed that domain walls in a multiferroic ferroelectric such as BFO, can exhibit unusual

electronic transport behavior on a local scale that is quite different from that in the bulk of the material. Using a model (1 1 0)-oriented BFO/SRO/STO heterostructure with a smooth surface (Fig. 27(a)), the researchers were able to switch the BFO material in such a way that enabled them to create all the different types of domain walls possible in BFO (i.e., 71° , 109° , and 180° domain walls) in a local region (Fig. 27(b) and (c)). Conducting-atomic force microscopy (c-AFM) measurements (Fig. 27(d)) revealed conduction at 109° and 180° domain walls. Detailed high-resolution transmission electron microscopy studies (Fig. 27(e)) revealed this conductivity was, in part, structurally induced and can be activated and controlled on the scale of the domain wall width—about 2 nm in BFO. From the combined study of conductivity measurements, electron microscopy analysis, and density functional theory calculations, two possible mechanisms for the observed conductivity at the domain walls have been suggested: (1) an increased carrier density as a consequence of the formation of an electrostatic potential step at the wall; and/or (2) a decrease in the band gap within the wall and corresponding reduction in band offset with the c-AFM tip. It was noted that both possibilities are the result of structural changes at the wall and both may, in principle, be acting simultaneously, since they are not mutually exclusive.

6.4.3.5. Magnetoelectric coupling in BiFeO_3 . Although many researchers anticipated strong magnetoelectric coupling in BFO, until the first evidence for this coupling in 2003 there was no definitive proof. Two years after this first evidence, a detailed report was published in which researchers observed the first visual evidence for electrical control of antiferromagnetic domain structures in a single phase multiferroic at room temperature. By combining X-ray photoemission electron microscopy (PEEM) imaging of antiferromagnetic domains (Fig. 28(a) and (b)) and piezoresponse force microscopy (PFM) imaging of ferroelectric domains (Fig. 28(c) and (d)) the researchers were able to observe direct changes in the nature of the antiferromagnetic domain structure in BFO with application of an applied electric field (Fig. 28(e)) [381]. This research showed that the ferroelastic switching events (i.e., 71° and 109°) resulted in a corresponding rotation of the magnetization plane in BFO (Fig. 28(f)) and has paved the way for further study of this material in attempts to gain room temperature control of ferromagnetism (to be discussed in detail later). This work has since been confirmed by neutron diffraction experiments in bulk BFO as well [382].

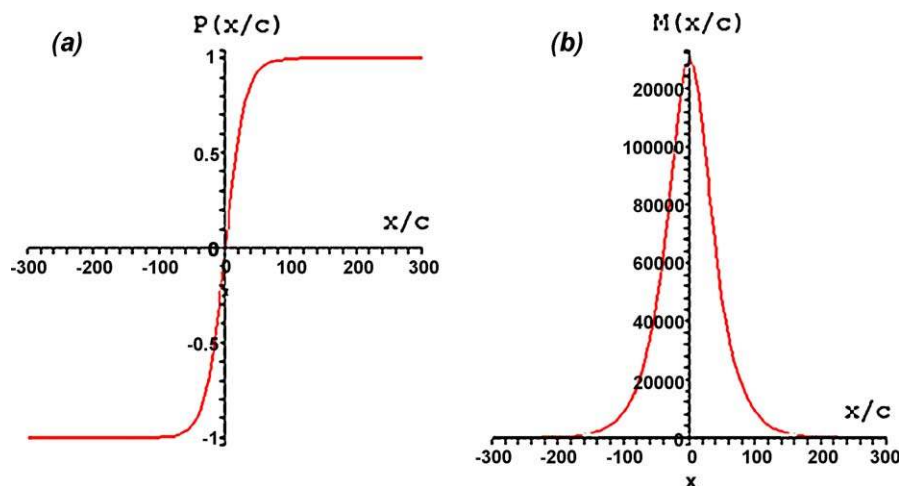


Fig. 26. Shape of ferroelectric polarization and magnetism across a domain wall in BiFeO_3 . (a) Ferroelectric polarization goes to zero at the center of the domain wall. (b) A net magnetization appears at the center of the domain wall even though the domains themselves do not possess a net moment. (Adapted from Refs. [377,378].)

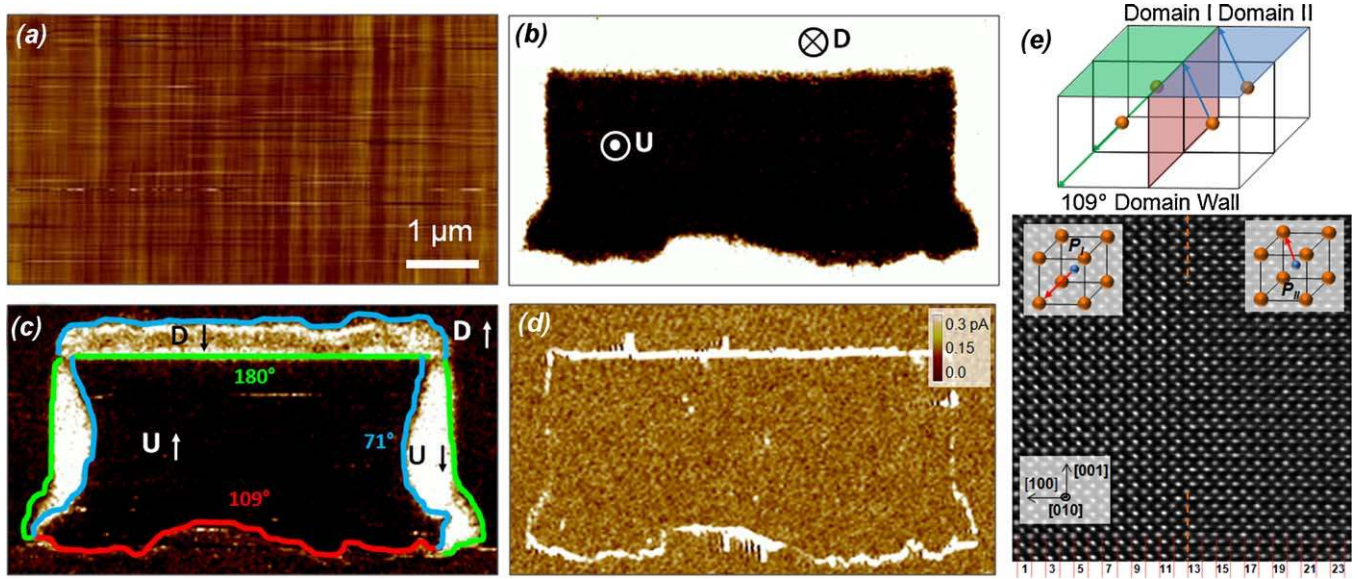


Fig. 27. Conduction at domain walls in BiFeO₃. (a) Topographic image of the surface of a model (1 1 0)-oriented BiFeO₃/SrRuO₃/SrTiO₃ (1 1 0) sample as image via atomic force microscopy. Corresponding out-of-plane (b) and in-plane (c) piezoresponse force microscopy images of a switch portion of the same film. Domain wall types and locations are labeled. (d) Conducting-atomic force microscopy image of switched portion of the film reveals certain types (name 109° and 180° domain walls) that conduct. (e) Schematic illustration of a 109° domain wall and corresponding high-resolution transmission electron microscopy image of a 109° domain wall. Analysis reveals the presence of a net polarization perpendicular to the domain wall and a change in the local structure at the domain wall – both of which could give rise to enhanced conduction. (Adapted from Ref. [380].)

6.4.3.6. Doped BiFeO₃ thin films. In the last few years, attention has also been given to studying doped BFO thin films (both *A*-site and *B*-site doping) in an attempt to reduce leakage currents and alter the magnetic properties [383]. Doping the *B*-site of BFO with Ti⁴⁺ has been shown to lead to an increase in film resistivity by over three orders of magnitude while doping with Ni²⁺ has been shown to decrease resistivity by over two orders of magnitude [384]. Likewise, doping with Cr has also been shown to greatly reduce leakage currents in BFO films [385]. Although there have been a number of studies focusing on doping BFO, little significant impact on the physical properties has been achieved until very recently. In 2009, Yang et al. [386], building off of the prior observation of the development of interesting materials phenomena such as high-*T_C* superconductivity in the cuprates and colossal magnetoresistance in the manganites arise out of a doping-driven competition between energetically similar ground states, investigated doped multiferroics as a new example of this generic concept of phase competition. The results were the observation of an electronic conductor–insulator transition by control of band-filling in Ca-doped BFO. Application of electric field enables us to control and manipulate this electronic transition to the extent that a p–n junction can be created, erased and inverted in this material. A ‘dome-like’ feature in the doping dependence of the ferroelectric transition is observed around a Ca concentration of 1/8, where a new pseudo-tetragonal phase appears and the electric modulation of conduction is optimized (Fig. 29(a)). c-AFM images (Fig. 29(b)) reveal that upon application of an electric field the material becomes conducting and that subsequent application of electric fields can reversibly turn the effect on and off. It has been proposed that this observation could open the door to merging magnetoelectrics and magnetoelectronics at room temperature by combining electronic conduction with electric and magnetic degrees of freedom already present in the multiferroic BFO. Fig. 29(c) shows the quasi-non-volatile and reversible modulation of electric conduction accompanied by the modulation of the ferroelectric state. The mechanism of this modulation in Ca-doped BFO is based on electronic conduction as a consequence of the naturally produced oxygen vacancies that act as donor impurities to

compensate Ca acceptors and maintain a highly stable Fe³⁺ valence state.

6.4.4. Other single phase multiferroic thin films

Finally, we note that a number of other candidate multiferroic materials with lone-pair active *A*-sites and magnetic transition metal *B*-sites have been produced in the last few years. As early as 2002, Hill et al. [387] had predicted BiCrO₃ to be antiferromagnetic and antiferroelectric, but not until 2006 were thin films of this material produced. Thin films of BiCrO₃ were grown on LaAlO₃ (0 0 1), SrTiO₃ (0 0 1), and NdGaO₃ (1 1 0) substrates and were shown to be antiferromagnetic, displaying weak ferromagnetism, with an ordering temperature of ~120–140 K. Early reports suggested that these films showed piezoelectric response and a tunable dielectric constant at room temperature [388] while others suggested that the films were antiferroelectric as predicted in theory [389]. Other phases of interest include BiCoO₃. Bulk work on BiCoO₃ [390] and theoretical predictions of giant electronic polarization of more than 150 μC/cm² [391] have driven researchers to attempt creating this phase as a thin film as well. To date only solid solutions of BiFeO₃–BiCoO₃ have been grown via MOCVD [392]. Another phase similar to BiCoO₃ that has been produced as a thin film is PbVO₃ [393]. PbVO₃ films were grown on LaAlO₃, SrTiO₃, (La_{0.18}Sr_{0.82})(Al_{0.59}Ta_{0.41})O₃, NdGaO₃, and LaAlO₃/Si substrates and were found to be a highly tetragonal perovskite phase with a *c/a* lattice parameter ratio of 1.32 (Fig. 30). Further analysis of this material using second harmonic generation and X-ray dichroism measurements revealed that PbVO₃ is both a polar, piezoelectric and likely an antiferromagnet below ~130 K [394]. There has also been attention given to double-perovskite structures such as Bi₂NiMnO₆ which have been shown to be both ferromagnetic (*T_C* ~ 100 K) and ferroelectric with spontaneous polarization of ~5 μC/cm² [395].

6.4.5. Horizontal multilayer heterostructures

Great strides have been made in the area of composite magnetoelectric systems. These systems operate by coupling the magnetic and electric properties between two materials, generally

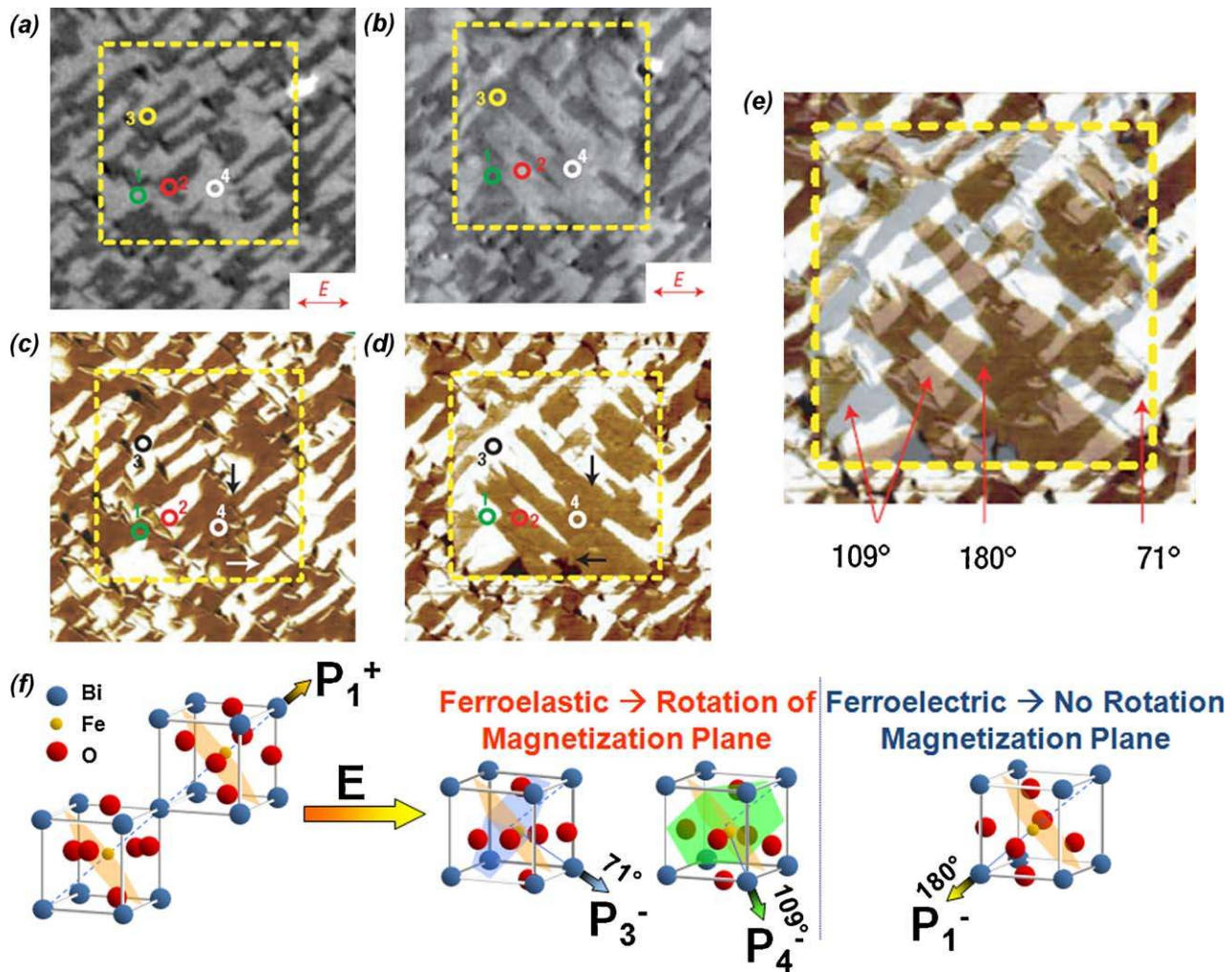


Fig. 28. Determination of strong magnetoelectric coupling in BiFeO₃. Photomission electron microscopy (PEEM) images before (a) and after (b) electric field poling. The arrows show the X-ray polarization direction during the measurements. In-plane PFM images before (c) and after (d) electric field poling. The arrows show the direction of the in-plane component of ferroelectric polarization. Regions 1 and 2 (marked with green and red circles, respectively) correspond to 109° ferroelectric switching, whereas 3 (black and yellow circles) and 4 (white circles) correspond to 71° and 180° switching, respectively. In regions 1 and 2 the PEEM contrast reverses after electrical poling. (e) A superposition of in-plane PFM scans shown in c and d used to identify the different switching mechanisms that appear with different colors and are labeled in the figure. (Adapted from Ref. [381].) (f) Schematic illustration of coupling between ferroelectricity and antiferromagnetism in BiFeO₃. Upon electrically switching BiFeO₃ by the appropriate ferroelastic switching events (i.e., 71° and 109° changes in polarization) a corresponding change in the nature of antiferromagnetism is observed. (Adapted from Ref. [285].) (For interpretation of the references to colour in this figure legend, the reader is referred to the web version of the article.)

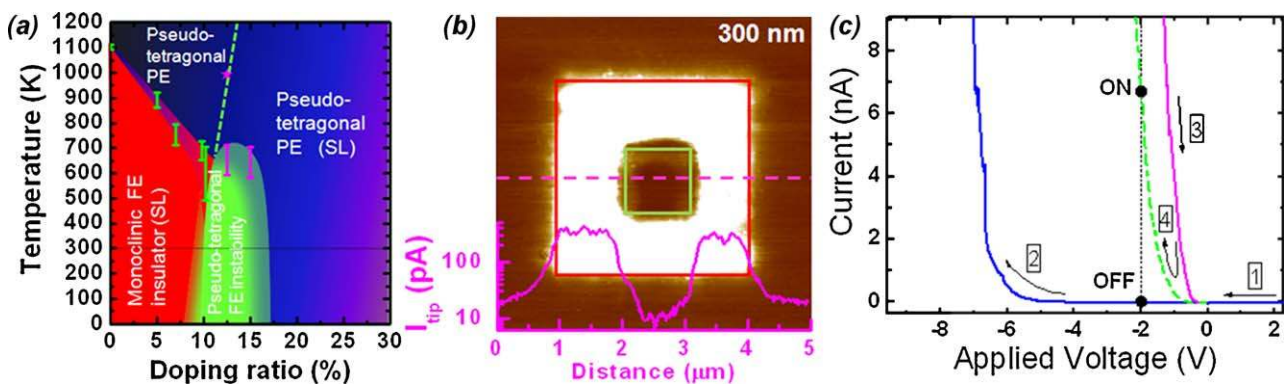


Fig. 29. Evolution of properties in doped multiferroics. (a) Pseudo-phase diagram of the evolution of structure and properties in Ca-doped BiFeO₃. (b) Conducting-atomic force microscopy image of an electrically poled and re-poled area of the doped BiFeO₃ film. In the as-grown state (outside red box), the sample is insulating in nature, in the electrically poled area (inside red and outside green box) the same has become conducting, and finally in the area that has been poled both up and down (inside green box) the sample is again insulating. (c) Illustration of the process to create a multi-state memory from these physical properties. (Adapted from Ref. [386].) (For interpretation of the references to colour in this figure legend, the reader is referred to the web version of the article.)

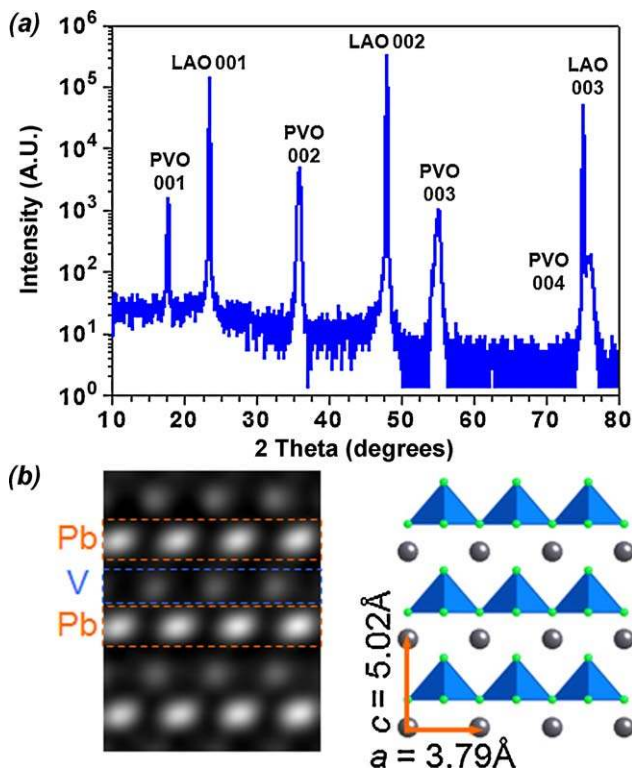


Fig. 30. Other multiferroics – PbVO₃. (a) X-ray diffraction of a fully epitaxial PbVO₃/LaAlO₃ (0 0 1) thin film. (b) High resolution, cross-sectional transmission electron microscopy image of the PbVO₃ structure along with a schematic illustration of the large c/a lattice parameter distortion in this super tetragonal phase. (Adapted from Ref. [393].)

a ferroelectric material and a ferrimagnetic material, via strain. An applied electric field creates a piezoelectric strain in the ferroelectric, which produces a corresponding strain in the ferrimagnetic material and a subsequent piezomagnetic change in magnetization or the magnetic anisotropy. Work started in the

field several decades ago using bulk composites, although experimental magnetoelectric voltage coefficients were far below those calculated theoretically [396]. In the 1990s theoretical calculations showed possible strong magnetoelectric coupling in a multilayer (2-2) configuration; an ideal structure to be examined by the burgeoning field of complex oxide thin-film growth [397]. In this spirit, researchers experimentally tested a number of materials in a laminate thick-film geometry, including ferroelectrics such as Pb(Zr_xTi_{1-x})O₃, [398–403] Pb(Mg_{0.33}Nb_{0.67})O₃–PbTiO₃ (PMN–PT), [404] and ferromagnets such as TbDyFe₂ (Terfenol-D) [398], NiFe₂O₄ [399,401], CoFe₂O₄ [403], Ni_{0.8}Zn_{0.2}Fe₂O₄ [400], La_{0.7}Sr_{0.3}MnO₃ [402], La_{0.7}Ca_{0.3}MnO₃ [402], and others. These experiments showed great promise and magnetoelectric voltage coefficients up to $\Delta E/\Delta H = 4680$ mV/cm Oe have been observed. Work also continued investigating thin-film heterostructures by combining such ferroelectrics as Ba_{0.6}Sr_{0.4}TiO₃, BaTiO₃ [405], and PMN–PT [406] with ferromagnets such as Pr_{0.85}Ca_{0.15}MnO₃ [405] and Tb–Fe/Fe–Co multilayers [406]; however, these attempts were unable to produce magnetoelectric voltage coefficients above a few tens of mV/cm Oe. Current theories suggest that the in-plane magnetoelectric interface is limiting the magnitude of this coefficient due to the clamping effect of the substrate on the ferroelectric phase [407]. Since the amount of strain that can be imparted by the ferroelectric phase is limited via this in-plane interfacial geometry, the magnetoelectric voltage coefficient can be reduced by up to a factor of five.

6.4.6. Vertical nanostructures

A seminal paper by Zheng et al. [408] showed that magnetoelectric materials could also be fabricated in a nanostructured columnar fashion (Fig. 31(a)). By selecting materials that spontaneously separate due to immiscibility, such as spinel and perovskite phases [396], one can create nanostructured phases made of pillars of one material embedded in a matrix of another. In this initial paper, researchers reported structures consisting of CoFe₂O₄ pillars embedded in a BaTiO₃ matrix. The large difference in lattice parameter between these phases leads to the formation of pillars with dimensions on the order of tens of nanometers, which

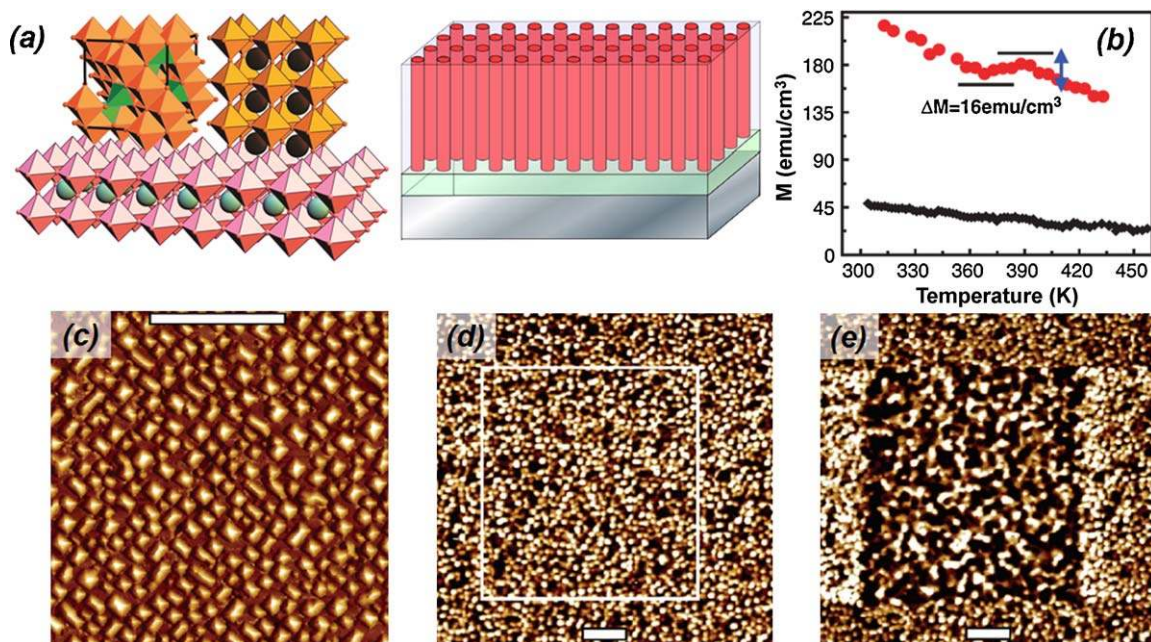


Fig. 31. Multiferroic nanostructures. (a) Schematic illustrations of vertical nanostructure of spinel pillars embedded in a perovskite matrix grown on a perovskite substrate. (b) Magnetization versus temperature curve measured at 100 Oe showing a distinct drop in magnetization at the ferroelectric Curie temperature – proof of strong magnetoelectric coupling. (c) Surface topography of a CoFe₂O₄/BiFeO₃ nanostructure as imaged by atomic force microscopy. Magnetic force microscopy scans taken in the same area before (d) and after electrical poling at –16 V (e) (Scale bars are 1 μm). (Adapted from Refs. [408,418].)

ensures a high interface-to-volume ratio, an important parameter when attempting to couple the two materials via strain. Such structures were shown to exhibit strong magnetoelectric coupling (Fig. 31(b)) via changes in magnetization occurring at the ferroelectric Curie temperature of the matrix material. These nanostructures, in which the interface is perpendicular to the substrate, remove the effect of substrate clamping and allow for better strain-induced coupling between the two phases. An explosion of research into alternate material systems followed as the design algorithm proved to be widely applicable to many perovskite-spinel systems. Nanostructured composites with combinations of a number of perovskite (BaTiO_3 , [409] PbTiO_3 [410], $\text{Pb}(\text{Zr}_x\text{Ti}_{1-x})\text{O}_3$ [411,412], and BiFeO_3 [413,414]) and spinel (CoFe_2O_4 [411,412], NiFe_2O_4 [410,413], and $\gamma\text{-Fe}_2\text{O}_3$ [414]) or corundum ($\alpha\text{-Fe}_2\text{O}_3$ [414]) structures have been investigated. The magnetic properties of such systems are generally well-behaved, but the ferroelectric properties are highly dependent on the synthesis technique. When satisfactory ferroelectric properties can be produced, more substantial magnetoelectric voltage coefficients are generally achieved. Pulsed laser deposition has proven to be a successful growth technique for achieving satisfactory properties in these nanostructured films [409,415,416].

Zavaliche et al. [417] showed $\Delta E/\Delta H = 100 \text{ V/cm Oe}$ at room temperature in a system comprised of CoFe_2O_4 pillars embedded in a BiFeO_3 matrix. These films were analyzed with scanning probe techniques that utilized both magnetized and conducting tips. Typical surface morphology for such samples is shown in Fig. 31(c). Magnetic measurements show the preference of such structures to maintain magnetization along the length of the nanopillars. Magnetic force microscopy scans both before (Fig. 31(d)) and after electric field poling (Fig. 31(e)) show a significant number of CoFe_2O_4 pillars switch their magnetic state from a downward direction to an upward direction upon application of an electric field [418]. This work further showed that the magnetization-switching event was non-deterministic and could be improved by applying a small magnetic field (700 Oe) to the sample. This field is essential to break time reversal symmetry and overcome the degeneracy between the up and down magnetization states. Nonetheless, these structures have been shown to be very versatile and offer an excellent opportunity for electrically controlled magnetic storage.

We also note that other interesting nano-scale composite geometries have been investigated. Using anodized aluminum

oxide templates, Liu et al. [419] successfully synthesized nanowires of NiFe_2O_4 surrounded by a shell of PZT. However, successful magnetoelectric coupling has been not yet shown in such a system. Overall, it has been shown that nanostructured composite multiferroics have shown significantly enhanced magnetoelectric properties over traditional multilayer heterostructures and are excellent candidates for a wide range of devices that would take advantage of the strong magnetoelectric coupling that can be achieved in these structures.

6.5. Engineering new functionalities with multiferroics

One of the major questions in the study of multiferroics today is how and when will multiferroics make their way into a room temperature device and what will these devices look like? In early 2005, a number of what were referred to as *magnetoelectronics* based on magnetoelectric materials were proposed [420]. The idea was a simple one, to use the net magnetic moment created by an electric field in a magnetoelectric thin film to change the magnetization of a neighboring ferromagnetic layer through exchange coupling. The authors went on to propose a number of electrically tunable giant magnetoresistance (GMR) spin valves (Fig. 32(a)) and tunnel magnetoresistance (TMR) (Fig. 32(b)) elements that could be made possible if such structures could be achieved. One additional field that could be greatly affected by this research is the burgeoning field of spintronics. Spin-based electronics, or spintronics, have already found successful application in magnetic read-heads and sensors that take advantage of GMR and TMR effects. The future of spintronics is partially focused on evolving beyond passive magnetoelectronic components, like those used today, to devices which combine memory and logic functions in one [421]. There has been growing interest in studying a direct method for magnetization reversal involving spin transfer from a spin-polarized current injected into the device. This effect has been theoretically predicted by Slonczewski [422,423] and Berger, [424] and has been experimentally confirmed by several groups [425–428]. And it is at this point that the first major stumbling block is met.

6.5.1. Electric field versus current control of magnetism

From these initial experiments and theoretical treatments, it was found that significant current densities (larger than 10^7 A cm^{-2}) were required for switching the orientation of even

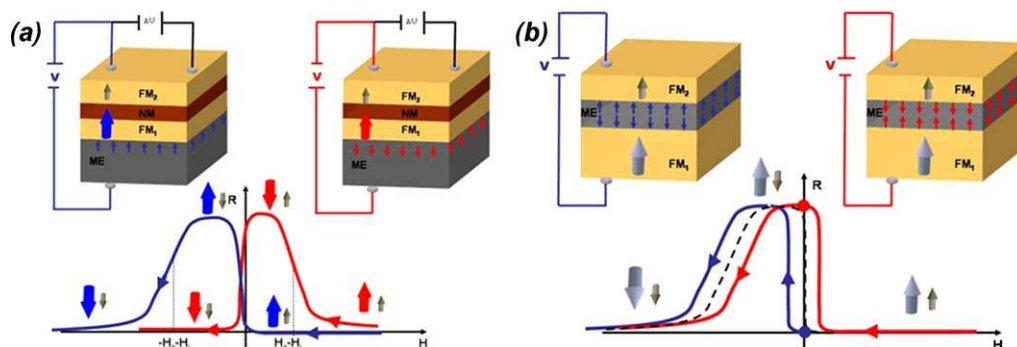


Fig. 32. Multiferroic-based magnetoelectronics. (a) Schematic of the magnetoresistance curve of a GMR device involving a magnetoelectric, multiferroic film as a pinning layer. Half-hysteresis curves are shown, after saturation at positive field values. The change of polarity of the magnetoelectric, multiferroic layer upon application of an electric field changes the direction of the net magnetization of the pinning field. The pinned layer (FM1) switches first at large positive field (red), or second at large negative field (blue). The low field magnetic configuration is therefore either antiparallel (red) or parallel (blue), controlled by the magnetoelectric, multiferroic. (b) Schematic of the magnetoresistance curve of a TMR device involving a magnetoelectric, multiferroic film as a tunnel barrier. Half-hysteresis curves are shown, after saturation at positive field values. The arrows denote the magnetization directions, with the bottom layer FM1 being harder (or pinned) than the top one FM2. The dashed curve is the expected TMR behavior. The change of voltage polarity changes the direction of the net magnetization of the magnetoelectric, multiferroic layer, adding an exchange bias magnetic field to the resistance curve. The two colors indicate shifting of half-hysteresis curves towards positive or negative fields, depending on the polarity of the applied voltage. At zero magnetic field, the change of voltage polarity changes the resistance value of the device (dashed). (Adapted from Ref. [420].) (For interpretation of the references to colour in this figure legend, the reader is referred to the web version of the article.)

a magnetic nanowire [426]. One option is to further scale down materials so that spin-transfer becomes a more attractive alternative to stray magnetic field techniques. In the end, integration of such effects into actual devices has been limited because there are a number of technical difficulties involved in reliably making such small structures, applying such large currents—while avoiding heating of the samples, and based on the fact that the intrinsic sample resistance (on the order of a few ohms) further limits the practical use for GMR devices. Similar issues are found in TMR devices, which are hindered by fact that a large current density must pass through a very thin insulator and the few reports on TMR systems to date have been inconclusive [429,430].

At the heart of what Binek and Doudin [420] were asking in 2005 was whether we should attempt to use currents or some alternative method (i.e., electric field) to create actual devices with new functionalities? Materials discoveries aside, a critical materials physics question emerges from this question that lies at the heart of the last 20 years of research on correlated oxides as well. This has to do with the role of energy scales (as well as time and length scales) of relevance to the ultimate implementation of these materials into actual devices. Let us explore this issue in a bit more detail using the data presented in Fig. 33 for the colossal magnetoresistant (CMR) manganites (data shown here is for $\text{La}_{0.7}\text{Ca}_{0.3}\text{MnO}_3$ (LCMO)) as a frame of reference. Over the past 20 years, there has been extensive research conducted on these materials. By far the most interesting aspect of these very intriguing materials is the large (coined colossal) change in resistance that occurs with the application of a magnetic field of several Tesla (6 T in the present example) (shown in the green data in Fig. 33(a)). It has also been demonstrated that a commensurate “colossal electroresistance” can be obtained with electric fields of the order of a few hundred kV (shown in blue in Fig. 33(a)) [431]. Let us now compare these two energy scales and ask the question: how do these two types of fields compare from the perspective of external power requirements?

We can understand this through a simple thought experiment. If one needed to generate the necessary magnetic field of 6 T at a distance of 1 μm from a metal wire (Fig. 33(b)), a current of ~ 30 A would be required! We note that a 6 T magnetic field translates to a temperature scale in the material of ~ 8 K, [432] which is

significantly smaller than the critical temperatures (for example the magnetic transition temperature or the peak in the resistivity). Regardless, this current is prohibitive both from the point of view of the integrity of the metal wire that would carry the current as well as the power requirements—especially as device sizes are decreased. Let us now examine an alternative pathway to achieve the same effect through the use of an electric field (Fig. 33(c)). If one desires to create the appropriate electric field needed to observe colossal electroresistance in a 100 nm thick film, a potential of only 4 V is required. This is easily generated by standard semiconductor electronics circuitry. However, if the thickness of the material is, say 1 mm, then a potential of 40,000 V is required to generate the same field.

These two scenarios present a number of important considerations. First, if the energy scales for manipulation of these materials (be they CMR or multiferroics) do not become significantly smaller, then the use of magnetic fields to probe and manipulate them becomes technologically prohibitive. Indeed, this can be identified as the most important reason why CMR based systems have not become commercially viable. Second, if these energy scales are indeed maintained, it is clear that using thin film heterostructures and manipulating them with electric fields is a more attractive way to proceed in terms of technological manifestations of these phenomena. These ideas form the technological foundation for the next section of our treatment—a detailed look at the evolution of the ideas of Binek and Doudin to the first generation of multiferroic-based devices for next generation technologies.

6.5.2. Electric field control of ferromagnetism

The overall motivating question for this section is a simple one: can we deterministically control ferromagnetism at room temperature with an electric field? One possible solution to this question is to utilize heterostructures of existing multiferroic materials, such as BFO, to create new pathways to functionalities not presented in nature. Such a concept is illustrated in Fig. 34. The idea is to take advantage of two different types of coupling in materials—intrinsic magnetoelectric coupling like that in multiferroic materials such as BFO which will allow for electrical control of antiferromagnetism and the extrinsic exchange coupling between ferromagnetic and antiferromagnetic materials—to create new functionalities in materials (Fig. 34(a)). By utilizing these

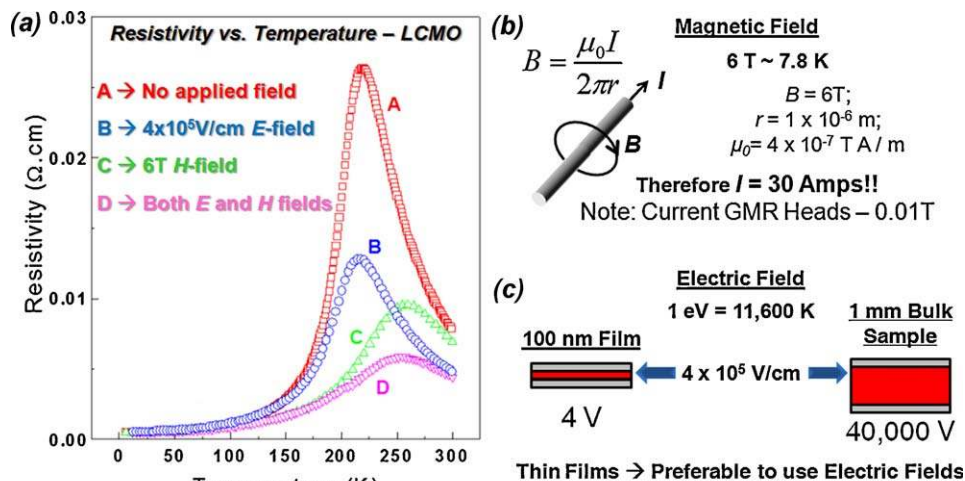


Fig. 33. Motivation for electric field control of properties. (a) Resistivity versus temperature for $\text{La}_{0.7}\text{Ca}_{0.3}\text{MnO}_3$ thin films with no applied field (red), applied electric field (blue), applied magnetic field (green), and both applied electric and magnetic fields (pink). Energy scales in materials dictate the eventual incorporation of such materials into device structures. (b) The production of the large magnetic fields (~ 6 T) required for colossal magnetoresistance in CMR materials requires large currents (~ 30 A) while (c) production of the appropriate electric fields to produce colossal electroresistance (~ 4 V for a 100 nm thick thin film) are much more reasonable and possible in standard semiconductor electronics circuitry. (Adapted from Ref. [431].) (For interpretation of the references to colour in this figure legend, the reader is referred to the web version of the article.)

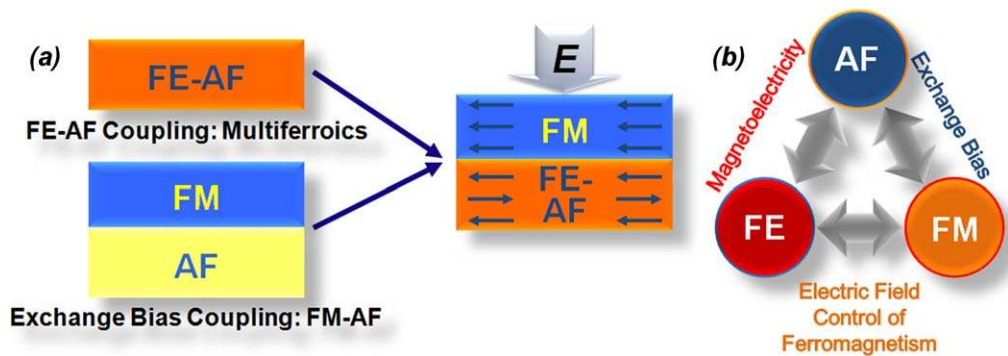


Fig. 34. Schematics illustrating the design algorithm for gaining electrical control of ferromagnetism. (a) By combining multiferroics together with traditional ferromagnets, we can create heterostructures that might have new functionalities. (b) These structure rely on two types of coupling – magnetoelectric and exchange bias – to gain electrical control of ferromagnetism. (Adapted from Ref. [285].)

different types of coupling we can then effectively couple ferroelectric and ferromagnetic order at room temperature and create an alternative pathway to electrical control of ferromagnetism (Fig. 34(b)). But what exactly are the opportunities for using multiferroics to gain electrical control over interactions like exchange bias anisotropy? Until recently the materials and the understanding of the appropriate materials did not exist to make this a plausible undertaking. Let us investigate, in detail, the work done in this field of study.

6.5.3. Exchange bias with multiferroic antiferromagnets

In the time since the proposal of these magnetoelectronics, studies have been done on a number of multiferroic materials. Among the earliest work was a study of heterostructures of the soft ferromagnet permalloy on YMO [433]. This report found that, indeed, the multiferroic layer could be used as an antiferromagnetic pinning layer that gives rise to exchange bias and enhanced coercivity, but suggested that YMO would likely be an inappropriate choice for continued study as these values varied greatly with crystal orientation and rendered actual device generation unlikely. Soon after this initial result, Marti et al. [434] reported the observation of exchange bias in all-oxide heterostructure of the ferromagnet SRO and the antiferromagnetic, multiferroic YMO. In both of these studies, the exchange bias existed only at very low

temperatures due to the low magnetic ordering temperature of the YMO. Around the same time, the first studies using BFO as the multiferroic, antiferromagnetic layer were appearing with hopes that these intriguing properties could be extended to high temperatures. As part of this Dho et al. [435] showed the existence of exchange bias in spin-valve structures based on permalloy and BFO at room temperature and Béa et al. [436] extended this idea to demonstrate how BFO films could be used in first generation spintronics devices. This work included the use of ultrathin BFO tunnel barriers in magnetic tunnel junctions with LSMO and Co electrodes where positive TMR up to $\sim 30\%$ was observed at 3K and also demonstrated that room temperature exchange bias could be generated using CoFeB/BFO heterostructures. Finally, Martin et al. [437] reported the growth and characterization of exchange bias and spin valve heterostructures based on $\text{Co}_{0.9}\text{Fe}_{0.1}$ /BFO heterostructures on Si substrates. In this work large negative exchange bias values (typically 150–200 Oe in magnitude) were observed along with the absence of a training effect – or a systematic decrease in the magnitude of the exchange bias with repeated magnetic cycling (confirming the results of Béa et al. [436]) – even with over 14,000 magnetic cycles. This work also demonstrated room temperature magnetoresistance of $\sim 2.25\%$ for spin valve structures of 2.5 nm CoFe/2 nm Cu/5 nm CoFe/100 nm BFO (Fig. 35). What these initial studies established was that exchange

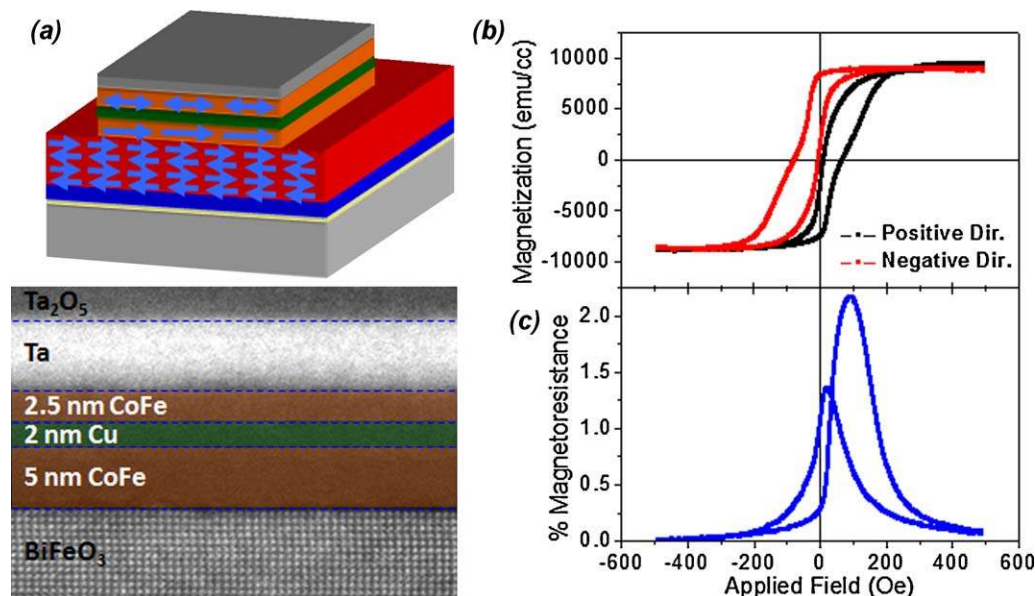


Fig. 35. Spin valve structures based on $\text{Co}_{0.9}\text{Fe}_{0.1}/\text{Cu}/\text{Co}_{0.9}\text{Fe}_{0.1}/\text{BiFeO}_3$ heterostructures. (a) Schematic illustration and scanning transmission electron microscopy image of the actual device. (b) Magnetic hysteresis loops of spin valve structures. (c) Current-in-plane magnetoresistance measurements. (Adapted from Ref. [437].)

bias with antiferromagnetic multiferroics was possible in a static manner, but these studies had not yet demonstrated dynamic control of exchange coupling in these systems.

A first attempt at this concept was done by Borisov et al. [438] who reported that they could affect changes on the exchange bias field in Cr_2O_3 (1 1 1)/(Co/Pt)₃ heterostructures by using the magnetoelectric nature of the substrate (Cr_2O_3) and a series of different cooling treatments with applied electric and magnetic fields. A unique aspect of this work was the ability to change the sign of the exchange bias with different field cooling treatments. Dynamic switching of the exchange bias field with an applied electric field, however, remained elusive until a report by Laukhin et al. [439] focusing on YMO at 2 K. Utilizing heterostructures of permalloy and (0 0 1) YMO films, the authors demonstrated that after cooling samples from 300 to 2 K in an applied field of 3 kOe and at various applied electric field biases, significant changes in the magnitude of magnetization was observed (Fig. 36(a)). Subsequent cycling of the voltage at low temperatures resulted in reversal of the magnetization direction in the heterostructure (Fig. 36(b)).

In the last few years, significant advancement in the understanding of the interactions present in such heterostructures has been presented. Initial reports noted an inverse relationship between domain size in BFO film and the exchange bias measured in CoFeB/BFO heterostructures [440]. This initial report offered

little detail on how the domain structures were controlled and the nature of the domain walls present in the films. A study that soon followed found a correlation not only to the density of domain walls, but to the density of certain types of domain walls [367]. What was observed was the presence of two distinctly different types of magnetic properties for CoFe/BFO heterostructures (Fig. 37(a) and (b)). Through careful control of the growth process – specifically controlling the growth rate of the BFO films – the authors were able to create two starkly different types of domains structures: so called stripe- (Fig. 37(c)) and mosaic-like (Fig. 37(d)) domain structures. These different structures were found to possess vastly different fractions of the different domain walls that can exist in BFO (Fig. 37(e) and (f)). It was observed that not only was there an inverse relationship between domain size and the magnitude of the exchange bias measured (Fig. 37(g)), but that it was directly related to the density and total length of 109° domain walls present in the sample (Fig. 37(h)). In addition to identifying the importance of 109° domain walls in creating exchange bias (and in turn suggesting the relationship with enhanced magnetism in BFO thin films), this report outlined the idea that two distinctly different types of exchange interactions are occurring in these exchange bias heterostructures. The first interaction was called an *exchange bias* interaction and takes place between pinned, uncompensated spin occurring at 109° domain walls in BFO and spins in the CoFe layer. This interaction results in a shift of the magnetic hysteresis loop for the ferromagnetic layer. The second interaction has been called an *exchange enhancement* interaction and it arises from an interaction of the spins in the ferromagnet and the fully compensated (0 0 1) surface of the G-type antiferromagnetic surface of BFO. This interaction results in an enhancement of the coercive field of the ferromagnetic layer.

6.5.3.1. Room temperature electric field control of ferromagnetic domain structures. Utilizing these findings, researchers have moved to create the first room temperature devices designed to enable control of ferromagnetism with an electric field. Initial results point to the ability to utilize the above *exchange enhancement* interaction to deterministically change the direction of ferromagnetic domains by 90° upon application an applied electric field (Fig. 38) [441]. By creating very high quality $\text{Co}_{0.9}\text{Fe}_{0.1}/\text{BFO}/\text{SRO}/\text{STO}$ (0 0 1) heterostructures, the authors were able to demonstrate the first example of a room temperature device structure that utilizes a multiferroic material to access new functionalities in materials. This work also outlined the complexity of such an undertaking. It has become apparent that in order to achieve significant advances with such systems one will need to understand and be able to control (at least at some level) the coupling between the two (in this case dissimilar) materials which requires that one have a perfunctory understanding of the various energies-scales at play (including shape anisotropy effects, how processing effects the interfacial coupling strength, magnetostriction effects, and more). This initial work also demonstrated the importance of length scales in this work as the observed ferromagnetic domain structures were typically much more complex than the underlying ferroelectric domain structures suggesting that diminished feature sizes could give rise to single magnetic domain configurations and therefore a more robust and simple device. In this spirit, current work is focused on making the coupling in such heterostructures more robust in hopes of extending this coupling to high temperatures and producing more deterministic control of electric field switching.

In pursuit of this idea, researchers are also working on understanding how the coupling in such heterostructures are changed in an all-oxide, heteroepitaxially grown structure. Preliminary evidence focused on 20–75 nm BFO/5 nm LSMO/STO (0 0 1) heterostructures suggests that by changing the coupling

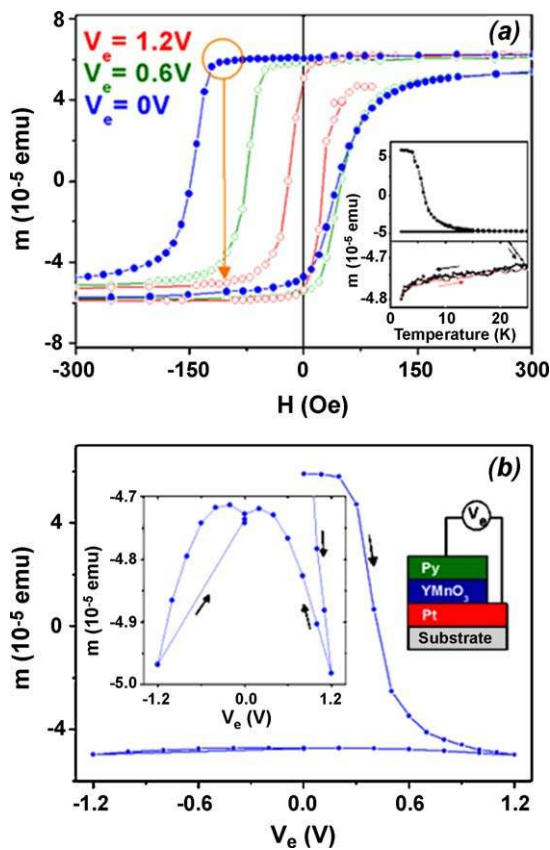


Fig. 36. Low temperature electric field control of ferromagnetism. (a) Magnetization loops for permalloy/YMnO₃/Pt, measured at 2 K, after cooling the sample from 300 K in a 3 kOe field, under various biasing-voltage (V_e) values. The circle and arrow illustrate schematically the expected change of magnetization when biasing the sample by an electric field. The inset shows the temperature dependence of the magnetization at $H = 100$ Oe and $V_e = 0$ when heating the sample from 2 K to 25 K (top panel) and subsequent cooling-heating-cooling cycles between 25 K and 2 K (bottom panel). (b) Dependence of the magnetization on V_e measured at 2 K in $H = 100$ Oe field after cooling the sample from 300 K in 3 kOe field. The inset shows (left) a zoom of the -1.2 V to 1.2 V portions of the bias excursion and (right) a sketch of the sample structure and electric biasing. (Adapted from Ref. [439].)

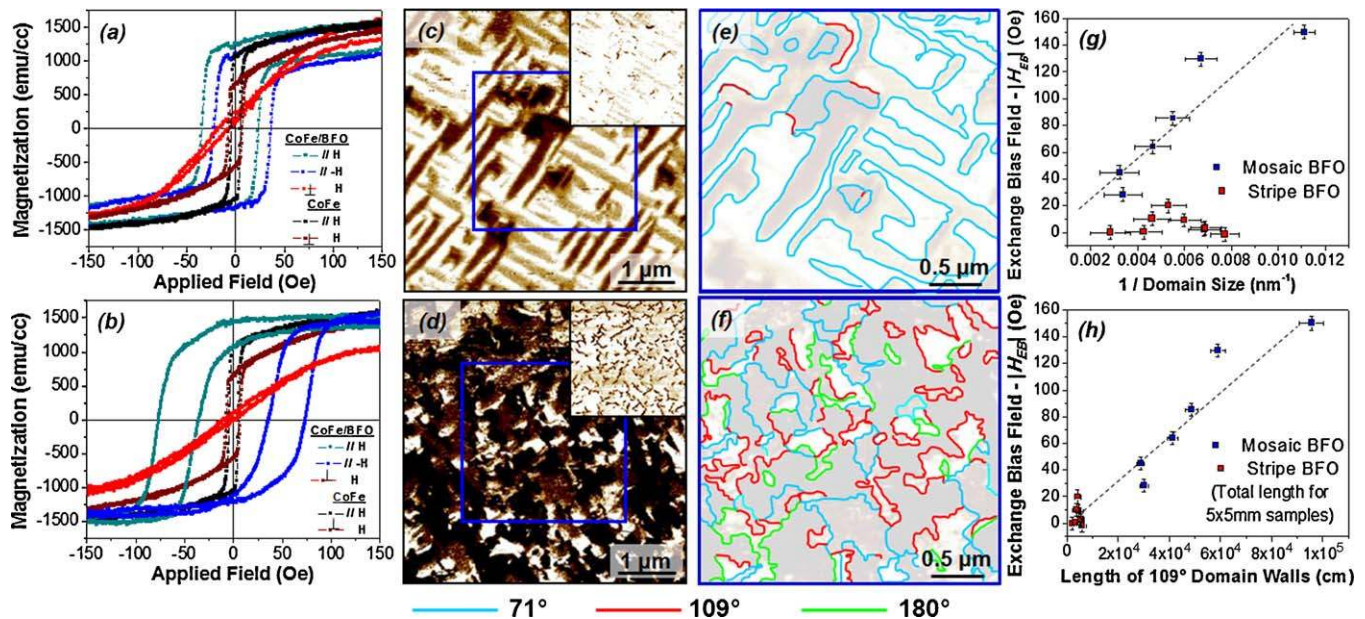


Fig. 37. Domain control of exchange bias. Room temperature magnetic properties for heterostructures exhibiting (a) exchange enhancement and (b) exchange bias properties. In-plane and out-of-plane (inset) PFM contrast for typical BiFeO₃ films that exhibit (c) exchange enhancement and (d) exchange bias, respectively. Detailed domain wall analysis for (e) stripe-like and (f) mosaic-like BFO films. (g) Dependence of exchange bias field on domain size for Co_{0.9}Fe_{0.1}/BiFeO₃ heterostructures grown on mosaic-like (blue) and stripe-like (red) BFO films. (h) Exchange bias field of the same samples here graphed as a function of the total length of 109° domain walls/sample surface area in 5 × 5 mm samples. (Adapted from Ref. [367].) (For interpretation of the references to colour in this figure legend, the reader is referred to the web version of the article.)

from being direct in nature to indirect across an interface possessing a continuous chemical structure (i.e., Mn–O–Fe bonds that extend across the interface) complex interactions can occur (Fig. 39) [442]. This work has shown that, due to the strong coupling between spin, lattice, orbital, and charge degrees-of-freedom in these oxide materials, interactions across these interfaces can become quite complex with changes in bond angle and length, electron density, orbital order, and more dictating the effects observed. In the end, it is such structures, however, that might represent the ultimate manifestation of new functionality if one can engineer and control these different degrees-of-freedom to some effect.

6.6. Advanced multiferroic-based devices

In 2007, Scott offered a brief, but elegant summary of where multiferroic-based devices, especially memory applications, might make an impact [443]. It is important to note that although ferroelectric random access memories (FeRAMs) have achieved fast access speeds (5 ns) and high densities (64 Mb) in a number of different materials, they remain limited by the need for a destructive read and reset operation. By comparison, magnetic random access memories (MRAMs) have been lagging far behind, although Freescale Corporation reported commercial production in 2006 of a smaller MRAM for testing. The appeal of multiferroics

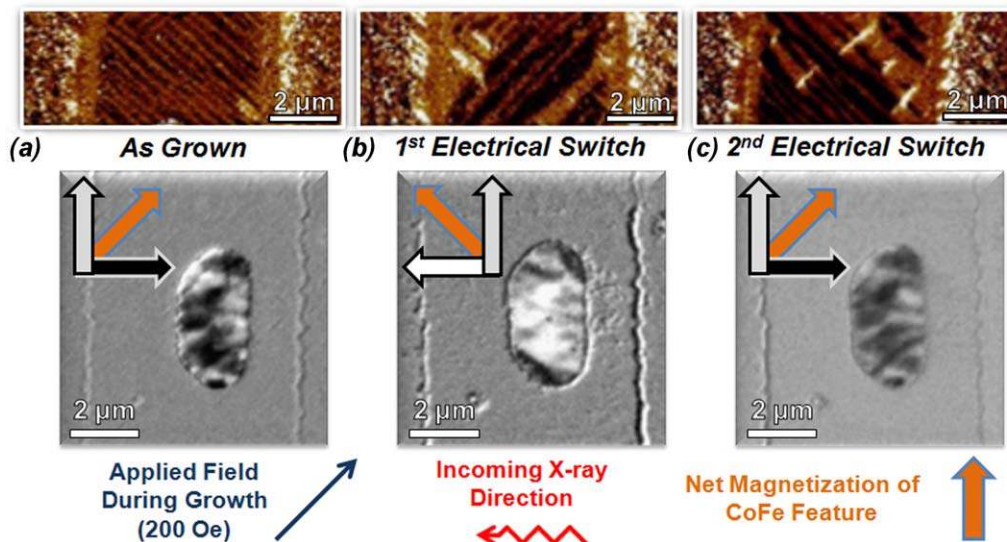


Fig. 38. Electric field control of ferromagnetic domain structures at room temperature. In-plane piezoresponse force microscopy images of ferroelectric domain structure (top) and corresponding photoemission electron microscopy image of ferromagnetic domain structure (bottom) of Co_{0.9}Fe_{0.1} features on BiFeO₃ as a function of applied electric field in the (a) as-grown state, (b) after application of an electric field, and (c) following application of the opposite electric field. This represents the first demonstration of reversible electric field control of ferromagnetic domain structures at room temperature. (Adapted from Ref. [441].)

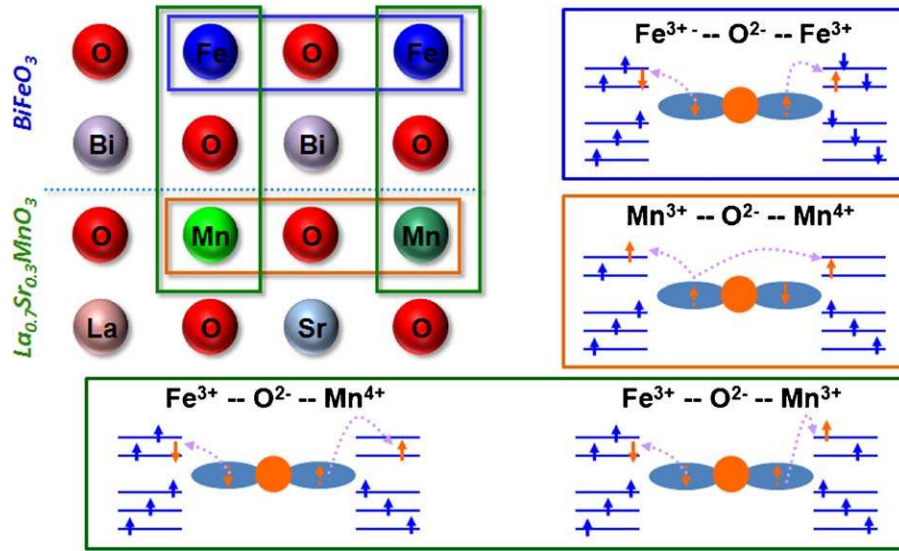


Fig. 39. Magnetic coupling across all-oxide interfaces. Schematic illustrating the complexity of all-oxide interfaces in multiferroic-based heterostructures. In all-oxide heterostructures there is competition between different types of indirect coupling: antiferromagnetic superexchange in BiFeO_3 (blue box), ferromagnetic double exchange in $\text{La}_{0.7}\text{Sr}_{0.3}\text{MnO}_3$ (orange box), and cross-interface coupling between Fe^{3+} – Mn^{3+} and Fe^{3+} – Mn^{4+} (green box). (For interpretation of the references to colour in this figure legend, the reader is referred to the web version of the article.)

is that they offer the possibility of combining the best qualities of FeRAMs and MRAMs: fast low-power electrical write operation, and non-destructive magnetic read operation. At the 256 Mbit level, such memory devices, in the words of Christensen [444], would be a “disruptive technology” and could eliminate competition such as EEPROMs (electrically erasable programmable read-only memories) for applications including megapixel photomemories for digital cameras or audio memories in devices such as mp3 players.

With this in mind, over the last few years, a number of new devices based on multiferroic materials and heterostructures have been demonstrated and proposed. In early 2007, Ju et al. [445] presented a theoretical investigation of an electrically controllable spin filter based on a multiferroic tunnel junction that could be switched between multiple resistance states. Soon after this, Gajek et al. [332] demonstrated the production of four logic states based on ultrathin multiferroic films used as barriers in spin-filter-type tunnel junctions. The junctions were made of $\text{La}_{0.1}\text{Bi}_{0.9}\text{MnO}_3$ which was proven to be both ferroelectric and magnetic down to film

thickness of only 2 nm and the devices exploited the magnetic and ferroelectric degrees of freedom of that layer. The ferromagnetism permitted read operations reminiscent of MRAM and the electrical switching evoked FeRAM write operations without the need for destructive ferroelectric readout. The results (Fig. 40(a)) suggest that it is possible to encode quaternary information by both ferromagnetic and ferroelectric order parameters, and to read it non-destructively by a resistance measurement. This work represented the starting point for future studies on the interplay between ferroelectricity and spin-dependent tunneling using multiferroic barrier layers and, in a wider perspective, suggested a new pathway toward novel reconfigurable logic spintronic architectures.

Soon after this work, Yang et al. [446] proposed that eight different logic states could be achieved by combining spin-filter effects and the screening of polarization charges between two electrodes through a multiferroic tunnel barrier (Fig. 40(b)). In this work, the conductance ratio was found to be dependent on the magnitude of the ferroelectric polarization, exchange splitting,

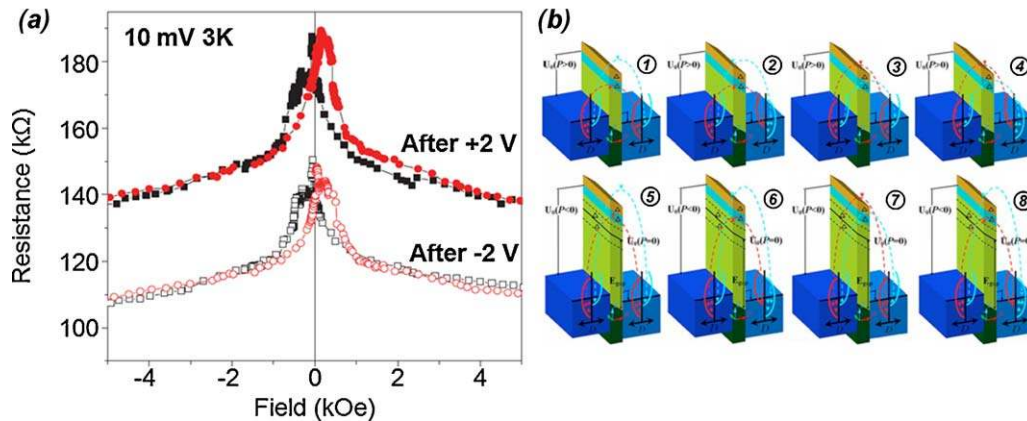


Fig. 40. Multiferroic-based devices. (a) Tunnel magnetoresistance curves at 4 K at $V_{dc} = 10$ mV in an $\text{La}_{2/3}\text{Sr}_{1/3}\text{MnO}_3/\text{La}_{0.1}\text{Bi}_{0.9}\text{MnO}_3$ (2 nm)/Au junction, after applying a voltage of +2 V (filled symbols) and –2 V (open symbols). The combination of the electroresistance effect and the tunnel magnetoresistance produces a four-resistance-state system. (Adapted from Ref. [332].) (b) The sketch of the potential profiles for each of the eight configurations of a multiferroic-based tunnel junction. Here, the red and light blue arrows denote majority- and minority-spin carriers, D displays the electronic density of states. (Adapted from Ref. [446].)

barrier width, and bias voltage. In 2009, Jia and Berakdar [447] proposed a modified spin-field-effect transistor fabricated in a two-dimensional electron gas (2DEG) formed at the surface of multiferroic oxides with a transverse helical magnetic order. The local magnetic moments in the oxide are said to induce a resonant momentum-dependent effective spin-orbit interaction acting on the 2DEG and thus the carrier spin precession is dependent on the magnetic spin helicity that can be electrically controlled in the multiferroic. Such a device could, in turn, be used as a nanometer-scale, decoherence-suppressed spin field-effect transistor and as a nanometer flash-memory device.

7. Future directions and conclusions

We hope that this review has captured some of the exciting new developments in the field of complex oxides, multiferroics and magnetoelectrics, especially from a thin film perspective. New developments are occurring at a rapid pace, throwing further light onto the intricacies of these materials. The dramatic progress in thin film heterostructure and nanostructure growth has been a key enabler fueling these discoveries. Since the advent of the superconducting cuprates, complex oxides have emerged as wonderful tools to probe the role of complexity induced by the interactions between the spin, charge, orbital, and lattice degrees of freedom that are pervasive in transition metal oxides. Soon after the cuprates, work on ferroelectric oxides emerged, followed by the colossal magnetoresistance effect in the doped manganites. It is critical to note that although more than 40,000 papers have been written on these topics put together, only the ferroelectric oxides have reasonably transitioned into real technologies (FRAM's), while the cuprates have experienced only limited market acceptance, mainly in wires and tapes. Transitioning fundamental materials discoveries into real products involves many steps, including pathways to design and create device structures that can then be inserted into systems architectures and the understanding of how these new technologies impact existing markets. As industrial supported research and development dwindles in magnitude, the onus falls more heavily on academic and national laboratory-based research programs to show the pathway to large-scale production of exotic new materials. A continued limitation of investment into manufacturing may remain a concern for the oxide field for years to come.

In turn, one of the biggest challenges facing the field of multiferroics today is the need for room temperature functionality. Despite a concerted effort by a wide number of researchers, the search for intrinsic multiferroics that are simultaneously both ferromagnetic and ferroelectric at room temperature remains a difficult one. Inherent to this the fact that one of the two order parameters, either electronic or magnetic, is often a weak property resulting from either a complicated phase transformation, orbital ordering, geometric frustration, etc. in materials. Such order parameters are typically very small in magnitude and occur only in the low temperature phase. Thus, it is essential that the field works to include both thin film heterostructure and bulk synthesis methods and broadens its search for new candidate multiferroics. The interplay between *ab initio*, density functional theoretical approaches and controlled synthetic approaches (be it single crystal growth or MBE-like heteroepitaxial thin film growth) is critical. Thin film heterostructures, further provide an additional degree of freedom through the mismatch strain; here again, the intimate interplay between theoretical predictions [448] and film growth is imperative. Additionally, the authors believe that the field can make significant strides towards room temperature functionality if additional attention is given to utilizing the current materials and technologies widely used in the field today. The work of Chu et al. [441] represents one pathway to creating new

functionalities based on intrinsic multiferroics at room temperature and could be a guide to device designers looking to utilize CMOS compatible control of ferromagnetism in room temperature devices. Finally, it is essential that the field outlines the needs and directions of research in the near future. If magnetoelectric coupling is the most interesting figure of merit, composite multiferroics offer extraordinary coupling at room temperature and above. Regardless, the field remains poised to impact everything from basic science to device design in the near future.

With this said, however, there remain a number of important areas for immediate future research. Paramount among these is that we establish a full understanding of the mechanisms by which the magnetic and dielectric order parameters couple in such materials. If deterministic control and manipulation of ferromagnetism is desired, then interactions across heterointerfaces will become important as we attempt to design systems capable of these functionalities. Domains, domain walls, and defects will undoubtedly play a critical role in unraveling the coupling phenomena. Further, in such heterostructure based coupling, differences between interactions with classical itinerant ferromagnets and double exchange ferromagnets (such as the manganite) need to be explored in depth as well. In thin films, heteroepitaxial constraints (such as strain, clamping, and possibly surface termination) are going to become important variables. What is clear from the research in this field thus far is that these heterostructure systems, although promising, represent extraordinarily complex systems which will require careful attention to develop further. Of course, the most desirable situation would be to discover a truly multiferroic material, one that is ferromagnetic and ferroelectric at room temperature and exhibits coupling between these two order parameters. This is truly a challenge for interdisciplinary condensed matter research.

At a more fundamental science level, complex oxides provide the ultimate playground for the exploration of the coupling and interplay among the charge, spin, orbital and lattice degrees of freedom. These interactions lead to novel (and exotic) ground states for the system that can be manipulated by external perturbations. The ability to engineer artificial heterostructures down to the unit cell level through MBE and related techniques is an incredible opportunity to explore quantum phenomena in oxides. At the crystal chemistry level, the interplay between cationic sizes and oxygen coordination chemistry leads to tilts and rotations of the oxygen octahedra. Control and manipulation of these degrees of freedom, especially at heterointerfaces where symmetry breaking is easily achieved, has captured the interest of researchers in the field and is likely to be an active area of research. The orbital degree of freedom, however, is still a relatively less explored aspect. An ideal manifestation would be room temperature electric field control of the orbital order in perovskites such as the manganites. Another area that presents both scientific challenges and opportunities relates to the properties of domain walls, especially conduction at domain walls in otherwise insulating ferroelectrics. A critical question is this: can we possibly create an insulator-metal transition at the wall, i.e., can the walls exhibit metallic conduction? If this is possible through careful control of the electronic structure at the wall as well as through external constraints (epitaxy, defect chemistry, etc.), this is likely to be a major breakthrough, since the domain walls in ferroelectrics are truly “nano-objects” (width of the order of a few nm) and they can be manipulated (written, erased and relocated) using electric fields.

In the end, as we look back at the development of modern complex oxide research we see a series of exciting discoveries from high T_c superconductivity, to ferroelectricity, to colossal magnetoresistance, to multiferroism and magnetoelectricity that have propelled the greater field of oxides to the forefront of condensed

matter physics. The field today stands poised for another great discovery that will usher in a new era of discovery. The diverse functionality of oxide materials means that this breakthrough could drive the field towards many of the major scientific questions that face us today – from energy, to medicine, to communications, and beyond.

Acknowledgements

The authors acknowledge the support of the Director, Office of Basic Energy Sciences, Materials Science Division of the U.S. Department of Energy under Contract No. DE-AC02-05CH11231 and previous contracts, ONR-MURI under Grant No. E21-6RU-G4 and previous contracts, and the Western Institute of Nanoelectronics program as well as significant intellectual and financial support from scientists and engineers at Intel. Over the past 8–10 years, R.R. has also benefitted significantly through funding from the Office of Naval Research (through a MURI program from 2003–2008) as well as funding from the National Science Foundation during his tenure at the University of Maryland, College Park.

References

- [1] C.N.R. Rao, B. Raveau, *Transition Metal Oxides*, 2nd edn., Wiley-VCH, New York, 1998.
- [2] D. Norton, *Mater. Sci. Eng. R* 43 (2004) 139.
- [3] S.N. Ruddlesden, P. Popper, *Acta. Crystallogr.* 11 (1958) 54.
- [4] Y. Maeno, H. Hashimoto, K. Yoshida, S. Nishizaki, T. Fujita, J.G. Bednorz, F. Lichtenberg, *Nature* 372 (1994) 532.
- [5] G. Cao, S. McCall, J.E. Crow, *Phys. Rev. B* 55 (1997) 672.
- [6] S. Ikeda, Y. Maeno, T. Fujita, *Phys. Rev. B* 57 (1998) 978; S. Ikeda, Y. Maeno, *Physica B* 259–261, (1999) 947; S. Ikeda, Y. Maeno, M. Kosaka, Y. Uwatoko, *Phys. Rev. B* 62 (2000) 1.
- [7] M. Imada, A. Fujimori, Y. Tokura, *Rev. Mod. Phys.* 70 (1998) 1039.
- [8] J.B. Goodenough, *Prog. Solid State Chem.* 5 (1971) 145.
- [9] D.G. Schlom, J.H. Haeni, J. Lettieri, C.D. Theis, W. Tian, J.C. Jiang, X.Q. Pan, *Mater. Sci. Eng. B* 87 (2001) 282.
- [10] M. Ohring, *Materials Science of Thin Films: Deposition and Structure*, Academic Press, San Francisco, 2002.
- [11] D.L. Smith, *Thin-Film Deposition: Principles and Practice*, McGraw Hill, San Francisco, 1995.
- [12] D.B. Chrisey, G.K. Hubler, *Pulsed Laser Deposition of Thin Films*, John Wiley & Sons, Inc., New York, 1994.
- [13] R. Eason, *Pulsed Laser Deposition of Thin Films: Applications-Led Growth of Functional Materials*, John Wiley & Sons, Hoboken, NJ, 2007.
- [14] H.M. Christen, G. Eres, J. Phys. Condens. Matter 20 (2008) 264005.
- [15] G. Bednorz, K.A. Muller, *Z. Phys. B* 64 (1986) 189.
- [16] D. Dijkkamp, T. Venkatesan, X.D. Wu, S.A. Shaheen, N. Jisrawi, Y.H. Min-Lee, W.L. McLean, M. Croft, *Appl. Phys. Lett.* 51 (1987) 619.
- [17] X.D. Wu, T. Venkatesan, A. Inam, X.X. Xi, Q. Li, W.L. McLean, C.C. Chang, D.M. Hwang, R. Ramesh, L. Nazar, B. Wilkens, S.A. Schwartz, R.T. Ravi, J.A. Martinez, P. England, J.M. Tarascon, R.E. Muenchausen, S. Foltyn, R.C. Dye, A.R. Garcia, N.S. Nogar, *Mater. Res. Soc. Symp. Proc.* 191 (1990) 129.
- [18] H.M. Smith, A.F. Turner, *Appl. Opt.* 4 (1965) 147.
- [19] H. Schwarz, H.A. Tourtellotte, *J. Vac. Sci. Technol.* 6 (1969) 373.
- [20] H. Christen, D.P. Norton, L.A. Gea, L.A. Boatner, *Thin Solid Films* 312 (1998) 156.
- [21] D.H. Kim, H.N. Lee, M.D. Biegalski, H.M. Christen, *Appl. Phys. Lett.* 91 (2007) 042906.
- [22] H.M. Christen, S.D. Silliman, K.S. Harshavardhan, *Rev. Sci. Instrum.* 72 (2001) 2673.
- [23] H.M. Christen, C.M. Rouleau, I. Ohkubo, H.Y. Zhai, H.N. Lee, S. Sathiyamurthy, D.H. Lowndes, *Rev. Sci. Instrum.* 74 (2003) 4058.
- [24] I. Ohkubo, H.M. Christen, S.V. Kalinin, C.M. Rouleau, D.H. Lowndes, *Appl. Phys. Lett.* 84 (2004) 1350.
- [25] H.M. Christen, G.E. Jellison Jr., I. Ohkubo, S. Huang, M.E. Reeves, E. Cicerella, J.L. Freeouf, Y. Jia, D.G. Schlom, *Appl. Phys. Lett.* 88 (2006) 262906.
- [26] G. Rijnders, D.H.A. Blank, in: O. Auciello, R. Ramesh (Eds.), *Thin Films and Heterostructures of Oxide Electronics*, Springer Science, New York, 2005.
- [27] M. Huijben, L.W. Martin, Y.-H. Chu, M.B. Holcomb, P. Yu, G. Rijnders, D.H.A. Blank, R. Ramesh, *Phys. Rev. B* 78 (2008) 094413.
- [28] H. Koinuma, M. Kawasaki, S. Ohashi, M. Lippmaa, N. Nakagawa, M. Iwasaki, X.G. Qiu, *Proc. SPIE* 3481 (1998) 153.
- [29] H. Tanaka, T. Kawai, *Appl. Phys. Lett.* 70 (2000) 425.
- [30] S. Ohashi, M. Lippmaa, N. Nakagawa, H. Nasagawa, H. Koinuma, M. Kawasaki, *Rev. Sci. Instrum.* 70 (1999) 178.
- [31] P. Chen, S.Y. Xu, J. Lin, C.K. Ong, D.F. Cui, *Appl. Surf. Sci.* 137 (1999) 98.
- [32] G.Z. Yang, H.B. Lu, F. Chen, T. Zhao, Z.H. Chen, *J. Cryst. Growth* 929 (2001) 227.
- [33] S. Hasegawa, S. Ino, Y. Yamamoto, H. Daimon, *Jpn. J. Appl. Phys.* 24 (1985) L387.
- [34] A.R. Krauss, M. Rangaswamy, Y. Lin, D.M. Gruen, J.A. Schultz, H.K. Schmidt, R.P.H. Chang, in: O. Auciello, J. Engemann (Eds.), *Multicomponent and Multilayered Thin Films for Advanced Microtechnologies, Techniques, Fundamentals, and Devices*, Kluwer, The Netherlands, 1993.
- [35] A.R. Krauss, Y. Lin, O. Auciello, G.J. Lamich, D.M. Gruen, J.A. Schultz, R.P.H. Chang, *J. Vac. Sci. Technol. A* 12 (1994) 1943.
- [36] Y. Lin, A.R. Krauss, R.P.H. Chang, O. Auciello, D.M. Gruen, J.A. Schultz, *Thin Solid Films* 253 (1995) 247.
- [37] M.S. Hammond, J.A. Schultz, A.R. Krauss, *J. Vac. Sci. Technol. A* 13 (1995) 1136.
- [38] K. Horiba, H. Ohguchi, H. Kumigashira, M. Oshima, K. Ono, N. Nakagawa, M. Lippmaa, *Rev. Sci. Instrum.* 74 (2003) 3406.
- [39] G. Eres, J.Z. Tischler, M. Yoon, B.C. Larson, C.M. Rouleau, D.H. Lowndes, P. Zschack, *Appl. Phys. Lett.* 80 (2002) 3379.
- [40] V. Vonk, S. Konings, L. Barthe, B. Gorges, H. Graafsmas, *J. Synchrotron Rad.* 12 (2005) 833.
- [41] D. Dale, Y. Suzuki, J.D. Brock, *J. Phys. Condens. Matter* 20 (2008) 264008.
- [42] C. Web, S.-L. Weng, J.N. Eckstein, N. Missert, K. Char, D.G. Schlom, E.S. Hellman, M.R. Beasley, A. Kapitulnik, J.S. Harris Jr., *Appl. Phys. Lett.* 51 (1987) 1191.
- [43] E.S. Hellman, D.G. Schlom, N. Missert, K. Char, J.S. Harris Jr., M.R. Beasley, A. Kapitulnik, T.H. Gaballe, J.N. Eckstein, S.-L. Weng, C. Web, *J. Vac. Sci. Technol. B* 6 (1988) 799.
- [44] D.D. Berkley, B.R. Johnson, N. Anand, K.M. Beauchamp, L.E. Conroy, A.M. Goldman, J. Maps, K. Mauersberger, M.L. McCartney, J. Morton, M. Tuominen, Y.-J. Zhang, *Appl. Phys. Lett.* 53 (1988) 1973.
- [45] J.N. Eckstein, I. Bozovic, *Ann. Rev. Mater. Sci.* 25 (1995) 679.
- [46] S.A. Chambers, *Surf. Sci. Rep.* 39 (2000) 105.
- [47] S.A. Chambers, *Adv. Mater.* 22 (2010) 219.
- [48] P.J. Kelly, R.D. Arnell, *Vacuum* 56 (2000) 159.
- [49] S.M. Rossnagel, in: W.D. Sproul, K.O. Legg (Eds.), *Opportunities for Innovation: Advanced Surface Engineering*, Technomic Publishing, Switzerland, 1995.
- [50] K. Wasa, M. Kitabatake, H. Abachi, *Thin Film Materials Technology—Sputtering of Compound Materials*, William Andrew Publishing, Norwich, NY, 2004.
- [51] U. Kruger, R. Kutzner, R. Wordenweber, *IEEE Trans. Appl. Supercond.* 3 (1993) 1687.
- [52] X.X. Xi, T. Venkatesan, Q. Li, X.D. Wu, A. Inam, C.C. Chang, R. Ramesh, D.M. Hwang, T.S. Ravi, A. Findikoglu, D. Hemmick, S. Etamad, J.A. Martinez, E. Wilkens, *IEEE Trans. Magn.* 27 (1991) 982.
- [53] D.J. Lichtenwalner, C.N. Soble II, R.R. Woolcott Jr., O. Auciello, A.I. Kington, *J. Appl. Phys.* 70 (1991) 6952.
- [54] C.B. Eom, J.Z. Sun, K. Yamamoto, A.F. Marshall, K.E. Luther, T.H. Geballe, S.S. Laderman, *Appl. Phys. Lett.* 55 (1989) 595.
- [55] J. Schwarzkopf, R. Fornari, *Prog. Cryst. Growth Charact. Mater.* 52 (2006) 159.
- [56] A. Leskelä, H. Mölsä, L. Niinistö, *Supercond. Sic. Technol.* 6 (1993) 627.
- [57] F.F. Lange, *Science* 273 (1996) 903.
- [58] R.W. Schwartz, *Chem. Mater.* 9 (1997) 2325.
- [59] T.P. Niesen, M.R. De Guire, *J. Electroceram.* 6 (2001) 169.
- [60] K. Aizu, *Phys. Rev. B* 2 (1970) 754.
- [61] M.E. Lines, A.M. Glass, *Principles, Applications of Ferroelectrics and Related Materials*, Oxford University Press, Oxford, 2004.
- [62] N.A. Hill, *J. Phys. Chem. B* 104 (2000) 6694.
- [63] J.M. Gauguain, C. R. Acad. Sci. Paris 42 (1856) 1264, 43 (1856) 916.
- [64] J. Curie, P. Curie, C. R. Acad. Sci. Paris 91 (1880) 294.
- [65] J. Valasek, *Phys. Rev.* 15 (1920) 537, 17 (1921) 475.
- [66] I.V. Kurchatov, *Segnetoelektriki (Ferroelectrics)* M GTTI (1933).
- [67] G. Busch, P. Scherrer, *Naturwissenschaft* 23 (1935) 737.
- [68] G. Busch, *Helv. Phys. Acta* 11 (1938) 269.
- [69] J.C. Slater, *J. Chem. Phys.* 9 (1941) 16.
- [70] B. Wul, I.M. Goldman, C. R. Acad. Sci. URSS 46 (1945) 139, 49 (1945) 177.
- [71] B.T. Matthias, *Phys. Rev.* 75 (1949) 1771.
- [72] B.T. Matthias, J.P. Remeika, *Phys. Rev.* 76 (1949) 1886.
- [73] G. Shirane, S. Hoshino, K. Suzuki, *Phys. Rev.* 80 (1950) 1105.
- [74] V.L. Ginzburg, *Zh. Eksp. Teor. Fiz* 15 (1945) 739, 19 (1949) 36.
- [75] A.F. Devonshire, *Phil. Mag* 40 (1949) 1040, 42 (1951) 1065.
- [76] C. Kittel, *Phys. Rev.* 82 (1951) 729.
- [77] P.W. Anderson, in: G.I. Skanavi (Ed.), *Fizika Dielektrikov*, Akad. Nauk. SSSR, Moscow, 1960.
- [78] W. Cochran, *Adv. Phys.* 9 (1960) 357.
- [79] V.L. Ginzburg, *Ferroelectrics* 267 (2002) 23.
- [80] J.F. Scott, C.A. Paz de Araujo, *Science* 246 (1989) 1400.
- [81] T. Tybell, C.H. Ahn, J.-M. Triscone, *Appl. Phys. Lett.* 75 (1999) 856.
- [82] P. Ghosez, K.M. Rabe, *Appl. Phys. Lett.* 76 (2000) 2767.
- [83] B. Meyer, D. Vanderbilt, *Phys. Rev. B* 63 (2001) 205426.
- [84] J. Junquera, P. Ghosez, *Nature* 422 (2003) 506.
- [85] D.D. Fong, G.B. Stephenson, S.K. Streiffer, J.A. Eastman, O. Auciello, P.H. Fuoss, C. Thompson, *Science* 304 (2004) 1650.
- [86] V. Nagarajan, S. Prasertchoung, T. Zhao, H. Zheng, J. Ouyang, R. Ramesh, W. Tian, X.Q. Pan, D.M. Kim, C.B. Eom, H. Kohlstedt, R. Waser, *Appl. Phys. Lett.* 84 (2004) 5225.
- [87] C.-L. Jia, V. Nagarajan, J.-Q. He, L. Houben, T. Zhao, R. Ramesh, K. Urban, R. Waser, *Nature Mater.* 6 (2007) 64.
- [88] M. Stengel, D. Vanderbilt, N.A. Spaldin, *Nature Mater.* 8 (2009) 392.
- [89] W. Lee, H. Han, A. Lotnyk, M.A. Schubert, S. Senz, M. Alexe, D. Hesse, S. Baik, U. Gösele, *Nature Nanotechnol.* 3 (2008) 402.
- [90] H. Masuda, K. Fukuda, *Science* 266 (1995) 1466–1468.
- [91] D.G. Schlom, L.-Q. Chen, C.-B. Eom, K.M. Rabe, S.K. Streiffer, J.-M. Triscone, *Ann. Rev. Mater. Res.* 37 (2007) 589.

- [92] J.H. Haeni, P. Irvin, W. Chang, R. Uecker, P. Reiche, Y.L. Li, S. Choudhury, W. Tian, M.E. Hawley, B. Craigo, A.K. Tagantsev, X.Q. Pan, S.K. Streiffer, L.Q. Chen, S.W. Kirchoefer, J. Levy, D.G. Schlom, *Nature* 430 (2004) 758.
- [93] K.J. Choi, M. Biegalski, Y.L. Li, A. Sharan, A.J. Hatt, C.-H. Yang, A. Kumar, C.H. Wang, A. Melville, C. Adamo, G. Sheng, Y.-H. Chu, J.F. Ihlefeld, R. Erni, C. Ederer, V. Gopalan, L.Q. Chen, D.G. Schlom, N.A. Spaldin, L.W. Martin, R. Ramesh, *Science* 306 (2004) 1005.
- [94] C. Ederer, N.A. Spaldin, *Phys. Rev. Lett.* 95 (2005) 257601.
- [95] R.J. Zeches, M.D. Rossell, J.X. Zhang, A. Hatt, C.-H. Yang, A. Kumar, C.H. Wang, A. Melville, C. Adamo, G. Sheng, Y.-H. Chu, J.F. Ihlefeld, R. Erni, C. Ederer, V. Gopalan, L.Q. Chen, D.G. Schlom, N.A. Spaldin, L.W. Martin, R. Ramesh, *Science* 326 (2009) 977.
- [96] B. Jaffe, R.S. Roth, S. Marzullo, *J. Appl. Phys.* 25 (1954) 809.
- [97] E. Cross, *Nature* 432 (2004) 24.
- [98] C. Ederer, N.A. Spaldin, *Phys. Rev. Lett.* 95 (2005) 257601.
- [99] P. Ravindran, R. Vidy, A. Kjekshus, H. Fjellvag, *Phys. Rev. B* 74 (2006) 224412.
- [100] D. Ricinchi, K.-Y. Yun, M. Okuyama, *J. Phys. Condens. Matter* 18 (2006) L97.
- [101] H. Béa, B. Dupé, S. Fusil, R. Mattana, E. Jacquet, B. Warnot-Fonrose, F. Wilhelm, A. Rogalev, S. Petit, V. Cros, A. Anane, F. Petroff, K. Bouzehouane, G. Geneste, B. Dkhil, S. Lisenkov, I. Ponomareva, L. Bellaiche, M. Bibes, A. Barthélémy, *Phys. Rev. Lett.* 102 (2009) 217603.
- [102] M. Sepiarsky, S.R. Phillpot, M.G. Stachiotti, R.L. Migoni, *J. Appl. Phys.* 91 (2002) 3165.
- [103] M. Sepiarsky, M.G. Stachiotti, R.L. Migoni, *Phys. Rev. B* 72 (2005) 014110.
- [104] O. Diéguez, S. Tinte, A. Antons, C. Bungaro, J.B. Neaton, K.M. Rabe, D. Vanderbilt, *Phys. Rev. B* 69 (2004) 212101.
- [105] B.K. Lai, I.A. Kornev, L. Bellaiche, G.J. Salamo, *Appl. Phys. Lett.* 86 (2005) 132904.
- [106] J. Iñiguez, S. Ivantchev, J.M. Perez-Mato, A. García, *Phys. Rev. B* 63 (2001) 144103.
- [107] Y.L. Li, L.Q. Chen, *Appl. Phys. Lett.* 88 (2006) 072905.
- [108] L.Q. Chen, *Annu. Rev. Mater. Res.* 32 (2002) 113.
- [109] S. Li, J.A. Eastman, J.M. Vetrone, R.E. Newnham, L.E. Cross, *Phil. Mag.* B 76 (1997) 47.
- [110] J.B. Neaton, K.M. Rabe, *Appl. Phys. Lett.* 82 (2003) 1586.
- [111] N. Sai, B. Meyer, D. Vanderbilt, *Phys. Rev. Lett.* 84 (2000) 5636.
- [112] M. Nakhmanson, K.M. Rabe, D. Vanderbilt, *Appl. Phys. Lett.* 87 (2005) 102906.
- [113] M. Nakhmanson, K.M. Rabe, D. Vanderbilt, *Phys. Rev. B* 73 (2006), 060101(R).
- [114] H.N. Lee, H.M. Christen, M.F. Chisholm, C.M. Rouleau, D.H. Lowndes, *Nature* 433 (2005) 395.
- [115] H.M. Christen, L.A. Knauss, K.S. Harshavardhan, *Mater. Sci. Eng. B* 56 (1998) 200.
- [116] T. Shimuta, O. Nakagawara, T. Makino, S. Arai, H. Tabata, T. Kawai, *J. Appl. Phys.* 91 (2002) 2290.
- [117] L. Kim, D. Jung, J. Kim, Y.S. Kim, J. Lee, *Appl. Phys. Lett.* 82 (2003) 2118.
- [118] H.M. Christen, E.D. Sprecht, S.S. Silliman, K.S. Harshavardhan, *Phys. Rev. B* 68 (2003), 020101.
- [119] M. Dawber, C. Lichtensteiger, M. Cantoni, M. Veithen, P. Ghosez, K. Johnston, K.M. Rabe, J.-M. Triscone, *Phys. Rev. Lett.* 95 (2005) 177601.
- [120] W. Tian, J.C. Jiang, X.Q. Pan, J.H. Haeni, Y.L. Li, L.Q. Chen, D.G. Schlom, J.B. Neaton, K.M. Rabe, *Appl. Phys. Lett.* 89 (2006) 092905.
- [121] D.A. Tenne, A. Bruchhausen, N.D. Lanzillotti-Kimura, A. Fainstein, R.S. Katiyar, A. Cantarero, A. Soukiasian, V. Vaithyanathan, J.H. Haeni, W. Tian, D.G. Schlom, K.J. Choi, D.M. Kim, C.B. Eom, H.P. Sun, X.Q. Pan, Y.L. Li, L.Q. Chen, Q.X. Jia, S.M. Nakhmanson, K.M. Rabe, X.X. Xi, *Science* 313 (2006) 5793.
- [122] M.P. Warusawithana, E.V. Colla, J.N. Eckstein, M.B. Weissman, *Phys. Rev. Lett.* 90 (2003) 036802.
- [123] M.H. Corbett, R.M. Bowman, J.M. Gregg, D.T. Ford, *Appl. Phys. Lett.* 79 (2001) 815.
- [124] V. Berger, *Phys. Rev. Lett.* 81 (1998) 4136.
- [125] S.V. Kalinin, D.A. Bonnell, T. Alvarez, X. Lei, Z. Hu, R. Shao, J.H. Ferris, *Adv. Mater.* 17 (2005) 795.
- [126] A.L. Roytburd, *Phys. Stat. Sol. A* 37 (1976) 329.
- [127] C.S. Ganpule, V. Nagarajan, B.K. Hill, A.L. Roytburd, E.D. Williams, R. Ramesh, S.P. Alpay, A. Roelofs, R. Waser, *L.M. Eng. J. Appl. Phys.* 91 (2002) 1477.
- [128] Y.L. Li, S.Y. Hu, L.Q. Chen, *J. Appl. Phys.* 97 (2005) 034112.
- [129] V. Nagarajan, C.S. Ganpule, H. Li, L. Salamanca-Riba, A.L. Roytburd, E.D. Williams, R. Ramesh, *Appl. Phys. Lett.* 79 (2001) 2805.
- [130] S.K. Streiffer, C.B. Parker, A.E. Romanov, M.J. Lefevre, L. Zhao, J.S. Speck, W. Pompe, C.M. Foster, G.R. Bai, *J. Appl. Phys.* 83 (1998) 2742.
- [131] J.X. Zhang, Y.L. Li, S. Choudhury, L.Q. Chen, Y.H. Chu, F. Zavaliche, M.P. Cruz, R. Ramesh, Q.X. Jia, *J. Appl. Phys.* 103 (2008) 094111.
- [132] Y.-H. Chu, Q. Zhan, L.W. Martin, M.P. Cruz, P.-L. Yang, G.W. Pabst, F. Zavaliche, S.-Y. Yang, J.-X. Zhang, L.-Q. Chen, D.G. Schlom, I.-N. Lin, T.-B. Wu, R. Ramesh, *Adv. Mater.* 18 (2006) 2307.
- [133] G.W. Pabst, L.W. Martin, Y.-H. Chu, R. Ramesh, *Appl. Phys. Lett.* 90 (2007) 072902.
- [134] Y.-H. Chu, M.P. Cruz, C.-H. Yang, L.W. Martin, P.-L. Yang, J.-X. Zhang, K. Lee, P. Yu, L.-Q. Chen, R. Ramesh, *Adv. Mater.* 19 (2007) 2662.
- [135] Y.-H. Chu, Q. He, C.-H. Yang, P. Yu, L.W. Martin, P. Shafer, R. Ramesh, *Nano Lett.* 9 (2009) 1726.
- [136] F. Zavaliche, S.-Y. Yang, T. Zhao, Y.-H. Chu, M.P. Cruz, R. Ramesh, *Phase Trans.* 79 (2006) 991.
- [137] M.P. Cruz, Y.-H. Chu, J.X. Zhang, P.-L. Yang, F. Zavaliche, Q. He, P. Shafer, L.Q. Chen, R. Ramesh, *Phys. Rev. Lett.* 99 (2007) 217601.
- [138] P. Shafer, F. Zavaliche, Y.-H. Chu, P.-L. Yang, M.P. Cruz, R. Ramesh, *Appl. Phys. Lett.* 90 (2007) 202909.
- [139] K.J. Hubbard, D.G. Schlom, *J. Mater. Res.* 11 (1996) 2757.
- [140] H.F. Luan, B.Z. Wu, L.G. Kang, B.Y. Kim, R. Vrtis, D.L. Kwong, *IEDM Tech. Dig.* (1998) 609.
- [141] B. He, T. Ma, S.A. Campbell, W.L. Gladfelter, *IEDM Tech. Dig.* (1998) 1038.
- [142] L. Manchanda, W.H. Lee, J.E. Bower, F.H. Bauman, W.L. Brown, *IEDM Tech. Dig.* (1998) 605.
- [143] G.D. Wilk, R.M. Wallace, *Appl. Phys. Lett.* 74 (1999) 2854.
- [144] J.C. Chen, G.H. Shen, L.J. Chen, *Appl. Surf. Sci.* 142 (1999) 120.
- [145] J. Ramdani, R. Droopad, Z. Yu, J.A. Curless, C.D. Overgaard, J. Finder, K. Eisesenbeiser, J.A. Hallmark, W.J. Ooms, V. Kaushik, P. Alluri, S. Pietambaram, *Appl. Surf. Sci.* 159–160 (2000) 127.
- [146] H. Mori, H. Ishiwara, *Jpn. J. Appl. Phys.* 30 (1991) L2059.
- [147] H. Nagata, *Thin Solid Films* 224 (1993) 1.
- [148] B.K. Moon, H. Ishiwara, *Jpn. J. Appl. Phys.* 33 (1994) L472.
- [149] T. Tambo, T. Nakamura, K. Maeda, H. Veba, C. Tatsuyama, *Jpn. J. Appl. Phys.* 37 (1998) 4454.
- [150] R.A. Mckee, F.J. Walker, M.F. Chisholm, *Phys. Rev. Lett.* 81 (1998) 3014.
- [151] S. Gaillard, Y. Rozier, C. Merckling, F. Ducroquet, M. Gendry, G. Hollinger, *Microelect. Eng.* 80 (2005) 146.
- [152] M.P. Warusawithana, C. Cen, C.R. Sleasman, J.C. Woicik, Y. Li, L. Fitting Kourkoutis, J.A. Klug, H. Li, P. Ryan, L.-P. Wang, M. Bedzyk, D.A. Muller, L.-Q. Chen, J. Levy, D.G. Schlom, *Science* 324 (2009) 367.
- [153] W. Tian, V. Vaithyanathan, D.G. Schlom, Q. Zhan, S.Y. Yang, Y.-H. Chu, R. Ramesh, *Appl. Phys. Lett.* 90 (2007) 172908.
- [154] S.Y. Yang, Q. Zhan, P.-L. Yang, M.P. Cruz, Y.-H. Chu, R. Ramesh, Y.R. Wu, J. Singh, W. Tian, D.G. Schlom, *Appl. Phys. Lett.* 91 (2007) 022909.
- [155] E.Y. Tsymbal, H. Kohlstedt, *Science* 313 (2006) 181.
- [156] S.S.P. Parkin, K.P. Roche, M.G. Samant, P.M. Rice, R.B. Beyers, R.E. Scheuerlein, E.J. O'Sullivan, S.L. Brown, J. Buccigiano, D.W. Abraham, Y. Lu, M. Rooks, P.L. Trouilloud, R.A. Wanner, W.J. Gallagher, *J. Appl. Phys.* 85 (1999) 5828.
- [157] M.Yu. Zhuravlev, R. Sabirianov, S.S. Jaswal, E.Y. Tsymbal, *Phys. Rev. Lett.* 94 (2005) 246802.
- [158] V. Garcia, S. Fusil, K. Bouzehouane, S. Enouz-Vedrenne, N.D. Mathur, A. Barthélémy, M. Bibes, *Nature* 460 (2009) 81.
- [159] P. Maksymovych, S. Jesse, P. Yu, R. Ramesh, A.P. Baddorf, S.V. Kalinin, *Science* 324 (2009) 1421.
- [160] D.E. Laughlin, M.A. Willard, M.E. McHenry, in: P. Turchi, A. Gonis (Eds.), *Phase Transformations and Evolutions in Materials, The Minerals, Metals, and Materials Society, Warrendale, PA*, 2000.
- [161] G.L. Verschuur, *Hidden Attraction, The Mystery and History of Magnetism*, Oxford University Press, Oxford, 1993.
- [162] J. Stöhr, H.C. Siegmann, *Magnetism, From Fundamentals to Nanoscale Dynamics*, Springer-Verlag, New York, 2006.
- [163] P. Weiss, *J. de Physique* 6 (1907) 661.
- [164] W. Heisenberg, *Z. Phys.* 49 (1928) 619.
- [165] L. Néel, *Ann. de Phys.* 18 (1932) 5.
- [166] J. Smit, H.P.J. Wijn, *Ferrites: Physical Properties of Ferrimagnetic Oxides in Relation to Their Technical Applications*, John Wiley and Sons, New York, 1959.
- [167] H.A. Kramers, *Physica* 1 (1934) 182.
- [168] P.W. Anderson, *Phys. Rev.* 79 (1950) 350.
- [169] C. Zener, *Phys. Rev.* 82 (1951) 403.
- [170] M.A. Ruderman, C. Kittel, *Phys. Rev.* 96 (1954) 99.
- [171] T. Kasuya, *Prog. Theor. Phys.* 16 (1956) 45.
- [172] K. Yosida, *Phys. Rev.* 106 (1957) 893.
- [173] J.L. Snoek, *New Developments in Ferromagnetic Materials*, Elsevier, New York, 1947.
- [174] C.L. Hogan, *Bell Syst. Tech. J.* 31 (1952) 1.
- [175] R.J. Gambino, T. Suzuki, *Magneto-optical Recording Materials*, IEEE Press, New York, 2000.
- [176] P.J. van der Zaag, J.J.M. Ruigrok, M.F. Gillies, *Philips J. Res.* 51 (1998) 173.
- [177] Z. Szotek, W.M. Temmerman, D. Ködderitzsch, A. Svane, L. Petit, H. Winter, *Phys. Rev. B* 74 (2006) 174431.
- [178] J.S. Moodera, L.R. Kinder, T.M. Wong, R. Meservey, *Phys. Rev. Lett.* 74 (1995) 3273.
- [179] Y. Suzuki, *Annu. Rev. Mater. Res.* 31 (2001) 265.
- [180] N. Tsuda, K. Nasu, A. Yanase, K. Siraatori, *Electronic Conduction in Oxides, Springer Series in Solid State Science*, New York, 1991.
- [181] M. Penicaud, B. Siberchocot, C.B. Sommers, J. Kubler, *J. Magn. Magn. Mater.* 103 (1992) 212.
- [182] E.J.W. Verwey, *Nature* 144 (1939) 327.
- [183] J. Yoshida, S. Iida, *J. Phys. Soc. Jpn.* 47 (1979) 1627.
- [184] J.P. Shepherd, J.W. Koenitzer, R. Aragon, J. Spalek, J.M. Honig, *Phys. Rev. B* 43 (1991) 8461.
- [185] H.S. Choi, J.S. Ahn, W. Jo, T.W. Noh, S.H. Chun, Z.G. Khim, *Mater. Res. Soc. Symp. Proc.* 341 (1994) 35.
- [186] D.T. Margulies, F.T. Parker, F.E. Spada, R.S. Goldman, J. Li, R. Sinclair, A.E. Berkowitz, *Phys. Rev. B* 53 (1996) 9175.
- [187] G.Q. Gong, A. Gupta, G. Xiao, W. Qian, V.P. Dravid, *Phys. Rev. B* 56 (1997) 5096.
- [188] S.A. Oliver, M.L. Chen, I. Kozulin, C. Vittoria, J. Magn. Magn. Mater. 213 (2000) 326.
- [189] M. Takeuchi, M. Hiramoto, M. Matsukawa, H. Adachi, S. Okamura, T. Shiosaki, H. Sakakima, *J. Magn. Soc. Jpn.* 25 (2001) 155.
- [190] S. Soeya, J. Hayakawa, H. Takahashi, K. Ito, C. Yamamoto, A. Kida, H. Asano, M. Matsui, *Appl. Phys. Lett.* 80 (2002) 823.
- [191] J.M.D. Coey, A.E. Berkowitz, L.I. Balcells, F.F. Putris, F.T. Parker, *Appl. Phys. Lett.* 72 (1998) 734.
- [192] X.W. Li, A. Gupta, G. Xiao, G.Q. Gong, *J. Appl. Phys.* 83 (1998) 7049.
- [193] X.W. Li, A. Gupta, G. Xiao, W. Qian, V.P. Dravid, *Appl. Phys. Lett.* 73 (1998) 3282.
- [194] P. Senor, A. Fert, J.-L. Maurice, F. Montaigne, F. Petroff, A. Vaurès, *Appl. Phys. Lett.* 74 (1999) 4017.

- [195] G. Hu, Y. Suzuki, *Phys. Rev. Lett.* 89 (2002) 276601.
- [196] M.G. Chapline, S.X. Wang, *Phys. Rev. B* 74 (2006) 014418.
- [197] P. Samarasekera, R. Rani, F.J. Cadieu, S.A. Shaheen, *J. Appl. Phys.* 79 (1996) 5425.
- [198] Y. Suzuki, R.B. van Dover, E.M. Gyorgy, J.M. Phillips, V. Korenivski, D.J. Werder, C.H. Chen, R.J. Felder, R.J. Cava, J.J. Krajewski, W.F. Peck Jr., *J. Appl. Phys.* 79 (1996) 5923.
- [199] S. Venzke, R.B. van Dover, J.M. Gyorgy, T. Siegrist, C.-H. Chen, D. Werder, R.M. Fleming, R.J. Felder, E. Coleman, R. Opila, *J. Mater. Res.* 11 (1996) 1187.
- [200] U. Lünders, M. Bibes, J.-F. Bobo, M. Cantoni, R. Bertacco, J. Fontcuberta, *Phys. Rev. B* 71 (2005) 134419.
- [201] P.C. Dorsey, P. Lubitz, D.B. Chrisey, J.S. Horwitz, *J. Appl. Phys.* 79 (1996) 6338.
- [202] S.A. Chambers, R.F.C. Farrow, S. Maat, M.F. Toney, L. Folks, J.G. Catalano, T.P. Trainor, G.E. Brown Jr., *J. Magn. Magn. Mater.* 246 (2002) 124.
- [203] G. Hu, J.H. Choi, C.B. Eom, V.G. Harris, Y. Suzuki, *Phys. Rev. B* 62 (2000) R779.
- [204] A.V. Ramos, J.-B. Moussy, M.-J. Guittet, M. Gautier-Soyer, C. Gatel, P. Bayle-Guillemaud, B. Warot-Fonrose, E. Snoeck, *Phys. Rev. B* 75 (2007) 224421.
- [205] S.M. Yuan, H.L. Glass, L.R. Adkins, *Appl. Phys. Lett.* 53 (1988) 340.
- [206] E.J. Donahue, D.M. Schleich, *J. Appl. Phys.* 71 (1992) 6013.
- [207] H.L. Glass, J.H.W. Liaw, *J. Appl. Phys.* 49 (1978) 1578.
- [208] C.A. Carosella, D.B. Chrisey, P. Lubitz, J.S. Horowitz, P. Dorsey, R. Seed, C. Vittoria, *J. Appl. Phys.* 71 (1992) 5107.
- [209] H.J. Masterson, J.G. Lunney, J.M. Coey, R. Atkinson, I.W. Salter, P. Papakonstantinou, *J. Appl. Phys.* 73 (1993) 3917.
- [210] S.R. Shinde, R. Ramesh, S.E. Lofland, S.M. Bhagat, S.B. Ogale, R.P. Sharma, T. Venkatesan, *Appl. Phys. Lett.* 72 (1998) 3443.
- [211] Y.-Y. Song, S. Kalarickal, C.E. Patton, *J. Appl. Phys.* 94 (2003) 5103.
- [212] Z. Yang, M. Lange, A. Volodin, R. Szymczak, V.V. Moshchalkov, *Nature Mater.* 3 (2004) 793.
- [213] Z.H. Chen, A. Yang, A. Gieler, V.G. Harris, C. Vittoria, P.R. Ohodnicki, K.Y. Goh, M.E. McHenry, Z.H. Cai, T.L. Goodrich, K.S. Ziemer, *Appl. Phys. Lett.* 91 (2007) 182505.
- [214] R.S. Teble, D.J. Craik, *Magnetic Materials*, Wiley-Interscience, New York, 1969.
- [215] D. Treves, *J. Appl. Phys.* 36 (1965) 1033.
- [216] D.J. Craik, *Magnetic Oxides*, Wiley, New York, 1975.
- [217] R. Krishnan, A. Lifsi, M. Guyot, V. Cagan, *J. Magn. Magn. Mater.* 147 (1995) L221.
- [218] D.S. Schmol, N. Keller, M. Guyot, R. Krishnan, M. Tessier, *J. Magn. Magn. Mater.* 195 (1999) 291.
- [219] Y. Ma, X.M. Chen, Y.Q. Lin, *J. Appl. Phys.* 103 (2008) 124111.
- [220] M.A. Gilileo, S. Geller, *Phys. Rev.* 110 (1958) 73.
- [221] A.P. Ramirez, *J. Phys. Condens. Matter* 9 (1997) 8171.
- [222] J.M.D. Coey, M. Viret, S. von Molnár, *Adv. Phys.* 48 (1999) 167.
- [223] Y. Tokura, Y. Tomioka, *J. Magn. Magn. Mater.* 200 (1999) 1.
- [224] M.B. Salamon, M. Jaime, *Rev. Mod. Phys.* 73 (2001) 583.
- [225] E. Dagotto, T. Hotta, A. Moreo, *Phys. Rep.* 344 (2001) 1.
- [226] S. Jin, T.H. Tiefel, M. McCormack, R.A. Fastnacht, R. Ramesh, L.H. Chen, *Science* 264 (1994) 413.
- [227] L. Zhang, C. Israel, A. Biswas, R.L. Greene, A. de Lozanne, *Science* 298 (2002) 805.
- [228] V. Moshnyaga, L. Sudheendra, O.I. Lebedev, S.A. Köster, K. Gehrke, O. Shapoval, A. Belenchuk, B. Damaschke, G. van Tendeloo, K. Samwer, *Phys. Rev. Lett.* 97 (2006) 107205.
- [229] S. Cox, J. Singleton, R.D. McDonald, A. Migliori, P.B. Littlewood, *Nature* 7 (2008) 25.
- [230] C.H. Chen, S. Mori, S.-W. Cheong, *Phys. Rev. Lett.* 83 (1999) 4792.
- [231] C.H. Chen, S.-W. Cheong, *Phys. Rev. Lett.* 76 (1996) 4042.
- [232] C.H. Chen, S.-W. Cheong, H.Y. Hwang, *J. Appl. Phys.* 81 (1997) 4326.
- [233] S. Mori, C.H. Chen, S.-W. Cheong, *Nature* 392 (1998) 473.
- [234] S.J. Hibbe, S.P. Copper, A.C. Hannon, I.D. Fawcett, M. Greenblatt, *J. Phys. Condens. Matter* 11 (1999) 9221.
- [235] F. Tsui, C. Smoak, T.K. Nath, C.B. Eom, *Appl. Phys. Lett.* 76 (2000) 2421.
- [236] D. Rubi, S. Dunhalde, M.C. Terzoli, G. Leyva, G. Polla, P. Levy, F. Parisi, R.R. Urbano, *Physica B* 320 (2002) 86.
- [237] L. Ranno, A. Llobet, R. Tiron, E. Favre-Nicolin, *Appl. Surf. Sci.* 188 (2002) 170.
- [238] P. Murugavel, J.H. Lee, J.-G. Yoon, T.W. Noh, J.S. Chang, M. Heu, S. Yoon, *Appl. Phys. Lett.* 82 (2003) 1908.
- [239] E.S. Vlahov, K.A. Nenkov, T.G. Donchev, E.S. Mateev, R.A. Chakalov, *Vacuum* 76 (2004) 249.
- [240] A.Y. Petrov, C. Aruta, S. Mercione, C. Adamo, I. Alessandri, L. Maritato, *Eur. Phys. J. B* 40 (2004) 11.
- [241] M. Angeloni, G. Balestrino, N.G. Boggio, P.G. Medaglia, P. Orgiani, A. Tebano, *J. Appl. Phys.* 96 (2004) 6387.
- [242] J. Cibert, J. Bobo, U. Lüders, C. R. Phys. 6 (2005) 977.
- [243] Y. Lu, J. Klein, F. Herbristrit, J.B. Philipp, A. Marx, R. Gross, *Phys. Rev. B* 73 (2006) 184406.
- [244] T. Dhakal, J. Tosado, A. Biswas, *Phys. Rev. B* 75 (2007) 092404.
- [245] C. Adamo, X. Ke, H.Q. Wang, H.L. Xin, T. Heeg, M.E. Hawley, W. Zander, J. Schubert, P. Schiffer, D.A. Muller, L. Maritato, D.G. Schlom, *Appl. Phys. Lett.* 95 (2009) 112504.
- [246] A.J. Millis, T. Darling, A. Migliori, *J. Appl. Phys.* 83 (1998) 1588.
- [247] B.A. Bernevig, T.L. Hughes, S.-C. Zhang, *Phys. Rev. Lett.* 95 (2005) 066601.
- [248] L. Abad, V. Laukhin, S. Valencia, A. Gaup, W. Gudat, L. Balcells, B. Martínez, *Adv. Funct. Mater.* 17 (2007) 3918.
- [249] H. Tanaka, J. Zhang, T. Kawai, *Phys. Rev. Lett.* 88 (2002) 027204.
- [250] N. Nakagawa, M. Asai, Y. Mukunoki, T. Susaki, H.Y. Hwang, *Appl. Phys. Lett.* 86 (2005) 082504.
- [251] J. Hoppler, J. Stahn, Ch. Niedermayer, V.K. Malik, H. Bouyanif, A.J. Drew, M. Rössle, A. Buzdin, G. Cristiani, H.-U. Habermeier, B. Keimer, C. Bernhard, *Nature Mater.* 8 (2009) 315.
- [252] S.D. Bader, *Proc. IEEE* 78 (1990) 909.
- [253] C. Kwon, M.C. Robson, K.-C. Kim, J.Y. Gu, S.E. Lofland, S.M. Bhagat, Z. Tranjanovic, M. Rajeswari, T. Venkatesan, A.R. Katz, R.D. Gomez, R. Ramesh, *J. Magn. Magn. Mater.* 172 (1997) 229.
- [254] Y. Suzuki, H.Y. Hwang, S.-W. Cheong, R.B. Van Dover, *Appl. Phys. Lett.* 71 (1997) 140.
- [255] H.L. Ju, M. Krishnan, D. Lederman, *J. Appl. Phys.* 83 (1998) 7073.
- [256] J.-H. Park, E. Vescovo, H.-J. Kim, C. Kwon, R. Ramesh, T. Venkatesan, *Phys. Rev. Lett.* 81 (1998) 1953.
- [257] K.S. Takahashi, M. Kawasaki, Y. Tokura, *Appl. Phys. Lett.* 79 (2001) 1324.
- [258] C. Adamo, X. Ke, P. Schiffer, A. Soukiasian, M. Warusawithana, L. Maritato, D.G. Schlom, *Appl. Phys. Lett.* 92 (2008) 112508.
- [259] A. Bhattacharya, S.J. May, S.G.E. te Velthuis, M. Warusawithana, X. Zhai, B. Jiang, J.-M. Zuo, M.R. Fitzsimmons, S.D. Bader, J.N. Eckstein, *Phys. Rev. Lett.* 100 (2008) 257203.
- [260] S.J. May, A.B. Shah, S.G.E. te Velthuis, M.R. Fitzsimmons, J.M. Zuo, X. Zhai, J.N. Eckstein, S.D. Bader, A. Bhattacharya, *Phys. Rev. B* 77 (2008) 174409.
- [261] S.J. May, P.J. Ryan, J.L. Robertson, J.-W. Kim, T.S. Santos, E. Karapetrova, J.L. Zarestky, X. Zhai, S.G.E. te Velthuis, J.N. Eckstein, S.D. Bader, A. Bhattacharya, *Nature Mater.* 8 (2009) 892.
- [262] S. Dong, R. Yu, S. Yunoki, G. Alvarez, J.-M. Liu, E. Dagotto, *Phys. Rev. B* 78 (2008) 201102.
- [263] C. Lin, A.J. Millis, *Phys. Rev. B* 78 (2008) 184405.
- [264] R. Yu, S. Yunoki, S. Dong, E. Dagotto, *Phys. Rev. B* 80 (2009) 125115.
- [265] B.R.K. Nanda, S. Satpathy, *Phys. Rev. Lett.* 101 (2008) 127201.
- [266] J. Nogués, I.K. Schuller, *J. Magn. Magn. Mater.* 192 (1999) 203.
- [267] W.H. Meiklejohn, C.P. Bean, *Phys. Rev.* 102 (1956) 1413.
- [268] W.H. Meiklejohn, C.P. Bean, *Phys. Rev.* 105 (1957) 904.
- [269] F.S. Lubrosky, *Electro-Technology*, 102 (Sept. 1962).
- [270] M. Ohkoshi et al., *IEEE Transl. J. Magn. Jpn.* 1 (1985) 37.
- [271] A.A. Glazer, et al. *Sov. Phys. JETP Lett.* 15 (1972) 259.
- [272] C. Tang, et al. *J. Appl. Phys.* 55 (1984) 2226.
- [273] B. Dieny, et al. *Phys. Rev. B* 43 (1991) 1297.
- [274] J.C.S. Kools, *IEEE Trans. Magn.* 32 (1996) 3165.
- [275] A.P. Malozemoff, *J. Appl. Phys.* 63 (1988) 3874.
- [276] A.E. Berkowitz, K. Takano, *J. Magn. Magn. Mater.* 200 (1999) 552.
- [277] T.C. Schulthess, W.H. Butler, *J. Appl. Phys.* 85 (1999) 5510.
- [278] M. Kiwi, *J. Magn. Magn. Mater.* 234 (2001) 584.
- [279] J. Nogués, J. Sort, V. Langlais, V. Skumryev, S. Suriñach, J.S. Muñoz, M.D. Baró, *Phys. Rep.* 422 (2005) 65.
- [280] A. Loidl, H. von Loehneysen, G.M. Kalvius, *J. Phys. Condens. Matter* 20 (2008) 430301.
- [281] H. Schmid, *Ferroelectrics* 162 (1994) 665.
- [282] M. Fiebig, *J. Phys. D* 38 (2005) R123.
- [283] W. Prellier, M.P. Singh, P. Murugavel, *J. Phys. Condens. Matter* 17 (2005) R803.
- [284] R. Ramesh, N.A. Spaldin, *Nature Mater.* 6 (2007) 21.
- [285] L.W. Martin, S.P. Crane, Y.-H. Chu, M.B. Holcomb, M. Gajek, M. Huijben, C.-H. Yang, N. Balke, R. Ramesh, *J. Phys. Condens. Matter* 20 (2008) 434220.
- [286] W. Eerenstein, N.D. Mathur, J.F. Scott, *Nature* 442 (2006) 759.
- [287] D. Khomskii, *Physics* 2 (2009) 20.
- [288] J. Wang, J.B. Neaton, H. Zheng, V. Nagarajan, S.B. Ogale, B. Liu, D. Viehland, V. Vaithyanathan, D.G. Schlom, U.V. Waghmare, N.A. Spaldin, K.M. Rabe, M. Wuttig, R. Ramesh, *Science* 299 (2003) 1719.
- [289] B.B. van Aken, T.T.M. Palstra, A. Filippetti, N.A. Spaldin, *Nature Mater.* 3 (2004) 164.
- [290] N. Ikeda, H. Ohsumi, K. Ohwada, K. Ishii, T. Inami, K. Kakurai, Y. Murakami, K. Yoshii, S. Mori, Y. Horibe, H. Kito, *Nature* 436 (2005) 1136.
- [291] T. Kimura, T. Goto, H. Shintani, K. Ishizaka, T. Arima, Y. Tokura, *Nature* 426 (2003) 55.
- [292] N. Hur, S. Park, P.A. Sharma, J.S. Ahn, S. Guha, S.-W. Cheong, *Nature* 429 (2004) 392.
- [293] P. Curie, *J. de Physique* 3 (1894) 393.
- [294] D.N. Astov, *Sov. Phys. JETP* 11 (1960) 708; 13 (1961) 729.
- [295] G.T. Rado, V.J. Folen, *Phys. Rev. Lett.* 7 (1961) 310; V.J. Folen, G.T. Rado, E.W. Stalder, *Phys. Rev. Lett.* 6 (1961) 607.
- [296] V.E. Wood, A.E. Austin, *Int. J. Magn. S* (1973) 303.
- [297] M. Fiebig, *J. Phys. D* 38 (2005) R123.
- [298] H.L. Yakel, W.D. Koehler, E.F. Bertaut, F. Forrat, *Acta Crystallogr.* 16 (1963) 957.
- [299] T. Lottermoser, T. Lonkai, U. Amann, D. Hohlwein, J. Ihlinger, M. Fiebig, *Nature* 430 (2004) 541.
- [300] T. Kimura, T. Goto, H. Shintani, K. Ishizaka, T. Arima, Y. Tokura, *Nature* 426 (2003), 55.
- [301] T. Kimura, G. Lawes, T. Goto, Y. Tokura, A.P. Ramirez, *Phys. Rev. B* 71 (2005) 224425.
- [302] N. Fujimura, T. Ishida, T. Yoshimura, T. Ito, *Appl. Phys. Lett.* 69 (1996) 1011.
- [303] H.L. Yakel, W.C. Koehler, E.F. Bertaut, E.F. Forrat, *Acta Crystallogr.* 16 (1963) 957.
- [304] E.F. Bertaut, R. Pauthenet, M. Mercier, *Phys. Lett.* 7 (1963) 110.
- [305] P. Salvador, T.-D. Doan, B. Mercey, B. Raveau, *Chem. Mater.* 10 (1998) 2592.
- [306] D.C. Yoo, J.Y. Lee, I.S. Kim, Y.T. Kim, *Thin Solid Films* 416 (2002) 62.
- [307] K. Suzuki, D. Fu, K. Nishizawa, T. Miki, K. Kato, *Jpn. J. Appl. Phys.* 42 (2003) 5692.
- [308] J. Dho, C.W. Leung, J.L. MacManus-Driscoll, M.G. Blamire, *J. Cryst. Growth* 267 (2004) 548.
- [309] A. Posadas, J.-B. Yau, C.H. Ahn, J. Han, S. Gariglio, K. Johnston, K.M. Rabe, J.B. Neaton, *Appl. Phys. Lett.* 87 (2005) 171915.
- [310] Y. Chye, T. Liu, D. Li, K. Lee, D. Lederman, T.H. Myers, *Appl. Phys. Lett.* 88 (2006) 132903.

- [311] K.T. Kim, C.L. Kim, J. Eur. Ceram. Soc. 24 (2004) 2613.
- [312] L. Zhou, Y.P. Wang, Z.G. Liu, W.Q. Zou, Y.W. Du, Phys. Status Solidi A 201 (2004) 497.
- [313] N. Shigemitsu, H. Sakata, D. Ito, T. Yoshimura, A. Ashida, N. Fujimura, Jpn. J. Appl. Phys. 43 (2004) 6613.
- [314] D. Kim, D. Klingensmith, D. Dalton, V. Olariu, F. Gnadinger, M. Rahman, A. Mahmud, T.S. Kalkur, Integr. Ferroelectr. 68 (2004) 75.
- [315] D. Ito, N. Fujimura, T. Yoshimura, T. Ito, J. Appl. Phys. 93 (2003) 5563.
- [316] N. Fujimura, H. Sakata, D. Ito, T. Yoshimura, T. Yokota, T. Ito, J. Appl. Phys. 93 (2003) 6990.
- [317] T. Choi, J. Lee, Appl. Phys. Lett. 84 (2004) 5043.
- [318] A. Sundaresan, A. Maignan, B. Raveau, Phys. Rev. B 56 (1997) 5092.
- [319] A.A. Nugroho, N. Bellido, U. Adem, G. Nénert, Ch. Simon, M.O. Tjia, M. Mostovoy, T.T.M. Palstra, Phys. Rev. B 75 (2007) 174435.
- [320] A.A. Bosak, A.A. Kamenev, I.E. Graboy, S.V. Antonov, O.Y. Gorbenco, A.R. Kaul, C. Dabourdieu, J.P. Senateur, V.L. Svechnikov, H.W. Zandbergen, B. Holländer, Thin Solid Films 400 (2001) 149.
- [321] K. Suzuki, K. Nishizawa, T. Miki, K. Kato, J. Cryst. Growth 237 (2002) 482.
- [322] J.-H. Lee, P. Murugavel, H. Ryu, D. Lee, J.Y. Jo, J.W. Kim, H.J. Kim, K.H. Kim, Y. Jo, M.-H. Jung, Y.H. Oh, Y.-W. Kim, J.-G. Yoon, J.-S. Chung, T.W. Noh, Adv. Mater. 18 (2006) 3125.
- [323] K.R. Balasubramaniam, S. Havelia, P.A. Salvador, H. Zheng, J.F. Mitchell, Appl. Phys. Lett. 91 (2007) 232901.
- [324] D.K. Shukla, R. Kumar, S.K. Sharma, P. Thakur, R.J. Choudhary, S. Mollah, N.B. Brookes, M. Knobel, K.H. Chae, W.K. Choi, J. Phys. D 42 (2009) 125304.
- [325] A.M. dos Santos, S. Parashar, A.R. Raju, Y.S. Zhao, A.K. Cheetham, C.N. Rao, Solid State Commun. 122 (2002) 49.
- [326] M. Azuma, N. Seiji, A. Belik, I. Shintaro, S. Takashi, T. Kazuhide, Y. Ikuya, S. Yuichi, T. Mikio, Trans. Mater. Res. Soc. Jpn. 31 (2006) 41.
- [327] A.M. dos Santos, A.K. Cheetham, W. Tian, X. Pan, Y. Jia, N.J. Murphy, J. Lettieri, D.G. Schlom, Appl. Phys. Lett. 84 (2004) 91.
- [328] A. Sharan, J. Lettieri, Y. Jia, W. Tian, X. Pan, D.G. Schlom, V. Gopalan, Phys. Rev. B 69 (2004) 214109.
- [329] T. Atou, H. Chiba, K. Ohoyama, Y. Yamaguichi, Y. Syono, J. Solid State Chem. 145 (1999) 639.
- [330] J.Y. Son, B.G. Kim, C.H. Kim, J.H. Cho, Appl. Phys. Lett. 84 (2004) 4971.
- [331] M. Gajek, M. Bibes, A. Barthélémy, K. Bouzehouane, S. Fusil, M. Varela, J. Fontcuberta, A. Fert, Phys. Rev. B 72 (2005), 020406 (R).
- [332] M. Gajek, M. Bibes, S. Fusil, K. Bouzehouane, J. Fontcuberta, A. Barthélémy, A. Fert, Nature Mater. 6 (2007) 296.
- [333] C.H. Yang, S.H. Lee, T.Y. Koo, Y.H. Jeong, Phys. Rev. B 75 (2007) 140104.
- [334] A.A. Belik, S. Iikubo, K. Kodama, N. Igawa, S. Shamoto, M. Maie, T. Nagai, Y. Matsui, S.Y. Stefanovich, B.I. Lazoryak, E. Takayama-Muromachi, J. Am. Chem. Soc. 128 (2005) 706.
- [335] P. Baettig, R. Seshadri, N.A. Spaldin, J. Am. Chem. Soc. 129 (2007) 9854.
- [336] T. Shishidou, N. Mikamo, Y. Uratani, F. Ishii, T. Oguchi, J. Phys. Condens. Matter. 16 (2004) S5677.
- [337] R. Schmidt, W. Eerenstein, P.A. Midgley, Phys. Rev. B 79 (2009) 214107.
- [338] P. Royen, K. Swars, Angew. Chem. 24 (1957) 779.
- [339] F. Kubel, H. Schmid, Acta. Cryst. B46 (1990) 698.
- [340] S.V. Kiselev, R.P. Ozerov, G.S. Zhdanov, Sov. Phys. Dokl. 7 (1963) 742.
- [341] J.R. Teague, R. Gerson, W.J. James, Solid. State. Commun. 8 (1963) 1073.
- [342] C. Michel, J.M. Moreau, G.D. Achenbach, R. Gerson, W.J. James, Solid State Commun. 7 (1969) 701.
- [343] J.M. Moreau, C. Michel, R. Gerson, W.J. James, J. Phys. Chem. Solids 32 (1971) 1315.
- [344] C. Tabares-Muñoz, J.P. Rivera, A. Bezing, A. Monnier, H. Schmid, Jpn. J. Appl. Phys. 24 (1985) 1051.
- [345] F. Zavaliche, S.Y. Yang, T. Zhao, Y.H. Chu, M.P. Cruz, C.B. Eom, R. Ramesh, Phase Transit 79 (2006) 991.
- [346] P. Fischer, M. Polomska, I. Sosnowska, M. Szymanski, J. Phys. C 13 (1980) 1931.
- [347] I. Sosnowska, T. Peterlin-Neumaier, E. Steichele, J. Phys. C 15 (1982) 4835.
- [348] I.E. Dzyaloshinskii, Sov. Phys. JETP 5 (1957) 1259.
- [349] T. Moriya, Phys. Rev. 120 (1960) 91.
- [350] D. Lebeugle, D. Colson, A. Forget, M. Viret, P. Bonville, J.F. Marucco, S. Fusil, Phys. Rev. B 76 (2007) 024116.
- [351] J.B. Neaton, C. Ederer, U.V. Waghmare, N.A. Spaldin, K.M. Rabe, Phys. Rev. B 71 (2005) 014113.
- [352] C. Ederer, N.A. Spaldin, Phys. Rev. B 71 (2005), 060401 (R).
- [353] W. Eerenstein, F.D. Morrison, J. Dho, M.G. Blamire, J.F. Scott, N.D. Mathur, Science 307 (2005) 1203a.
- [354] H. Béa, M. Bibes, S. Fusil, K. Bouzehouane, E. Jacquet, K. Rode, P. Bencok, A. Barthélémy, Phys. Rev. B 74 (2006) 020101.
- [355] J. Wang, A. Scholl, H. Zheng, S.B. Ogale, D. Viehland, D.G. Schlom, N.A. Spaldin, K.M. Rabe, M. Wuttig, L. Mohaddes, J. Neaton, U. Waghmare, T. Zhao, R. Ramesh, Science 307 (2005) 1203b.
- [356] F. Gao, X. Chen, K. Yin, S. Dong, Z. Ren, F. Yuan, T. Yu, Z. Zou, J.M. Liu, Adv. Mater. 19 (2007) 2889.
- [357] V.R. Palkar, J. John, R. Pinto, Appl. Phys. Lett. 80 (2002) 1628.
- [358] Y.H. Lee, C.C. Lee, Z.X. Liu, C.S. Liang, J.M. Wu, Electrochem. Solid-State Lett. 8 (2005) F55.
- [359] R.R. Das, D.M. Kim, S.H. Baek, F. Zavaliche, S.-Y. Yang, X. Ke, S.K. Streiffer, M.S. Rzhowski, R. Ramesh, C.B. Eom, Appl. Phys. Lett. 88 (2006) 242904.
- [360] S.-Y. Yang, F. Zavaliche, L. Mohaddes-Ardabili, V. Vaithyanathan, D.G. Schlom, Y.J. Lee, Y.-H. Chu, M.P. Cruz, T. Zhao, R. Ramesh, Appl. Phys. Lett. 87 (2005) 102903.
- [361] R. Ueno, S. Okaura, H. Funakubo, K. Saito, Jpn. J. Appl. Phys. 44 (2005) L1231.
- [362] S.K. Singh, Y.K. Kim, H. Funakubo, H. Ishiura, Appl. Phys. Lett. 88 (2006) 062502.
- [363] J. Wang, H. Zheng, Z. Ma, S. Prasertchoung, M. Wuttig, R. Droopad, J. Yu, K. Eisenbeiser, R. Ramesh, Appl. Phys. Lett. 85 (2004) 2574.
- [364] W. Tian, V. Vaithyanathan, D.G. Schlom, Q. Zhan, S.-Y. Yang, Y.-H. Chu, R. Ramesh, Appl. Phys. Lett. 90 (2007) 172908.
- [365] Y.-H. Chu, T. Zhao, M.P. Cruz, Q. Zhan, P.-L. Yang, L.W. Martin, M. Huijben, C.-H. Yang, F. Zavaliche, H. Zheng, R. Ramesh, Appl. Phys. Lett. 90 (2007) 252906.
- [366] M.B. Holcomb, L.W. Martin, A. Scholl, Q. He, P. Yu, C.-H. Yang, S.Y. Yang, P.-A. Glans, M. Valvidares, M. Huijben, J.B. Kortright, J. Guo, Y.-H. Chu, R. Ramesh, Phys. Rev. B 81 (2010) 134406.
- [367] L.W. Martin, Y.-H. Chu, M.B. Holcomb, M. Huijben, S.J. Han, D. Lee, A. Arenholz, S.X. Wang, R. Ramesh, Nano Lett. 8 (2008) 2050.
- [368] J. Přivratská, V. Janovec, Ferroelectrics 204 (1997) 321.
- [369] J. Přivratská, V. Janovec, Ferroelectrics 222 (1999) 23.
- [370] L. Thomas, M. Hayashi, X. Jiang, R. Moriya, C. Rettner, S. Parkin, Science 315 (2007) 1553.
- [371] V. Goltsev, et al. Phys. Rev. Lett. 90 (2003) 177204.
- [372] M. Mostovoy, Phys. Rev. Lett. 96 (2006) 067601.
- [373] S.-W. Cheong, M. Mostovoy, Nature. Mater. 6 (2007) 13.
- [374] A. Aird, E.K.H. Salje, J. Phys.: Condens. Matter. 10 (1998) L377.
- [375] M. Bartels, V. Hagen, M. Burianek, M. Getzlaff, U. Bismayer, R. Wiesendanger, J. Phys.: Condens. Matter. 15 (2003) 957.
- [376] P. Zubko, et al. Phys. Rev. Lett. 99 (2007) 167601.
- [377] M. Daraktchiev, G. Catalan, J.F. Scott, Ferroelectrics 375 (2008) 122.
- [378] G. Catalan, J.F. Scott, Adv. Mater. 21 (2009) 2463.
- [379] Q. He, M. Daraktchiev, G. Catalan, E. Arenholz, A. Scholl, A. Fraile-Rodríguez, S.-Y. Yang, C.-H. Yang, P. Yu, J. Wu, D. Lee, Z. Q. Qiu, S. X. Wang, Y.-H. Chu, J. F. Scott, L. W. Martin, R. Ramesh, Nature Mater., submitted for publication.
- [380] J. Seidel, L.W. Martin, Q. He, Q. Zhan, Y.-H. Chu, A. Rother, M.E. Hawkrig, P. Maksymovych, P. Yu, M. Gajek, N. Balke, S.V. Kalinin, S. Gemming, F. Wang, G. Catalan, J.F. Scott, N.A. Spaldin, J. Orenstein, R. Ramesh, Nature Mater. 8 (2009) 229.
- [381] T. Zhao, A. Scholl, F. Zavaliche, K. Lee, M. Barry, A. Doran, M.P. Cruz, Y.-H. Chu, C. Ederer, N.A. Spaldin, R.R. Das, D.M. Kim, S.H. Baek, C.B. Eom, R. Ramesh, Nature Mater. 5 (2006) 823.
- [382] D. Lebugle, D. Colson, A. Forget, M. Viret, A.M. Bataille, A. Gukasov, Phys. Rev. Lett. 100 (2008) 227602.
- [383] Y.-H. Lee, J.-M. Wu, C.-H. Lai, Appl. Phys. Lett. 88 (2006) 042903.
- [384] X. Qi, J. Dho, R. Tomov, M.G. Blamire, J.L. MacManus-Driscoll, Appl. Phys. Lett. 86 (2005) 062903.
- [385] J.K. Kim, S.S. Kim, W.-J. Kim, A.S. Bhalla, R. Guo, Appl. Phys. Lett. 88 (2006) 132901.
- [386] C.-H. Yang, J. Seidel, S.Y. Kim, P.B. Rossen, P. Yu, M. Gajek, Y.-H. Chu, L.W. Martin, M.B. Holcomb, Q. He, P. Maksymovych, N. Balke, S.V. Kalinin, A.P. Baddorf, S.R. Basu, M.L. Scullin, R. Ramesh, Nature Mater. 8 (2009) 485.
- [387] N.A. Hill, P. Battig, C. Daul, J. Phys. Chem. B 106 (2002) 3383.
- [388] M. Murakami, S. Fujino, S.-H. Lim, C.J. Long, L.G. Salamanca-Riba, M. Wuttig, I. Takeuchi, V. Nagarajan, A. Varatharajan, Appl. Phys. Lett. 88 (2006) 152902.
- [389] D.H. Kim, H.N. Lee, M. Varela, H.M. Christen, Appl. Phys. Lett. 89 (2006) 162904.
- [390] A.A. Belik, S. Iikubo, K. Kodama, N. Igawa, S. Shamota, S. Niitaka, M. Azuma, Y. Shimakawa, M. Takano, F. Izumi, E. Takayama-Muromachi, Chem. Mater. 18 (2006) 798.
- [391] Y. Uratani, T. Shishidou, F. Ishii, T. Oguchi, Jpn. J. Appl. Phys. 44 (2005) 7130.
- [392] S. Yasui, K. Nishida, H. Naganuma, S. Okamura, T. Iijima, H. Funakubo, Jpn. J. Appl. Phys. 46 (2007) 6948.
- [393] L.W. Martin, Q. Zhan, Y. Suzuki, R. Ramesh, M. Chi, N. Browning, T. Mizoguchi, J. Kreisel, Appl. Phys. Lett. 90 (2007) 062903.
- [394] A. Kumar, L.W. Martin, S. Denev, J.B. Kortright, Y. Suzuki, R. Ramesh, V. Gopalan, Phys. Rev. B 75 (2007) 060101 (R).
- [395] M. Sakai, A. Msauno, D. Kan, M. Hashisaka, K. Takata, M. Azuma, M. Takano, Y. Shimakawa, Appl. Phys. Lett. 90 (2007) 072903.
- [396] J. van den Boomgaard, D.R. Terrell, R.A.J. Born, J. Mater. Sci. 9 (1974) 1705.
- [397] M. Avellaneda, G. Harshe, J. Intel. Mat. Syst. Str. 5 (1994) 501.
- [398] J. Ryu, S. Priya, A.V. Carazo, K. Uchino, H. Kim, J. Am. Ceram. Soc. 84 (2001) 2905.
- [399] S. Ryu, J.H. Park, H.M. Jang, App. Phys. Lett. 91 (2007) 142910.
- [400] J. Ryu, A.V. Carazo, K. Uchino, H. Kim, J. Electroceram. 7 (2001) 17.
- [401] G. Srinivasan, E.T. Rasmussen, J. Gallegos, R. Srinivasan, Phys. Rev. B 64 (2001) 214408.
- [402] G. Srinivasan, E.T. Rasmussen, B.J. Levin, R. Hayes, Phys. Rev. B 65 (2002) 134402.
- [403] G. Srinivasan, E.T. Rasmussen, A.A. Bush, K.E. Kametsev, App. Phys. A 78 (2004) 721.
- [404] J. Ryu, S. Priya, K. Uchino, H.E. Kim, J. Electroceram. 8 (2002) 107.
- [405] P. Murugavel, M.P. Singh, W. Prellier, B. Mercey, C. Simon, B. Raveau, J. Appl. Phys. 97 (2005) 103914.
- [406] S. Stein, M. Wuttig, D. Viehland, E. Quandt, J. Appl. Phys. 97 (2005), 10Q301.
- [407] M.I. Bichurin, V.M. Petrov, G. Srinivasan, Phys. Rev. B 68 (2003) 054402.
- [408] H. Zheng, J. Wang, S.E. Lofland, Z. Ma, L. Mohaddes-Ardabili, T. Zhao, L. Salamanca-Riba, S.R. Shinde, S.B. Ogale, F. Bai, D. Viehland, Y. Jia, D.G. Schlom, M. Wuttig, A. Roytburg, R. Ramesh, Science 303 (2004) 661.
- [409] H. Zheng, Q. Zhan, F. Zavaliche, M. Sherburne, F. Straub, M.P. Cruz, L.-Q. Chen, U. Dahmen, R. Ramesh, Nanolett 7 (2006) 1401.
- [410] J. Li, I. Levin, J. Slutsker, V. Provenzano, P.K. Schenck, R. Ramesh, J. Ouyang, A.L. Roytburd, Appl. Phys. Lett. 87 (2005) 072909.
- [411] J.G. Wan, X.W. Wang, Y.J. Wu, M. Zeng, Y. Wang, H. Jiang, W.Q. Zhou, G.H. Wang, J.M. Liu, Appl. Phys. Lett. 86 (2005) 122501.
- [412] S. Ren, M. Wuttig, Appl. Phys. Lett. 91 (2007) 083501.

- [413] Q. Zhan, R. Yu, S.P. Crane, H. Zheng, C. Kisielowski, R. Ramesh, *Appl. Phys. Lett.* 89 (2006) 172902.
- [414] M. Murakami, S. Fujino, S.-H. Lim, L.G. Salamanca-Riba, M. Wuttig, I. Takeuchi, B. Varughese, H. Sugaya, T. Hasegawa, S.E. Lofland, *Appl. Phys. Lett.* 88 (2006) 112505.
- [415] H. Ryu, P. Murugavel, J.H. Lee, S.C. Chae, T.W. Noh, Y.S. Oh, H.J. Kim, K.H. Kim, J.H. Jang, M. Kim, C. Bae, J.-G. Park, *Appl. Phys. Lett.* 89 (2006) 102907.
- [416] J.-G. Wan, Y. Weng, Y. Wu, Z. Li, J.-M. Liu, G. Wang, *Nanotechnology* 18 (2007) 465708.
- [417] F. Zavaliche, H. Zheng, L. Mohaddes-Ardabili, S.-Y. Yang, Q. Zhan, P. Shafer, E. Reilly, R. Chopdekar, Y. Jia, P. Wright, D.G. Schlom, Y. Suzuki, R. Ramesh, *Nano Lett.* 5 (2005) 1793.
- [418] F. Zavaliche, T. Zhao, H. Zheng, F. Straub, M.P. Cruz, P.-L. Yang, D. Hao, R. Ramesh, *Nano Lett.* 7 (2007) 1586.
- [419] M. Liu, X. Li, H. Imrane, Y. Chen, T. Goodrich, Z. Cai, K.S. Ziemer, J.Y. Huang, *Appl. Phys. Lett.* 90 (2007) 152501.
- [420] Ch. Binek, B. Doudin, *J. Phys. Condens. Matter.* 17 (2005) L39.
- [421] A. Ney, C. Pampuch, R. Koch, K.H. Ploog, *Nature* 425 (2003) 485.
- [422] J. Slonczewski, *J. Magn. Magn. Mater.* 159 (1996) L1.
- [423] J. Slonczewski, *J. Magn. Magn. Mater.* 195 (1999) 261.
- [424] L. Berger, *Phys. Rev. B* 54 (1996) 9353.
- [425] M. Tsoi, A.G.M. Jansen, W.-C. Chiang, M. Seck, V. Tsoi, P. Wyder, *Phys. Rev. Lett.* 80 (1998) 4281.
- [426] J.E. Wegrowe, D. Kelly, Y. Jaccard, Ph. Guittienne, J.-Ph. Ansermet, *Europhys. Lett.* 45 (1999) 626.
- [427] E.B. Myers, D.C. Ralph, J.A. Katine, R.N. Louie, R.A. Buhrman, *Science* 285 (1999) 867.
- [428] S. Urazhdin, N.O. Birge, W.P. Pratt Jr., J. Bass, *Phys. Rev. Lett.* 91 (2003) 146803.
- [429] Y. Liu, Z. Zhang, P.P. Freitas, J.L. Martins, *Appl. Phys. Lett.* 82 (2003) 2871.
- [430] Y. Huai, F. Albert, P. Nguyen, M. Pakala, T. Valet, *Appl. Phys. Lett.* 84 (2004) 3118.
- [431] T. Wu, S.B. Ogale, J.E. Garrison, B. Nagaraj, A. Biswas, Z. Chen, R.L. Greene, R. Ramesh, T. Venkatesan, *Phys. Rev. Lett.* 86 (2001) 5998.
- [432] E. Dagotto, *Nanoscale Phase Separation and Colossal Magnetoresistance*, Springer-Verlag, New York, 2003.
- [433] J. Dho, M.G. Blamire, *Appl. Phys. Lett.* 87 (2005) 252504.
- [434] X. Martí, F. Sánchez, J. Fontcuberta, M.V. García-Cuenca, C. Ferrater, M. Varela, *J. Appl. Phys.* 99 (2006), 08P302.
- [435] J. Dho, X. Qi, H. Kim, J.L. MacManus-Driscoll, M.G. Blamire, *Adv. Mater.* 18 (2006) 1445.
- [436] H. Béa, M. Bibes, S. Cherifi, *Appl. Phys. Lett.* 89 (2006) 242114.
- [437] L.W. Martin, Y.-H. Chu, Q. Zhan, R. Ramesh, S.J. Han, S.X. Wang, M. Warusawithana, D.G. Schlom, *Appl. Phys. Lett.* 91 (2007) 172513.
- [438] P. Borisov, A. Hochstrat, X. Chen, W. Kleeman, C. Binek, *Phys. Rev. Lett.* 94 (2005) 117203.
- [439] V. Laukhin, V. Skumryev, X. Martí, D. Hrabovsky, F. Sánchez, M.V. García-Cuenca, C. Ferrater, M. Varela, U. Lüders, J. Fontcuberta, *Phys. Rev. Lett.* 97 (2006) 227201.
- [440] H. Béa, M. Bibes, F. Ott, B. Dupé, X.H. Zhu, S. Petit, S. Fusil, C. Deranlot, K. Boussehouane, A. Barthélémy, *Phys. Rev. Lett.* 100 (2008) 017204.
- [441] Y.-H. Chu, L.W. Martin, M.B. Holcomb, M. Gajek, S.J. Han, N. Balke, C.-H. Yang, D. Lee, W. Hu, Q. Zhan, P.-L. Yang, A. Fraile-Rodriguez, A. Scholl, S.X. Wang, R. Ramesh, *Nature Mater.* 7 (2008) 478.
- [442] P. Yu, J.-S. Lee, M.D. Rossell, M. Huijben, C.-H. Yang, Q. He, J.-X. Zhang, S.-Y. Yang, M. Lee, Q.M. Ramasse, R. Erni, Y.-H. Chu, D. Arena, C.-C. Kao, L.W. Martin, R. Ramesh, *Phys. Rev. Lett.*, in press.
- [443] J.F. Scott, *Nature Mater.* 6 (2007) 256.
- [444] C.M. Cristensen, *The Innovator's Dilemma*, Harvard Business School Press, Boston, 1997.
- [445] S. Ju, T.-Y. Cai, G.-Y. Guo, Z.-Y. Li, *Phys. Rev. B* 75 (2007) 064419.
- [446] F. Yang, M.H. Tang, Z. Ye, Y.C. Zhou, X.J. Zheng, J.X. Zheng, J.J. Zhang, J. He, *J. Appl. Phys.* 102 (2007) 044504.
- [447] C. Jia, J. Berakdar, *Appl. Phys. Lett.* 95 (2009) 012105.
- [448] C.J. Fennie, K.M. Rabe, *Phys. Rev. Lett.* 97 (2007) 267602.